Nucleation Control: Microwave, Ultrasound and Laser as Tools to Control the Number of Nuclei in Crystallization Processes

Kacker, Rohit

Important note
To cite this publication, please use the final published version (if applicable).
Please check the document version above.

Nucleation Control: Microwave, Ultrasound and Laser as Tools to Control the Number of Nuclei in Crystallization Processes

Rohit KACKER

Nucleation Control: Microwave, Ultrasound and Laser as Tools to Control the Number of Nuclei in Crystallization Processes

Proefschrift

ter verkrijging van de graad van doctor
aan de Technische Universiteit Delft,
op gezag van de Rector Magnificus prof. dr. ir. T. H. J. J. van der Hagen,
voorzitter van het College voor Promoties,
in het openbaar te verdedigen op dinsdag 8 mei 2018 om 15:00 uur

door

Rohit KACKER

Master of Science in Chemical Engineering,
Technische Universiteit Delft, Delft, Nederland,
geboren te Lucknow, India.

Dit proefschrift is goedgekeurd door de

promotor: Prof. dr. ir. A. I. Stankiewicz
copromotor: Dr. H. B. Eral

Samenstelling promotiecommissie:

Rector Magnificus,	voorzitter
Prof. dr. ir. A. I. Stankiewicz,	Technische Universiteit Delft
Dr. H. B. Eral,	Technische Universiteit Delft

Onafhankelijke leden:

Prof. dr. T. Van Gerven,	Katholieke Universiteit Leuven
Prof. dr. ir. J. H. ter Horst	University of Strathclyde Glasgow
Dr. R. M. Geertman,	The Janssen Pharmaceutical Companies of Jhonson & Jhonson
Prof. dr. ir. A. B. de Haan,	Technische Universiteit Delft
Prof. dr. ir. J. R. van Ommen,	Technische Universiteit Delft, reservelid

Overig lid:

Prof. dr. ir. H. J. M. Kramer,	Technische Universiteit Delft

Printed by:	Ridderprint
Front & Back:	Designed by R. Kacker

An electronic version of this dissertation is available at
http://repository.tudelft.nl/.

Contents

Summary

Nucleation is the first step in a crystallization process, where out of a supersaturated solution the new crystalline entities are created, which eventually grow out to the final product crystals. Nucleation is thus crucial for the process, as it determines both the crystal structure as well as the amount and properties such as the size and shape distribution of the final product. In this thesis, the development of approaches to control the nucleation in batch and continuous processes has been targeted to manipulate the number of crystals with the aim to control the product properties, such as , the size and shape distribution.

Chapters 2 and 3 focus on the Direct Nucleation Control approach (DNC). DNC is a model free feedback control strategy, to achieve desired crystal properties by controlling the number of particles during the batch processes through real time in-situ measurement of the crystal phase. The number of crystals is manipulated under the DNC framework by cycling between the supersaturated and undersaturated state, for instance by temperature manipulation. Due to the slow heating response of the conventional jacketed crystallizers, the efficiency of DNC is poor. Large number of control cycles and long cycle times lead to long batch times to achieve the targeted control over crystal properties. Hence, the efficiency enhancement of the DNC has been targeted through optimization of the dissolution cycles by rapid heating using microwaves. Chapter 2, covers the demonstration of the proof of the concept of microwave assisted DNC for efficiency enhancement. The demonstration has been carried out in a crystallizer with combined microwave heating, via an external circulation loop passing through a microwave oven. The rapid microwave heating in the microwave assisted DNC process, allowed curbing of nucleation by reducing the periods at high supersaturation and facilitated quick dissolution of the excess nuclei. Consequently, the impact of nucleation could be strongly mitigated, which resulted in a remarkable reduction in the number of heating cycles needed to keep the number of particle at their set-point value. As a result, the efficiency of the DNC process could be enhanced by achieving a 50% reduction in batch time. The focus of chapter 3, was the design of a novel crystallizer in which the microwave applicator was integrated to eliminate the external heating loop through a microwave oven. Through internal transmission of the microwaves directly into the crystallizer, a compact unit has been achieved with microwave heating, jacketed cooling and provision for safe implementation of PAT tools in presence of microwaves. The scale of the process has also been enhanced from $1\,L$ to $4\,L$. Similar to proof of concept study, a strong efficiency enhancement of DNC (50 % reduction in batch time) was achieved when compared to the performance using conventional heating.

Chapters 4 to 6, cover the topic of the optimal operation of continuous tubular crystallizers. Tubular crystallizer operated under plug flow conditions offer a well-defined residence time distribution, but rely on primary nucleation or seeding meth-

ods to provide the initial crystals at the beginning of the reactor. In this thesis, a COBC has been analysed and optimised. First, the optimal flow conditions to reach plug flow like behaviour have been ascertained and secondly the seeding of the COBC through controlled primary nucleation using ultrasounds has been investigated. During the study, the mixing in the COBC as the function of the fluid oscillation frequency and amplitude and the imposed flowrate has been characterized. The characterization is done by studying the residence time distribution of both the bulk liquid phase and the dispersed crystalline phase. Operation at low oscillation amplitude at several operating frequencies have been identified as optimal conditions leading to a narrow residence time distribution of the crystal suspension. At the optimal condition, good radial mixing was achieved in the COBC with slurry concentration of 10 % (w/w). Ensuring homogenous residence time of crystals implies that control over the growth and the secondary nucleation can be easily achieved by applying an appropriate temperature profile over the crystallizer. However, as under plug flow conditions there is no back mixing of crystals, continuous supply of seed crystal is needed to ensure steady operation without uncontrolled primary and secondary nucleation, which lead to fouling and plugging of the flow crystallizer.

Chapter 5, shows the development of in-situ imaging system for the monitoring of nucleation and characterization of the crystalline phase. Process monitoring and characterization is an essential part of implementing control strategies for ensuring steady operation with constant crystal density and the end product quality. In-situ imaging is a convenient tool for inline characterization of the number, size and shape of the crystals without the need for sampling. Unfortunately, the available image analysis tools are not robust enough to accurately estimate the crystals shape and size distribution from the images obtained from the in-line probes. In this chapter, two image analysis approaches, one based on pattern matching and the other based on segregation algorithms for identifying objects on an image, are examined to identify and characterize the crystals. Samples containing both small nuclei and the larger grown crystals (non-spherical and irregular in shape) which have very different appearances could not be reliably characterized by the pattern matching approach. The pattern matching based image analysis resulted in an overestimation of the crystal size, while shape information could not be obtained due to circular approximation of the crystals. Alternatively, a segmentation based algorithm resulted in better crystal size and shape characteristics. Sampled crystals for laser diffraction analysis resulted in overestimation of the particle sizes due to the agglomeration of particles upon filtration and drying, highlighting the advantage of in-situ imaging. The normalized trend in the particle counts determined by the image analysis probe was comparable with the trend measured by FBRM.

Finally, chapters 6 and 7 present the use of external energy fields to directly manipulate the nucleation rate for gaining control over the number of nuclei during the crystallization process. Use of ultrasound (US) to induce controlled nucleation in a continuous flow through cell has been targeted as a tool for continuous seed generation, which can be applied to continuous crystallizers. Batch operating conditions, in terms of supersaturation, have been identified where only application of US at low supersaturation (within the metastable zone width) leads to creation of nuclei

due to the enhanced nucleation rate. However, the design of the flow cell used for application of US was found to be limiting and resulted in poor control over crystal size distribution. When the flow cell was applied to the COBC, the effect of US was overshadowed by nucleation on the walls of the COBC., leading to uncontrolled nucleation. As a result of nucleation on walls, the crystal residence time deviated from the expected plug flow behaviour established in the previous chapter.

Similarly, research has been done to clarify the mechanism that is responsible for Non photochemical laser induced nucleation (NPLIN). First of all, the supersaturation conditions have been identified where application of laser energy leads to nucleation, which otherwise do not nucleate. Various mechanisms have been proposed to explain the enhanced nucleation rate due to the non-photochemical interaction of laser with the clear solution. In our study, the presence of impurities (<400 nm) have been found to aid NPLIN. Laser induced pressure (radiation pressure) was measured and found to be weak to influence nucleation, thereby elimination radiation pressure as possible mechanism explaining NPLIN. Finally, the enhanced nucleation probability upon exposure to short laser pulses, as a function of the laser intensity, wavelength and laser induced pressure has been characterized. The knowledge generated on application of US and laser induced nucleation has helped to identify conditions and areas of improvement to further develop the use of external energy as process actuator to manipulate the nucleation rate.

Samenvatting

Nucleatie is de eerste stap in een kristallisatieproces, waarbij uit een oververzadigde oplossing de nieuwe kristallijne entiteiten worden gemaakt, die uiteindelijk uitgroeien tot de kristallen van het eindproduct. Nucleatie is dus cruciaal voor het proces, omdat het zowel de kristalstructuur bepaalt als de hoeveelheid en eigenschappen zoals de grootte en vormverdeling van het eindproduct. In dit proefschrift is de ontwikkeling van benaderingen om de nucleatie te beheersen, in batch en continue processen, gericht op het beïnvloeden van de hoeveelheid kristallen. Daarbij is het gericht op het beheersen van de producteigenschappen, zoals de grootte en vormverdeling.

Hoofdstukken 2 en 3 richten zich op de Directe Nucleatie Controle aanpak (DNC). DNC is een modelvrije feedback controle strategie met als doel om de gewenste kristaleigenschappen te bereiken door het aantal deeltjes tijdens de batchprocessen te beheersen doormiddel van rechtstreeks in-situ meting van de kristalfase. De hoeveelheid kristallen wordt beïnvloed onder het DNC-context door te circuleren tussen de oververzadigde en onderverzadigde stadium. Dit kan bijvoorbeeld door temperatuur worden beïnvloed. De efficiëntie van DNC is slecht, vanwege de langzame verhittingsreactie van de conventionele, met mantel voorziene kristallisatie reactor. Een groot aantal controlecycli en lange cyclustijden leiden tot lange batchtijden om de gerichte controle over kristaleigenschappen te bereiken. Als gevolg, de efficiëntieverbetering van de DNC is gericht op de optimalisatie van de oplossingscycli door snel te verwarmen met behulp van microgolven. Hoofdstuk 2 bevat de demonstratie van het bewijs rondom het microgolf-ondersteunde DNC voor efficiëntieverbetering. De demonstratie is uitgevoerd in een kristallisatie reactor gecombineerd met microgolfverwarming, via een externe circulatie die door een magnetronoven passeert. De snelle microgolfverwarming in het door microgolven ondersteunde DNC-proces, maakte het mogelijk de nucleusvorming te beperken door de perioden bij hoge oververzadiging te verminderen en door het snel oplossen van de overtollige kernen mogelijk te maken. Als gevolg hiervan kon de impact van nucleatie sterk worden beperkt, wat resulteerde in een opmerkelijke vermindering van het aantal verwarmingscycli dat nodig is om het aantal deeltjes op hun instelwaarde te houden. Dit resulteert tot de efficiëntieverbetering van het DNC-proces door een batch-tijdbesparing van 50% te bereiken. Hoofdstuk 3 focust zich op het ontwerp van een nieuwe kristallisatie reactor, waarin een microgolfapplicator was geïntegreerd om de externe verwarmingskringloop door een magnetronoven te elimineren. Door de rechtstreekse transmissie van de microgolven in de kristallisatiereactor is een compacte eenheid bereikt, met daarbij een magnetron voor verwarming, dubbelwandige koeling en een voorziening voor veilige implementatie van PAT-gereedschappen in aanwezigheid van microgolven. De schaal van het proces is daarnaast van $1L$ naar $4L$ verbeterd. Net als bij de proof of concept-studie, werd een sterke efficiëntieverbetering van DNC (50% reductie in batchtijd) bereikt in vergelijking met de prestaties met conventionele verwarming.

Hoofdstukken 4 en 5 behandelen het onderwerp rondom de optimale werking van continue buisvormige kristallisatie reactoren. Buisvormige kristallisatie reactoren die werken onder propstroomomstandigheden, bieden een goed gedefinieerde verblijftijdverdeling, maar vertrouwen op primaire nucleatie of kiemvorming om de kristallisatie te initiëren aan het begin van de reactor. In dit proefschrift is een Continuous Oscillatory flow Baffled Crystallizer (COBC) geanalyseerd en geoptimaliseerd.

Eerst werden de optimale stromingscondities bepaald om het propstromingsverloop te bereiken en ten tweede werd de kiemvorming van het COBC onderzocht door middel van gecontroleerde primaire nucleatie met behulp van ultrasone golven. Tijdens de studie is het mengen in de COBC gekarakteriseerd, als functie van de vloeistofoscillatiefrequentie, -amplitude en de opgebrachte stroomsnelheid. De karakterisering wordt gedaan door de verblijftijdverdeling van zowel de vloeibare bulkfase als de gedispergeerde kristallijne fase te bestuderen. Werking bij lage oscillatie-amplitude bij verschillende werkfrequenties zijn geïdentificeerd als optimale omstandigheden die leidden tot een nauwe verblijftijdverdeling van de kristalsuspensie.

Bij de optimale conditie werd een goede radiale menging bereikt in het COBC met specieconcentratie tot 10% (w/w). Het garanderen van een homogene verblijftijd van kristallen houdt in dat controle over de groei en de secundaire nucleatie eenvoudig kan worden bereikt door een geschikt temperatuurprofiel over de kristallisatie reactor aan te houden. Omdat er onder plugstroomomstandigheden echter geen terug-menging van kristallen plaatsvindt, is de continue toevoer van kiemkristallen nodig om een stabiele werking zonder ongecontroleerde primaire en secundaire kiemvorming te waarborgen, hetgeen leidt tot vervuiling en verstopping van de stroom kristallisatie reactor.

Hoofdstuk 5 toont de ontwikkeling van in-situ imaging-systemen voor de monitoring van nucleatie en karakterisatie van de kristallijne fase. Procesbewaking en karakterisering is een essentieel onderdeel van het implementeren van besturingsstrategieën. Dit waarborgt een stabiele werking met constante kristaldichtheid en de kwaliteit van het eindproduct. In-situ beeldvorming biedt als een handig hulpmiddel voor in-lijn karakterisering van het aantal, de grootte en de vorm van de kristallen zonder bemonstering. Helaas zijn de beschikbare hulpmiddelen voor beeldanalyse niet robuust genoeg om de vorm van de kristallen en de grootteverdeling nauwkeurig te schatten op basis van de beelden die zijn verkregen van de sondes. In dit hoofdstuk worden twee benaderingen voor beeldanalyse onderzocht op nauwkeurige identificatie en karakterisering van de kristallen. Eén benaderd op basis van patroonvergelijking en de andere gebaseerd op segregatiealgoritmen voor het identificeren van objecten op een afbeelding. Monsters die zowel kleine kernen bevatten als de grotere gegroeide kristallen (niet-bolvormig en onregelmatig van vorm) die zeer verschillende verschijningsvormen hebben, konden niet op betrouwbare wijze worden gekarakteriseerd door de patroon-aanpassingsbenadering. De beeldanalyse gebaseerd op patroonafstemming, resulteerde in een overschatting van de kristalgrootte, terwijl vorminformatie niet verkregen kon worden vanwege de cirkelvormige benadering van de kristallen. Als alternatief resulteerde een op segmenten gebaseerd algoritme, in betere kristalafmetingen en vormkenmerken. Het gebruik van bemonsterde kristallen voor laserdiffractie-analyse resulteerde in een overschatting van de

deeltjesgrootten als gevolg van de agglomeratie van deeltjes bij filtratie en drogen, wat het voordeel van in-situ beeldvorming benadrukt. De genormaliseerde trend in de deeltjestellingen bepaald door de beeldanalysesonde was vergelijkbaar met de trend gemeten door FBRM.

Ten slotte presenteren hoofdstukken 6 en 7 het gebruik van externe energievelden om de nucleatiesnelheid direct te manipuleren, zodat er controle verkregen wordt over het aantal kernen tijdens het kristallisatieproces. Gebruik van ultrasone trillingen (US) om gecontroleerde nucleatie in een continue stroom door cel te induceren, is als een hulpmiddel voor continue kiemvorming bedoeld, dat op continue kristallisatie reactoren kan worden toegepast. Operationele omstandigheden, in termen van oververzadiging, zijn geïdentificeerd waarbij alleen toepassing van de US bij lage oververzadiging (binnen de breedte van de metastabiele zone) leidt tot het creëren van kernen vanwege de verbeterde nucleatiesnelheid. Het ontwerp van de "flow cell" die werd gebruikt voor toepassing van de US bleek echter beperkend en resulteerde in slechte controle over kristalgrootteverdeling als gevolg van slecht mengen.

Als alternatief zijn de oververzadigingstoestanden geïdentificeerd waar toepassing van laserenergie leidt tot kiemvorming in oververzadigde oplossingen, die anders geen nucleaties vormen. Verschillende mechanismen zijn voorgesteld om de verbeterde kiemvormingssnelheid te verklaren vanwege de niet-fotochemische interactie van laser met de heldere oplossing. In ons onderzoek is gevonden dat de aanwezigheid van onzuiverheden ($<400\ nm$) de niet-fotochemische door laser geïnduceerde nucleatie (NPLIN) bevordert. Door laser veroorzaakte druk (stralingsdruk) werd gemeten en bleek zwak te zijn om kiemvorming te beïnvloeden, waardoor stralingsdruk als mogelijk mechanisme dat NPLIN verklaart. Tenslotte is de verbeterde kans van nucleatievorming als een functie van de laserintensiteit, golflengte en laser-geïnduceerde druk gekarakteriseerd. De kennis die is gegenereerd door toepassing van door de US en door laser geïnduceerde nucleatie heeft bijgedragen tot het identificeren van omstandigheden en verbetergebieden om het gebruik van externe energie als procesactuator verder te ontwikkelen om de nucleatiesnelheid te hanteren.

Vertaald door Hanaa el Hilali.

Preface

My firm belief in innovation being the key to value creation is the guiding beacon in the journey to quell inquisitiveness and to contribute. The experience leading to the completion of the PhD is just a start.

Rohit KACKER
Voorburg, January 2018

1

Introduction

The chapter aims to provide a brief overview on fundamentals of crystallization technology, challenges and the current research direction in the field of process control strategies and the presents the research questions and objectives addressed in the thesis.

1.1. Overview of Crystallization

The crystallization unit operation is the process of purification and separation of solutes molecules in a solid form (usually crystalline) by phasing them out from a multicomponent solution or vapour phase. The solid crystals during crystallization can be obtained from melts, liquid or vapour phase directly. Depending on the arrangement of the molecules the solid phase can be classified as crystalline, semi-crystalline, amorphous, or sub cooled liquid [1]. Crystalline solids have a well- defined lattice structure in which the ions, atoms or molecules are arranged in a unit cell which repeats itself. Crystallization is one of the preferred separation processes in industry, as a compound can be separated from a mixture in a single unit operation with high purity and with the desired end product properties such as size, shape and crystal structure. The physical characteristics of the crystals are of the utmost importance as properties such as solubility, flowabilty, etc. are dependent on the properties of the product crystals. Given the wide application of the crystallization products, different end product requirements are put forward. In general, purity (inclusions, solvates, etc.), crystal structure, shape, size, and surface properties of the crystals are important and need to be controlled. Poor control over crystal shape and size during crystallization will also affect the downstream processes like filtration or tableting resulting in loss of product. In industrial practice these complications arise, as the control of the crystallization process and its specific product properties is complex. Hence controlled engineering of the product crystals, through robust process design, is important to guarantee reliable and consistent production of crystals with the desired product specifications.

Nucleation being the onset of the crystallization process is a critical step to control for ensuring product with the right qualities. However, the inaccessibility of the nucleation time and spatial scales and the steep dependency of the nucleation rate on supersaturation has made characterization of the nucleation troublesome. Thus, two challenges arise; firstly the difficulty to predict the nucleation rate, due to the limited nucleation kinetics knowledge, leads to poor crystallization process design [2]. Secondly, the non-linear dependence of the primary nucleation rate on the process condition, makes nucleation control challenging. Hence, control by a simple temperature trajectory or anti-solvent addition rate is often inadequate to control the nucleation rate and it's variation is the main cause for the variability in the product quality from batch to batch. Therefore, control of the nucleation rate is essential to achieve the desired product quality.

In this research, the development of novel approaches to control nucleation is targeted. Due to the uncertain relation between the nucleation rate and the supersaturation and the limited robustness of the supersaturation sensors, model free control approach is investigated. First of all, the intensification of the Direct Nucleation Control(DNC) strategy, which is a model free approach based on direct monitoring and characterization of the number of nuclei in the process, is studied. It is shown and demonstrated in this thesis that application of microwave heating can lead to an considerable improvement in the efficiency of the direct nucleation control.

Secondly, alternative seeding strategy is investigated to eliminate the difficult to control primary nucleation. By maintaining an optimum number of particles in the

batch or continuous processes, along with controlled process conditions, a growth dominated crystallization process is targeted. In the context of continuous crystallization processes, a continuous supply of seed crystals is important to ensure the steady state operation with a fixed crystal density. Secondary nucleation which is dominant in continuous processes such as the mixed suspension mixed product removal (MSMPR) crystallizer, may not ensure a sufficient number and quality of nuclei in the process. In addition to controlling nucleation, the growth of crystals also needs to be controlled, which is not possible in MSMPRs, as the intrinsic broad residence time distribution results in a broad crystal size distribution. Therefore, alternative crystallizer designs are required which ensure a narrow residence time distribution. Tubular crystallizers offer better control over the mixing to realize plug flow like characteristics only under turbulent flow conditions, which are difficult to achieve for crystallization systems. The desired turbulent conditions for the plug flow can can be achieved by fluid oscillations, in helical coils or at very high flow rates through the tubes. In this study Continuous Oscillatory Flow Baffled Crystallizers(COBC) has been studied and it is shown that the desired plug flow behaviour can be achieved by optimization of the oscillation parameters in the flow crystallizer

However, at the inlet of the continuous plug flow crystallizer primary nucleation needs to be avoided, as due to the large surface area, nucleation on the wall and scaling will lead to operation problems. As secondary nucleation cannot be relied upon to provide sufficient nuclei due to the plug flow characteristics, seeding is needed to ensure a steady number of crystals in the process for guaranteeing a consistent product quality. To achieve the continuous seeding of the COBC, internal seed generation systems which provide seeds with a constant particle size and controllable concentration, through primary nucleation, are examined.

Application of external energy fields provide as an alternative driving force for controlling the nucleation rates. In the literature, use of ultrasounds and laser to induce nucleation at low supersaturations has been shown to produce particles with narrow size and shape distribution and to result in selective nucleation of the desired polymorph [3, 4]. In this study, the effect of ultrasounds and laser pulses on nucleation has been quantified. Application of such a internal seeding strategy using ultrasound induced nucleation in the COBC is studied. However the application appeared to be difficult to achieve, due to the large surface volume ratio of this type of crystallizers and the inefficiency of US induced nucleation under flow conditions in the flow cell.

Common to all nucleation control strategies is the requirement to estimate the relevant process variables and characterize the crystal properties. A variety of process analytical tools (PAT) have been developed, to enable nucleation monitoring and to determine the crystal shape and size distribution for example, the FBRM and image analysis based tools. In-situ imaging tools are being preferred as it allows quantitative characterization of the size and shape of the crystals, unlike the FBRM which measures the chord length distribution. In-situ characterization does not interfere with the process and avoids product sampling, which may introduce a bias in the measured properties [5]. Rapid analysis and estimation of the process through in-situ monitoring tools is a development area which has the potential to enable real-time

control. Thus, in this research, we investigated use of pattern matching and segregation based image analysis algorithms to enable accurate detection of the crystals from images taken in-situ in the COBC. A large set of images have been processed to ascertain the robustness of the analysis for estimating the crystal shape and size distribution.

In the subsequent sections of this introductory chapter, a brief overview of the fundamentals of the crystallization process is described to aid readers new to the field of crystallization. Subsequently, an overview of the current research and developments in nucleation control and monitoring approaches is provided with highlights of the key challenges still to be addressed. Finally, the objective of the thesis to address control of nucleation during batch and continuous processes by aiding the development of novel approaches is elaborated, and an overview of the chapters is presented.

1.2. Crystallization Fundamentals

The first step in crystallization, the creation of a new phase is referred to as nucleation. Nucleation occurs in a supersaturated solution when solute molecules assemble and align into clusters, and transform themselves into a stable ordered structure (critical nuclei) once they reach the critical size through growth. The growth process occurs as solute molecules attach to the nuclei and continues to aid the development of the critical nuclei into small crystals which already possess most of the properties of the larger crystals. The small crystals grow out to the desired product specifications under controlled conditions to achieve a high yield. The growth rates have to be controlled as high growth rates lead to low quality crystals with surface defect, irregular shapes and impurity inclusion.

1.2.1. The Driving Force

For nucleation to happen a driving force is needed. Two phases are in equilibrium if their chemical potential, temperature and pressure are equal. The driving force for nucleation is the difference in the chemical potential between the solution and the crystalline phase. In case of cooling crystallization, a change in temperature changes the saturation level which creates a metastable state in which the stability of the system is maintained only for a finite time, after which the system reaches equilibrium (a state of minimum energy) via nucleation and subsequent growth of the created nuclei. Usually, the chemical potential is expressed as the difference between the initial and the final concentration of the solute in the solution.

$$\Delta\mu = RT \ln(C/C\_eq) = RT \ln(S) \tag{1.1}$$

In the equation 1, $\Delta\mu$ is the chemical potential difference, R is the universal gas constant, T is the equilibrium temperature, C and C_eq are the solute concentration of the initial state and the equilibrium state respectively. The ratio of C over C_eq is termed as the supersaturation ratio S. This simplified form of equation 1.1 is obtained using the definition that the chemical potential of the crystalline phase is the same as that of solute at the equilibrium conditions and the assumption that the activity

coefficient relating the chemical potential of the solute to concentration are assumed to be independent of the concentration.

Various methods of supersaturation generation are used for crystallization process operation, such as, cooling, evaporation, anti-solvent addition etc. The design of the crystallization process is based on the choice of supersaturation generation, which is based on factors, such as the sensitivity of the solute or the solute solubility to temperature.

1.2.2. Nucleation

The classical nucleation theory is widely relied upon to explain the primary nucleation phenomenon. The number of stable nuclei formed per unit volume and per unit time is termed as the nucleation rate. The nucleation rate is generally expressed in the form of Arrhenius reaction rate equation; an exponential equation with a proportionality factor and an activation energy term, also referred to as the work of nucleation or nucleation barrier. In the classical theory, it is assumed that the change in free energy associated with nucleation of a cluster of a finite size is the sum of surface excess free energy and the volume excess free energy [6]. This change is free energy is maximum when the cluster reaches a critical size, leading to nucleation of the new phase. Assuming spherical nuclei, under classical nucleation theory the change in free energy has been expressed in terms of supersaturation as shown in equation 1.2

$$J = A \exp(-16\pi\gamma^3 v^2 / 3k^3 T^3 (lnS)^2) \tag{1.2}$$

Where, J represents the nucleation rate as a function of the supersaturation (S), interfacial tension γ, molecular volume v, the Boltzmann's constant (k), the Temperature (T) and the pre-exponential factor A.

The combination of the pre-exponential factor and the exponential term in equation 1.2 is often interpreted as the number of possible nucleation sites and nucleation barrier required to be crossed for nucleation to occur at these sites. This highlights the probabilistic nature of nucleation, making nucleation a stochastic process. The probability of nucleation depends on the operating conditions such as the temperature, supersaturation, volume etc. As seen from nucleation rate derived based on the classical nucleation theory, the change in supersaturation changes the nucleation rate exponentially, therefore in order to control nucleation a tight control over supersaturation is recommended.

Although the classical nucleation theory predicts the rate of homogeneous nucleation, in reality, presence of foreign particles or surfaces lowers the nucleation energy barrier resulting in heterogeneous nucleation at lower supersaturation. Secondary nucleation occurs in the vicinity of crystals. Several mechanisms are described for secondary nucleation where single nuclei can disintegrate into smaller fragments which can grow into crystals. Breakage and disintegration, especially of larger crystals are considered as important mechanisms [7].

Measurement of nucleation rate is not straightforward as the formation of nuclei which are very small (a few nanometers) is not easily observable and the strong

1

non-linear dependence on supersaturation makes control of nucleation rates challenging. Additionally, mostly heterogeneous nucleation occurs as the presence of foreign particles cannot be avoided. Also distinguishing between primary and secondary nucleation during a crystallization process is very difficult. Furthermore, tools used to monitor nucleation are unable to access the nucleation length scales and rely on nuclei to grow to a certain size before being detected. Metastable zone width (MSZW) and induction time are two commonly used measures to characterize the crystallization kinetics. As nucleation seldom occurs instantaneously after generation of supersaturation (depending upon the nucleation rate), the time required to observe nucleation in a supersaturated solution is defined as the induction time. Similarly, MSZW is the supersaturation required for spontaneous nucleation to occur in a crystal free solution. By monitoring the nucleation in a clear solution in which the supersaturation is increased slowly the meta stable zone width (MSZW) of the system can be determined. The MSZW gives an indication of the operation window for the crystallization process [8]. Thus, the MSZW and induction time measurements are the tools to characterize nucleation kinetics of a crystallization process.

The recent outlook towards classical nucleation theory being the most acceptable mechanism for nucleation has been shifting. Studies have shown experimental observations which contradicts the classical nucleation theory, especially in the crystallization of proteins and polymers [9, 10]. A new two-step nucleation theory has been proposed to explain the contradictions observed during nucleation. In the first step clustering of molecules (density fluctuation) occurs followed by a second step in which the molecules are ordered into a crystal lattice [11]. Under such a multi-step mechanism the nucleation rate becomes dependent on the rate limiting step. Another theory for primary nucleation has been proposed recently, the single nucleation mechanism according to which only one or a few nuclei are formed by a primary nucleation mechanism, while the bulk of the crystals in the system are formed by secondary nucleation of these nuclei after growth. The various mechanisms which have been proposed still need to be developed and a gap exists in understanding nucleation fundamentally.

1.2.3. Crystal Growth, Attrition & Agglomeration

The nucleated crystals grow by consuming the supersaturation in the solution. Crystal growth is understood as the deposition of solute molecules to the lattice of the nuclei. Several mechanisms have been proposed to explain the growth of the crystals. Usually the different facets of the crystals experience different growth rates which dictate the final shape of the crystals. The final shape of the crystal is such that the total surface energy is minimized. The attachment of the solute molecules onto the crystal surface can be described as a two-stage process, where the solute molecule first diffuses through the diffusion layer and then attaches to the crystal lattice according to known growth mechanisms [12–14]. Contrary explanations have also envisioned the growth process to be analogous to adsorption which is a one step process just driven by the concentration difference [12].

The control over the growth rate is important as high growth rates often result in rough crystals with surface imperfections, irregular shapes or impurity inclusions.

Also, during the crystallization operation the crystals collide with other crystals, the crystallizer wall and the crystal impeller. The collisions can lead to attrition and dislocation of the crystals which result in additional particles in the system and a loss of shape and size control. The new particles can act as nuclei which compete for the supersaturation to grow into larger crystals. Similarly, under high shear from flow around crystals, dislocation occurs at the crystal surfaces leading to formation of additional particles in the system. On the contrary agglomeration cements many crystals into an aggregate. Agglomeration is undesired as it results in a loss of material properties such as solubility, compactibility, flowability etc. Supersaturation may have role in the agglomeration process but the usual practice to avoid agglomeration is to use additives which prevent crystals from adhering to each other. Thus the control of product shape and size control is complex.

1.2.4. Crystallizer Operation: Batch vs Continuous

The batch process continues to be the favoured mode of operation for the crystallization process as it offers the operational flexibility in terms of manipulating the process parameters such as the temperature, supersaturation, mixing etc. The flexibility to manipulate the operation trajectory also allows process control strategies to be easily implemented. However, most often the batch process suffers from variability in the end product quality, due to variability in nucleation which is difficult to control. Seeding is most commonly used to supress and avoid nucleation, but the challenge to guarantee consistent seed quality and the reproducibility of the seeding process also results in end products which variable quality.

Continuous operation has been gaining momentum as steady state operation mostly eliminates variability in the product quality, which can offer easier and more predictable scale up. In addition, a continuous process has the potential to be economical favourable as the operation volume can be reduced, resulting in reduced inventory and equipment footprint. Gains are also achieved in terms of safety as less material is handled. Given the existing operational knowledge of stirred tank reactors, the mixed suspension and mixed product removal (MSMPR) design is widely implemented for continuous crystallization. However, a number of challenges still need to be addressed. The inherently broad residence time distribution of such a design, results in poor crystal quality control which is difficult to manipulate due to inflexibility in the operation. Additional processing steps are required to meet the desired quality which adds cost to the process. Further, implementation of process monitoring becomes indispensable as steady state needs to be ensured and process disturbances (if any) needs to be monitored. New designs based on tubular flow crystallizers are being developed which eliminate the problem with broad residence time distribution by ensuring plug flow like conditions. The narrow residence time distribution as well as better control over the temperature and supersaturation distribution is promising for achieving a well-controlled process. Oscillatory flow baffled crystallizer is one such design which has been studied in this thesis.

1.3. Nucleation Control: Challenges and Trends

The control over nucleation is important to avoid excessive and uncontrolled outburst of nuclei which results in poor quality of the crystals due to impurity inclusion, nucleation of wrong polymorph, growth artefacts and due to the resulting broad shape and size distribution. Stochastic nature of nucleation and the strong non-linear dependence on supersaturation makes nucleation control difficult. Accurate measurement of nucleation is difficult and it is mostly indirectly deduced based on measuring the number of crystals which can be detected (assuming that all the nuclei that are formed grow out to larger crystals). Estimation of nucleation rate using classical nucleation model predicts primary homogenous nucleation rates which differs significantly from the observation as mostly heterogeneous nucleation takes place due to the unavoidable presence of foreign particle or surfaces. Thus, the prediction and control of nucleation is challenging.

In the literature, studies on nucleation control are focussed on development of approaches which aim to create conditions that allow better prediction and manipulation of the nucleation rate, such as switching from batch to continuous operation where primary nucleation is suppressed and secondary nucleation becomes the dominant and better controllable crystallization phenomenon or to develop robust implementation of feedback or feedforward control loops for nucleation kinetics control.

Prediction and understanding of the nucleation rate is being targeted through molecular simulations for verifying proposed nucleation mechanisms, high-throughput micro devices for characterizing nucleation rates [15] and through application of tools to access the nucleation length scale like x-ray spectroscopy, neutron scattering and solution chemistry tracking using Raman spectroscopy. Through use of additives, patterned surfaces and solvent selection control over molecular assembly process leading to nucleation is being targeted [16–19]. Use of external energy fields like ultrasounds and lasers have been shown to be alternatives to manipulate and control the nucleation rate at low supersaturation conditions [20]. To account for the nucleation stochasticity a high number of micro droplets or cavities in micro or milli channels, where good supersaturation control is achieved, are being used to accurately determine nucleation rates. The results in micro and nano-droplets have shown deviations from the classical nucleation theory based dependence of the nucleation rate on supersaturation [21–23].

Use of external fields as alternative tools to manipulate the nucleation rate has attracted special attention. The application of external fields has shown to enhance nucleation kinetics at low bulk supersaturations where no spontaneous nucleation is observed, unless the external energy is applied. Use of ultrasounds or laser are examples of application of external fields which offer an alternative lever to manipulate nucleation rate and to gain spatial and temporal control over nucleation by inducing nucleation in the volume exposed to the energy field with reduced induction time. Application of laser pulses in slightly supersaturated solutions have been reported to reduce drastically the induction time for nucleation and influence the crystal structure of the nuclei [24]. Similarly use of ultrasounds [3] and electric field has also been probed to gain control over nucleation [25]. One important problem in the application of these technologies is that the knowledge on the mechanisms through

which the nucleation is influenced, is still lacking. The large-scale implementation and demonstration of external field assisted crystallization processes need a lot of attention.

In MSMPRs, which are widely used for continuous processing, the broad residence time distribution is an intrinsic property resulting in poor control over the crystal size distribution. Also, in continuous operation, only limited manipulation opportunities are available to respond on deviations from the steady value. Novel tubular crystallizers have the opportunity to overcome poor control over the width of the crystal size distribution (CSD) by providing a narrow residence time distribution and a tight spatial control over the temperature and the supersaturation. Since the control over temperature, supersaturation and dispersion is governed by the prevalent fluid dynamics, control over mixing is one of the main design aspects for tubular crystallizers. Use of static mixers [26] or baffled orifices has been investigated to control the mixing in tubular devices. Helically coiled tube crystallizers have been shown to be an alternative for baffled tubes to improving the radial mixing within the tubes and to decrease the fluid dispersion. Control over supersaturation and residence time distribution can also be achieved by confining the crystallization process in slugs flowing in an immiscible bulk phase, which results in narrow crystal size distribution and avoids fouling of the tube surfaces during continuous operation [27]. Seeding is advised in flow rectors to ensure the steady crystal density and avoid primary nucleation which can lead to excessive nuclei in the process leading to plugging and fouling.

The continuous oscillatory flow baffled crystallizer (COBC) is designed to achieve plug flow conditions by oscillating the bulk flow around regularly spaced baffles which ensures good radial and lateral mixing [28]. The mixing is dependent on the oscillatory motion of the fluid and allows long residence times to be achieved in relatively short tube lengths in the COBC system. Additionally, the modular design of the COBC with tubes having separate jackets and multiple inputs/outputs offers flexibility for process manipulation through manipulation of the supersaturation profile by varying independently the temperature of the jacketed tubes or addition of solvent/anti-solvent at various input points [29]. However, to ensure continuous steady operation continuous supply of seed crystals is required to avoid the high supersaturations needed for primary nucleation. Especially, the high surface area in a COBC or other tubular reactor presents a risk of fouling and plugging. 'Internal seeding' in the COBC is preferred to avoid the complexities and variabilities arising from transferring seeds from external units. Use of impinging jets, controlled mixing of flow streams for supersaturation generation, use of contact secondary nucleation [30] and use of ultrasound are some of the techniques demonstrated to have potential for being developed into an efficient tools for seed generation through controlled nucleation within tubular crystallization systems [27].

Process models based on estimations of the process kinetics can be used to determine an optimum operation trajectory. For nucleation control strategies, like seeding, the optimum design is identified by models which take into account variables such as seed mass, particle size distribution or the ratio of nucleated mass to the seeded mass [31–34]. In literature, the models for a seeded process have also been implemented in a control framework to account for process deviations arising from

1

the variability in the seed quality [35]. Similarly fines removal through temperature cycling strategy, and use of external dissolution loops in continuous MSMPR crystallizers is also designed based on process modelling to gain control over the crystals shape and size distribution [35–37]. However, limited knowledge on crystallization kinetics, especially on nucleation, makes the nucleation rate unpredictable. Limited knowledge on the relation between nucleation and the process conditions, such as the supersaturation and the mixing conditions, results in poor accuracy of the models. Therefore, model based process optimization is not always feasible as the required a priori knowledge of the crystallization kinetics is not readily available.

Model-free control approaches offer an opportunity to overcome the drawback of the model based approaches. The model free approach allows process manipulation based on direct in-situ characterization of the process variables and the crystal properties such as crystal shape, size or structure. Direct Nucleation Control (DNC) is one example of the model free nucleation control approach. DNC works on the direct feed-back of the estimate of the number of crystals in the system from tools like FBRM, turbidity sensor or imaging based sensor. By controlling the number of crystals in the system the crystal properties such as the size and shape distribution can be directly manipulated. The nucleation control in DNC is realized through temperature cycling or addition of solvent/anti-solvent to alter between supersaturated and undersaturated process conditions [38]. During nucleation, when the number of crystals increases beyond the set point value, the controller creates undersaturation to dissolve the excess nuclei. When the number of crystals drops below the set point, the controller switches to cooling to trigger nucleation. The cycling between dissolution and nucleation continues till the number of crystals stabilizes at the set point value. The optimal number of particles is usually estimated from trial experiments, by maintaining either a low or high crystal counts to obtain, for example, large or small crystals respectively. The DNC technique has been shown to control particle size distribution, polymorphism, solvent inclusion and improve the surface property of the crystals [39].

The shortcoming of the DNC approach is the large amount of control cycles which are required to reach the control objective, making the process inefficient due to the significantly increased batch time. The efficiency of the DNC approach can be improved in a combined feedforward-feedback control framework where an iterative learning process for the controller based on information from previous batches improves the response. Combination of supersaturation control and DNC is also a possibility, where limiting the supersaturation accessible to DNC avoids overshoot in the nucleation and the dissolution targets. Thus, further development is required to achieve an efficient implementation of model free control.

Process monitoring plays an important role in implementing control over the crystallization process by facilitating accurate process estimation. Advancement of process monitoring capabilities and improvement of the accuracy of process estimation is a rapidly developing area [40]. The developments and improvements in the process analytical tools (PAT) tools have allowed the implementation of robust model predictive control objectives by eliminating process uncertainties and reducing the plant-model mismatch [39] in both open and closed loop control framework [41].

Nevertheless, development is needed of rapid measurement of the process for real time control, which allows immediate action against process deviations and hence avoids the wastage of the off-spec products. In-situ techniques have been identified as development targets to avoid the need sampling procedures which may disturb the process. Hence, in-situ characterization tools like the FBRM and PVM have become preferred tools. But these techniques only provide qualitative information, for example, chord length distributions in the case of FBRM and hence imagining based tools which characterize crystal shape and size distributions (2D or 3D) are being developed. In-situ imaging probes, based on stroboscopic endoscope, include a number of high resolution systems for example, Particle Imaging System (PARIS) of Dupont, PVM from Mettler Toledo, Process Image Analyzer (PIA) of MessTechnik Schwartz GmbH, In-Situ Particle Viewer (ISPV) of Perdix Analytical Systems and the more recently introduced imaging system from SOPAT GmbH [42]. In order to facilitate the use of these new tools, correct implementation and accurate image analysis procedure needs to be developed and limitations in process estimation needs to be identified.

1.3.1. Challenges Addressed in the Thesis

In line with the developments and progress in the field of nucleation control, presented in the previous section, a select few challenges have been addressed.

- Efficiency enhancement of DNC:

  Since model free approaches are not based on a priori knowledge of the process kinetics, manipulation of the process conditions, especially the supersaturation in the DNC, leads to large overshoots in the number of particles during the nucleation and dissolution phases. These overshoots will extend both the cycle time and the number of control cycles, which adds to the valuable batch time. The efficiency can be enhanced through enabling rapid response against nucleation through quicker heating and faster switch to cooling to avoid excessive dissolution. Developments of process is thus required to identify an optimal strategy for improving the efficiency of the model free approach.

- In-situ imaging for nucleation and crystal phase characterization:

  In-situ imagining has the potential to develop as a tool for rapid and accurate estimation of the crystal properties as soon as possible after their creation through nucleation. A number of image analysis methods and tools have been demonstrated and are now being made available as PAT probes for in-situ monitoring of nucleation. In order to facilitate the use of these new tools, correct implementation and accuracy of the imaging based PAT tools needs to be validated. In the current tools, there are still limitations in correctly identifying the crystals due to the high particle concentrations, overlapping, orientation and small size of the crystals. The latter remains the most important limitation in the nucleation research where the detection of very small crystals needs to be

addressed. Robustness of image analysis procedures and comparison of the estimated crystal characteristics needs to be validated against the true shape and size of the crystals.

- Continuous crystallization - flow crystallizers:

  Even though the tubular reactor technology has existed for long, the application in the field of crystallization has been more recent. Identification of optimal operating parameters, especially achieving plug flow mixing is required to provide crystals a narrow residence time distribution. In continuous operation, under plug flow conditions, consistent product properties can be ensured by implementing seeding strategies and optimum supersaturation profile to avoid unwanted nucleation which leads to poor control over product characteristics. In the COBC, in-depth analysis of the dispersion of both the bulk (solvent) and the dispersed (crystals) phase is targeted, by studying the residence time distribution (of both phases) as a function of the frequency and amplitude of oscillating slurry interacting with the regularly spaced baffles.

- Additional drivers for nucleation control:

  Application of external energy fields such as the laser light, electric field and acoustic waves (ultrasound) have been shown to offer alternative ways for controlling nucleation. The mechanisms through which the energy fields influence nucleation is still debated and needs further probing. Modelling the process kinetics, identification of the optimum operation space and proper equipment design to ensure controlled application of the energy fields for manipulating nucleation, are some of the tasks required to further the implementation of the technology. Use of US for continuous internal seed generation for the COBC is investigated. Mechanisms behind Non-photochemical Laser Induced Nucleation (NPLIN) is probed and the characterization of resulting nucleation kinetics is aimed.

1.4. Objective & Approaches

The principal objective for the research presented in this thesis is to intensify batch and continuous crystallization processes with enhanced nucleation control, proper plug flow conditions in continuous tubular crystallizers and development of advanced image analysis based PAT tool for process monitoring.

Nucleation control is addressed through manipulation of the number of crystals in the crystallizer; by either controlling the rate of nuclei formation or through dissolution of the excess nuclei to limit the nucleation overshoot or through continuous seeding in case of flow crystallizer to suppress nucleation in the tubes.

The efficiency of the DNC strategy applied to batch processes, in which the number of crystals in the crystallizer is controlled by the manipulation of nucleation and dissolution cycles, will be intensified through the use of microwave heating; rapid re-

1

sponse against excess nucleation and shorter temperature cycles for a more efficient batch is targeted.

On the other hand the induction of high nucleation rates at low supersaturation by the application of laser or ultrasound energy can facilitate the control of the formation of the nuclei under more modest process conditions. Combination of the ultrasound assisted internal seed generation in the COBC is studied as a strategy to ensure a constant number of seed crystals to avoid uncontrolled nucleation at the inlet. Similarly, the effect of laser pulses on the nucleation rate is studied as a driver to develop alternative technologies for seed generation in the crystallization process.

Plug flow conditions which minimize the dispersion of the crystals and the bulk phase in continuous tubular crystallizer will be measured and optimised using crystal suspensions in a COBC, to ensure a crystalline product with narrow mono-modal CSD. Good radial mixing is also essential to achieve the desired temperature/supersaturation distribution for better control of the crystallization process in the COBC.

Critical to the success of nucleation control strategy is the ability to monitor and characterize nucleation and the crystal properties. Development of in-situ imaging based PAT technology will be targeted through testing and validation of pattern matching and segregation approaches for characterizing the number, shape and size of the crystals during cooling crystallization in the COBC.

To summarize, the following research questions are addressed in the thesis:

- Can direct nucleation control efficiency be enhanced through restriction of nucleation and optimization of dissolution cycles using rapid microwave heating?.

- Can optimal mixing conditions in the COBC be obtained for controlled growth of crystals?

- Can in-situ imaging be applied as a robust tool for monitoring and control of nucleation through characterization of shape and size distribution of the newly formed crystals?

- Can application of laser pulses and ultrasound fields lead to a process actuator that realizes a reproducible seed generation system?

1

1.4.1. Overview of the Chapters

The work carried out in the thesis which addresses the research objectives is organized in the following chapters:

- *Microwave assisted Direct Nucleation Control (DNC): (Chapter 1)*

  Investigation into the efficiency enhancement of direct nucleation control strategy based on microwave heating for rapid dissolution of the excess or unwanted nuclei.

- *A novel design integrating a microwave applicator with crystallization for rapid temperature cycling: (Chapter 2)*

  Integration of the microwave applicator to introduce the microwave heating directly within the crystallizer, in presence of PAT tools, in a prototype design enabling efficient DNC.

- *Optimized operation of an Oscillatory Flow Baffled Crystallizer (OFBC) for continuous crystallization: (Chapter 3)*

  Identifying the optimal mixing regime in the COBC, through characterization of the residence time distribution of the bulk phase and the crystals in a seeded process.

- *Implementation of in-situ imaging technology for monitoring the start-up and the steady state operation in COBC: (Chapter 4)*

  Nucleation detection and particle size distribution characterization through in-situ imaging for monitoring the changes in the crystalline phase in the COBC.

- *Controlled nucleation at low supersaturations using ultrasound (US) for internal seeding of an OFBC: (Chapter 5)*

  Investigations into US as a reliable tool for controlled nucleation at low supersaturations for continuous seed generation.

- *Multi-parameter study into Laser induced nucleation (Chapter 6)*

  Role of laser as an alternative driver for nucleation. Quantification of nucleation kinetics and an insight into role of laser for internal seeding of crystallization processes through controlled nucleation

References

[1] S. Rohani, *Applications of the crystallization process in the pharmaceutical industry,* Frontiers of Chemical Engineering in China **4**, 2 (2010).

[2] H.-H. Tung, *Industrial perspectives of pharmaceutical crystallization,* Organic Process Research & Development **17**, 445 (2013).

[3] L. d. I. S. Castillo-Peinado and M. D. Luque de Castro, *The role of ultrasound in pharmaceutical production: sonocrystallization,* Journal of Pharmacy and Pharmacology **68**, 1249 (2016).

[4] J. Zaccaro, J. Matic, A. S. Myerson, and B. A. Garetz, *Nonphotochemical, laser-induced nucleation of supersaturated aqueous glycine produces unexpected gamma-polymorph,* Crystal Growth & Design **1**, 5 (2001), 519ch Times Cited:112 Cited References Count:22.

[5] J. Ulrich and P. Frohberg, *Problems, potentials and future of industrial crystallization,* Frontiers of Chemical Science and Engineering **7**, 1 (2013).

[6] J. W. Mullin, *5 - nucleation,* in *Crystallization (Fourth Edition)* (Butterworth-Heinemann, Oxford, 2001) pp. 181–215.

[7] T. W. Evans, G. Margolis, and A. F. Sarofim, *Mechanisms of secondary nucleation in agitated crystallizers,* AIChE Journal **20**, 950 (1974).

[8] S. A. Kulkarni, S. S. Kadam, H. Meekes, A. I. Stankiewicz, and J. H. ter Horst, *Crystal nucleation kinetics from induction times and metastable zone widths,* Crystal Growth & Design **13**, 2435 (2013).

[9] A. Sauter, F. Roosen-Runge, F. Zhang, G. Lotze, A. Feoktystov, R. M. J. Jacobs, and F. Schreiber, *On the question of two-step nucleation in protein crystallization,* Faraday Discuss. **179**, 41 (2015).

[10] J. R. Savage and A. D. Dinsmore, *Experimental evidence for two-step nucleation in colloidal crystallization,* Physical Review Letters **102**, 198302 (2009), pRL.

[11] P. G. Vekilov, *The two-step mechanism of nucleation of crystals in solution,* Nanoscale **2**, 2346 (2010).

[12] J. W. Mullin, *6 - crystal growth,* in *Crystallization (Fourth Edition)* (Butterworth-Heinemann, Oxford, 2001) pp. 216–288.

[13] W. B. Hillig and D. Turnbull, *Theory of crystal growth in undercooled pure liquids,* The Journal of Chemical Physics **24**, 914 (1956), https://doi.org/10.1063/1.1742646 .

[14] J. W. Cahn, *Theory of crystal growth and interface motion in crystalline materials,* Acta Metallurgica **8**, 554 (1960).

1

[15] K. Chen, L. Goh, G. He, P. Kenis, C. Zukoski, and R. Braatz, *Identification of nucleation rates in droplet-based microfluidic systems,* Chemical Engineering Science **77**, 235 (2012), 18th International Symposium on Industrial Crystallization.

[16] M. A. Lovette, M. Muratore, and M. F. Doherty, *Crystal shape modification through cycles of dissolution and growth: Attainable regions and experimental validation,* AIChE Journal **58**, 1465 (2012).

[17] X.-H. Guo, S.-H. Yu, and G.-B. Cai, *Crystallization in a mixture of solvents by using a crystal modifier: Morphology control in the synthesis of highly monodisperse caco3 microspheres,* Angewandte Chemie **118**, 4081 (2006).

[18] R. J. Davey, N. Blagden, S. Righini, H. Alison, M. J. Quayle, and S. Fuller, *Crystal polymorphism as a probe for molecular self-assembly during nucleation from solutions: the case of 2,6-dihydroxybenzoic acid,* Crystal Growth & Design **1**, 59 (2001).

[19] G. R. Desiraju, *Crystal engineering: From molecule to crystal,* Journal of the American Chemical Society **135**, 9952 (2013).

[20] A. Caridi, S. A. Kulkarni, G. Di Profio, E. Curcio, and J. H. ter Horst, *Template-induced nucleation of isonicotinamide polymorphs,* Crystal Growth & Design **14**, 1135 (2014).

[21] e. Selimović, Y. Jia, and S. Fraden, *Measuring the nucleation rate of lysozyme using microfluidics,* Crystal Growth & Design **9**, 1806 (2009).

[22] D. Knezic, J. Zaccaro, and A. S. Myerson, *Nucleation induction time in levitated droplets,* The Journal of Physical Chemistry B **108**, 10672 (2004).

[23] I. S. Lee, K. T. Kim, A. Y. Lee, and A. S. Myerson, *Concomitant crystallization of glycine on patterned substrates: The effect of ph on the polymorphic outcome,* Crystal Growth & Design **8**, 108 (2008).

[24] B. A. Garetz, J. E. Aber, N. L. Goddard, R. G. Young, and A. S. Myerson, *Nonphotochemical, polarization-dependent, laser-induced nucleation in supersaturated aqueous urea solutions,* Physical Review Letters **77**, 3475 (1996), vm032 Times Cited:108 Cited References Count:14.

[25] J. E. Aber, S. Arnold, B. A. Garetz, and A. S. Myerson, *Strong dc electric field applied to supersaturated aqueous glycine solution induces nucleation of the gamma polymorph,* Phys Rev Lett **94**, 145503 (2005), aber, Janice E Arnold, Stephen Garetz, Bruce A Myerson, Allan S eng Research Support, U.S. Gov't, Non-P.H.S. 2005/05/21 09:00 Phys Rev Lett. 2005 Apr 15;94(14):145503. Epub 2005 Apr 14.

[26] A. J. Alvarez and A. S. Myerson, *Continuous plug flow crystallization of pharmaceutical compounds,* Crystal Growth & Design **10**, 2219 (2010).

1

[27] M. Jiang, C. D. Papageorgiou, J. Waetzig, A. Hardy, M. Langston, and R. D. Braatz, *Indirect ultrasonication in continuous slug-flow crystallization,* Crystal Growth & Design **15**, 2486 (2015).

[28] S. Lawton, G. Steele, P. Shering, L. Zhao, I. Laird, and X.-W. Ni, *Continuous crystallization of pharmaceuticals using a continuous oscillatory baffled crystallizer,* Organic Process Research & Development **13**, 1357 (2009).

[29] A. Majumder and Z. K. Nagy, *Fines removal in a continuous plug flow crystallizer by optimal spatial temperature profiles with controlled dissolution,* AIChE Journal **59**, 4582 (2013).

[30] S. Y. Wong, Y. Cui, and A. S. Myerson, *Contact secondary nucleation as a means of creating seeds for continuous tubular crystallizers,* Crystal Growth & Design **13**, 2514 (2013).

[31] S. H. Chung, D. L. Ma, and R. D. Braatz, *Optimal seeding in batch crystallization,* The Canadian Journal of Chemical Engineering **77**, 590 (1999).

[32] J. D. Ward, D. A. Mellichamp, and M. F. Doherty, *Choosing an operating policy for seeded batch crystallization,* AIChE Journal **52**, 2046 (2006).

[33] A. N. Kalbasenka, L. C. P. Spierings, A. E. M. Huesman, and H. J. M. Kramer, *Application of seeding as a process actuator in a model predictive control framework for fed-batch crystallization of ammonium sulphate,* Particle & Particle Systems Characterization **24**, 40 (2007).

[34] R. J. P. Eder, E. K. Schmitt, J. Grill, S. Radl, H. Gruber-Woelfler, and J. G. Khinast, *Seed loading effects on the mean crystal size of acetylsalicylic acid in a continuous-flow crystallization device,* Crystal Research and Technology **46**, 227 (2011).

[35] S. Qamar, S. Mukhtar, and A. Seidel-Morgenstern, *Efficient solution of a batch crystallization model with fines dissolution,* Journal of Crystal Growth **312**, 2936 (2010).

[36] M. Jiang, X. Zhu, M. C. Molaro, M. L. Rasche, H. Zhang, K. Chadwick, D. M. Raimondo, K.-K. K. Kim, L. Zhou, Z. Zhu, M. H. Wong, D. O'Grady, D. Hebrault, J. Tedesco, and R. D. Braatz, *Modification of crystal shape through deep temperature cycling,* Industrial & Engineering Chemistry Research **53**, 5325 (2014).

[37] N. Bajcinca, V. de Oliveira, C. Borchert, J. Raisch, and K. Sundmacher, *Optimal control solutions for crystal shape manipulation,* Computer Aided Chemical Engineering **28**, 751 (2010).

[38] M. R. Abu Bakar, Z. K. Nagy, A. N. Saleemi, and C. D. Rielly, *The impact of direct nucleation control on crystal size distribution in pharmaceutical crystallization processes,* Crystal Growth & Design **9**, 1378 (2009).

[39] Z. K. Nagy and R. D. Braatz, *Advances and new directions in crystallization control,* Annual Review of Chemical and Biomolecular Engineering **3**, 55 (2012).

[40] R. J. Davey, S. L. M. Schroeder, and J. H. ter Horst, *Nucleation of organic crystals—a molecular perspective,* Angewandte Chemie International Edition **52**, 2166 (2013).

[41] Z. K. Nagy and R. D. Braatz, *Open-loop and closed-loop robust optimal control of batch processes using distributional and worst-case analysis,* Journal of Process Control **14**, 411 (2004).

[42] R. F. Li, R. Penchev, V. Ramachandran, K. J. Roberts, X. Z. Wang, R. J. Tweedie, A. Prior, J. W. Gerritsen, and F. M. Hugen, *Particle shape characterisation via image analysis: from laboratory studies to in-process measurements using an in situ particle viewer system,* Organic Process Research & Development **12**, 837 (2008).

1

2

Microwave Assisted Direct Nucleation Control for Batch Crystallization: Crystal Size Control with Reduced Batch Time

2

Direct nucleation control (DNC) is a feedback control strategy, based on an in situ measurement of number of particles. In batch cooling crystallization processes, the DNC approach utilizes temperature cycling to control the supersaturation profile during the batch. As a result of this cycling, product crystals with a large mean size and a narrow size distribution can be achieved due to the dissolution of undesired fines. However, implementing the temperature cycles may come at the expense of significantly prolonged batch times due to conventional heat transfer limitations and practical limitations for implementing both actuation for conventional heating and cooling. In this work, microwave heating in combination with DNC is presented to eliminate limitations of conventional heating and further improve the effectiveness of DNC. The results show a very rapid response when using microwave heating, which allowed for improved effectiveness of DNC. In particular, batch times obtained with DNC could be reduced with 50% by using microwave heating compared to conventional heating, producing crystals with a narrow distribution similar to experiments with conventionally heated DNC.

2.1. Introduction

Consistent and high product quality is of utmost importance in the pharmaceutical industry. Crystallization is a key separation and product formation technology for manufacturing of most active pharmaceutical ingredients (APIs). Among the wide variety in crystal quality attributes of API crystals (e.g., shape, size, purity, polymorphic form), the crystal size distribution (CSD) needs to be controlled to obtain a product with the desired performance and to reduce the costs of downstream processes. Consequently, many control strategies have been investigated to improve the CSD [4, 7–10]. In addition, novel designs of crystallizers to improve control over the CSD are also investigated recently [11–15]. Broadly speaking, control strategies for a desired CSD can be classified as either model-based or model-free or a combination of both [16]. Model-based approaches utilize mass, energy, and population balances to predict an optimized trajectory for state variables. Most commonly used strategies include programmed cooling [17] and seeding as a process actuator to control nucleation and growth rates [3, 4]. Drawbacks of model-based approaches include requirements of having validated models for crystallization kinetics, which are often difficult to obtain, especially, for pharmaceutical systems. In addition, susceptibility to process disturbances or uncertainties in the initial conditions lead to poor process control. Direct control or model free control, offers the advantages of process control without any a priori knowledge of crystallization kinetics [18]. Model-free control methods use in situ measurements of process variables with a feedback control structure to ensure that for instance a pre-defined supersaturation trajectory is closely followed.

With the advancement of process analytical tools (PAT) for in situ measurements, it is now possible to control directly product quality attributes such as particle size distribution, crystal habit and polymorphism as a controlled variable, an approach which fits well within 'Quality-by-Design' frameworks [16, 19, 21, 22]. Direct Nucleation Control (DNC) is a model free approach utilizing in situ particle count measurements as a controlled variable for feedback control [6]. Particle counts can be measured by the use of focused beam reflectance measurement FBRM or any other measurement technique that gives an indication of the number of particles in the system. By control of the number of particles through manipulation of the temperature profile and thus the supersaturation, nucleation and growth rates are optimized. The measured particle count is compared to a set point, which provides the input for the temperature controller of the batch cooling crystallization. Depending on whether the number of particles is above or below the set point, growth or dissolution cycles are implemented automatically. These cycles generate supersaturation for nucleation/growth or undersaturation for the dissolution of excess of nuclei, respectively. Similar temperature cycling approach has been previously demonstrated, where in situ fines dissolution cycle has been designed based on experimentally measured supersaturation [20] and more recently asymmetric linear temperature cycles has been designed based on available information on nucleation kinetics [5]. The DNC approach on the contrary results in temperature cycles directly based on observed (measured) dynamics of the crystallization process and is not limited by unpredictability due to process disturbances and variations in the estimation crystallization kinetics. DNC has been

shown to produce a desired crystal mean size, a reduction in solvent inclusion, an improved polymorphic purity and enhanced crystal surface properties [23–25], which is of major importance for industry.

However, the use of DNC comes at an expense of prolonged and varying batch times when compared to traditional approaches for control of batch crystallization. In case of cooling crystallization, practical challenges exist when equipping batch crystallization with both conventional actuation for heating and cooling. For example, fluids for heating and cooling need to be exchanged as the available surface area for heat exchange need to be shared. Furthermore, conventional heating suffers from heat transfer limitations. Consequently, the cycling times may be large, which increases batch time and, in case of the heating cycles, provides the opportunity for fines to grow (which were generated during the nucleation events), leading to an undesired product size distribution. Unmitigated fines may lead to even longer batch times as more time is needed to dissolve the grown fines or may lead to additional cycles that are required to reach the desired product size distribution. Approaches to mitigate extensive cycling have been proposed, which include an iterative learning control framework based on information from previous batches implemented with a combined feedforward-feedback control structure and a combined concentration control and DNC approach [23, 26]. Despite these important advances, inherent limitations related to conventional heating remain, which can only be eliminated by radically changing the heating mechanism.

The application of microwaves has been widely demonstrated to drastically reduce reaction times by accelerating chemical transformations through controlled flash heating [27]. Others areas of application for microwaves include the food, wood and rubber industry, waste processing and drying [28, 29]. In the field of crystallization, microwaves have been used for evaporative crystallization, melt crystallization, crystallization coupled with atomic layer deposition techniques and for nanopowder production [30–33]. The objective of the present study is to investigate the benefits of using microwave heating in combination with DNC. Microwave heating can fundamentally decouple the actuation for heating and cooling and, potentially, significantly reduce batch time. The direct heating property of microwaves provides a rapid response to nucleation events such that fines can be dissolved rapidly. Particle count measured by FBRM is used as the controlled variable. Automation and data processing is provided via the Crystallization Process Informatics System (CryPRINS)[34], which acts as a supervisory controller to the novel microwave based control strategy. Batch cooling crystallization of paracetamol from iso-propyl alcohol (IPA) is used as model system.

2.2. Experimental Section

2.2.1. Materials

Acetaminophen (Paracetamol, BioXtra ≥99%) and technical grade iso-propyl alcohol (IPA, 99%), bought from sigma Aldrich was used in this study.

2.2.2. Characterization of crystal chord length and size distribution

An FBRM probe (model G400, Mettler Toledo) was used for in situ particle counts and chord length distributions (CLD) measurements. The iC FBRM software provided by Mettler was used to record the data from the probe. The software was further used to couple the FBRM data with the CryPRINS controller. The measurement interval was 10 seconds in all experiments. The measuring mode was set to macro, which means that there was less sensitivity to edges when particles were close to each other. Furthermore, samples for particle size distribution measurement were prepared by filtering the slurry. The filter retentate, containing the product crystals, was washed with a small amount of IPA and left overnight for drying in an oven maintained at 30 $°C$. A laser diffractometer (Mircotrac S3500) was used for dry sample measurement of the crystal size distribution.

A schematic drawing of the experimental setup is given in Figure 2.1. The cooling crystallization was carried out in a baffled and jacketed glass vessel of 1 L. A thermostatic bath (Lauda RE-310 Ecoline Staredition) was connected to the jacket of the vessel to provide for feedback temperature control. A Pt-100 resistance thermometer was placed inside the crystallizer to control the temperature. FRBM was used to count the number of crystals in the crystallizer.

A custom built cavity was used with a 2.45 GHz microwave generator, 0–1200 W continuously variable (GMP 12K, Sairem SAS). This cavity was designed in-house as a versatile tool for microwave experimentation; it is based on a standard WR-340 rectangular waveguide, but with added features for improved access. Specifically, a lid and a pattern of many holes were included in the design for enhanced access to the microwave field in the cavity [35]. A circulation loop (Figure 2.2) has been installed to pump the slurry through the microwave cavity and back into the crystallizer. In this way the micro-wave heating can be utilized to heat the content of the crystallizer. An external loop has been installed for this investigation mainly because of practical considerations, but in principle microwave heating could also be applied in-situ in compact designs of novel crystallizers [36, 37]. The performance of the method is not expected to depend heavily on the exact location of the micro-wave heating source. In all experiments with microwaves, a peristaltic pump (model 520S, Watson-Marlow) was used for circulation with a typical flow rate of 1 L/min. The crystallizer was stirred by a pitched blade impeller connected to an overhead drive (IKA RW16 basic) maintained close to 300 rpm. The maximum input power of the system is 1200 W at 2.45 GHz. However, the amount of energy absorbed depends on the dielectric properties of the liquid and the crystals exposed to the microwaves. Additionally, temperatures close to boiling due to aggressive microwave heating could induce small vapor bubbles in the system which may have secondary effects on mass transfer in the system. Our operational temperatures were well below the boiling point of IPA and we didn't expect any bubble formation.

An in-house Labview program was written to control and manipulate the crystallizer operating temperature (named as MW controller in this paper). The program was coupled with the CryPRINS software which provided the temperature set point based on the measurements from FBRM. Therefore, CryPRINS worked as the super-

2
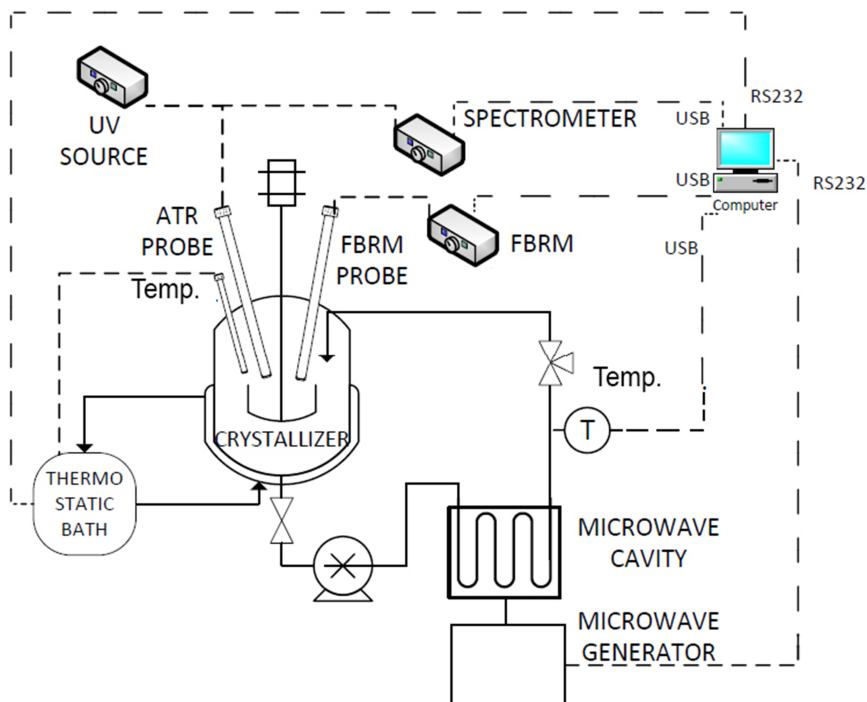
Figure 2.1: Schematic of the experimental set-up showing the crystallizer configuration along with the connected PAT instruments.

visory control layer. Detailed information about DNC using CryPRINS can be found in literature [23, 24]. The temperature set point from CryPRINS was sent to the MW controller, which regulated heating by switching the microwave generator on or off and cooling by regulating the jacket temperature via the thermostatic bath. In case of conventional experiments, the MW controller regulated the water bath to achieve heating and cooling. A schematic diagram of the control structure is presented in Figure 2.3.

2.2.3. Experimental Conditions

In addition to experiments with microwave heating, experiments with conventional heating were conducted for reference. In both cases, the experimental configuration was the same. Saturated solution at 40 $°C$, was prepared by dissolving 0.21 grams of paracetamol per gram of IPA. The solution was then heated to 50 $°C$ at those conditions to ensure complete dissolution. Subsequently, circulation was switched on and automated control was started according to a certain set point for the counts.

During all microwave-assisted experiments, the power was set at the maximum value. The heating rate was set at 4 $°C/min$ in the crystallizer with the maximum temperature set point restricted to 35 $°C$. This was done to avoid significant disso-
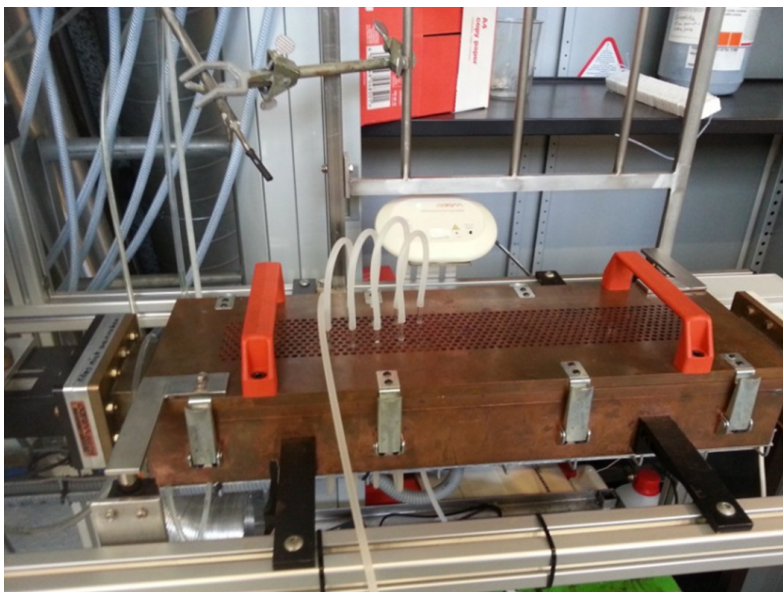
Figure 2.2: Circulation loop through the microwave cavity.
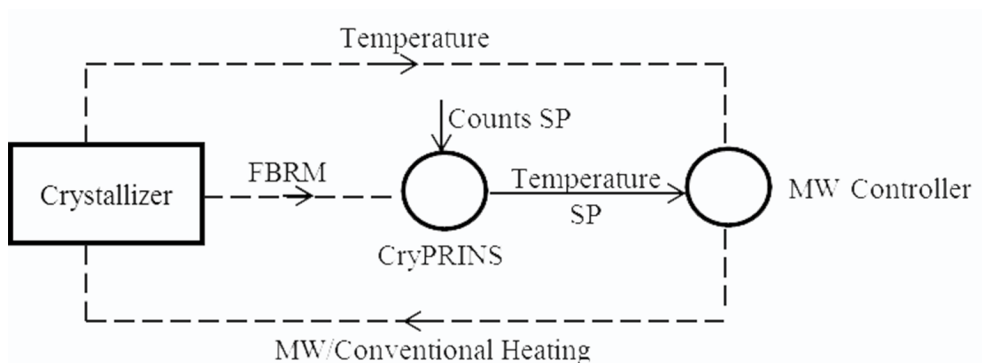
Figure 2.3: Schematic diagram showing the overall control framework.

lution of also the larger crystals due to rapid heating to high temperatures.

The conventional experiments were carried out with a heating rate of $0.2\,°C/min$, which was restricted by the used heat transfer area of the jacket, with a maximum set point of 50 $°C$. The cooling rate in all experiments was $0.2\,°C/min$ to avoid excessive secondary nucleation. Furthermore, two counts set points of 5,000 and 2,000 with an acceptable deviation of ± 1,000 were chosen to investigate the use of microwave assisted DNC under challenging conditions. The experimental conditions are summarized in Table 3.1.

Table 2.1: List of experiments and corresponding conditions. SP = Set Point

Experiment	Type Heating	Heating/Cooling Rate ($°C/min$)	Counts SP	Temp SP Upper Limit ($°C$)
Conv1	Jacket/conventional	0.2/0.2	5000	50
Conv2	Jacket/conventional	0.2/0.2	2000	50
MW1	Microwave	4/0.2	5000	35
MW2	Microwave	4/0.2	2000	35

2.3. Results and Discussions

Experiments with conventional heating were carried out with the aim to compare the performance of DNC in a conventionally heated and a microwave heated crystallizer. Two experiments with different set points for the number of counts were performed (see Table 3.1). First, a set point of 5000 counts was used and, after that, a set point of 2,000 was used with the aim to obtain bigger product crystals.

As can be seen from Figure 2.4, the system first deviates from the counts set point due to primary nucleation, which is reflected by the large peak in counts at the beginning. When starting from a clear solution the controller lowered the temperature set point to cool the crystallizer. As a result the required supersaturation is generated to trigger nucleation. As soon as nucleation occurred, the counts exceeded rapidly the set-point. The controller then switched to heating phase in order to generate undersaturation for dissolving the excess particles. Despite the switch to a dissolution cycle, the large supersaturation generated in the beginning (during the cooling phase) resulted in high nucleation rates and hence the count of particles exceeded 20000. The overshoot as a result of primary nucleation was different in each experiment, due to variable nucleation rates arising possibly from the differences in initial supersaturation and due to the stochastic nature of primary nucleation. The subsequent cycles seen in Figure 5, were due to secondary nucleation caused by the creation of supersaturation in the subsequent cooling phases. The system needed about three cycles before the counts set-point was maintained within the acceptable deviation range from the set-point. The temperature set-point also reached the lower temperature limit, which signifies the end point of the batch with a desired yield.

In case of a set point of 2000 counts, more temperature cycles were needed (see Figure 2.4). This was expected, as lowering the set-point for the counts implies a decrease in the amount of crystals that are available for growth, and hence increased secondary nucleation. Indeed more peaks attributed to secondary nucleation were observed with the set point of 2,000 counts. Consequently, the number of temperature cycles required were significantly greater before the system would converge gradually to the lower temperature limit. However, at least for the duration of the experiment, the system still cycled and did not stabilize.

A substantial improvement in control performance was achieved when microwave heating was used. Figure 2.5 shows the evolution of number of counts and the crystallizer temperature when microwave assisted heating was applied in combination with DNC for the two chosen set-points. For both the tested set points (5000 and 2000 counts), it was observed that only a few cycles were required before the system converged rapidly to the lower limit of the temperature set-point. Even though, after
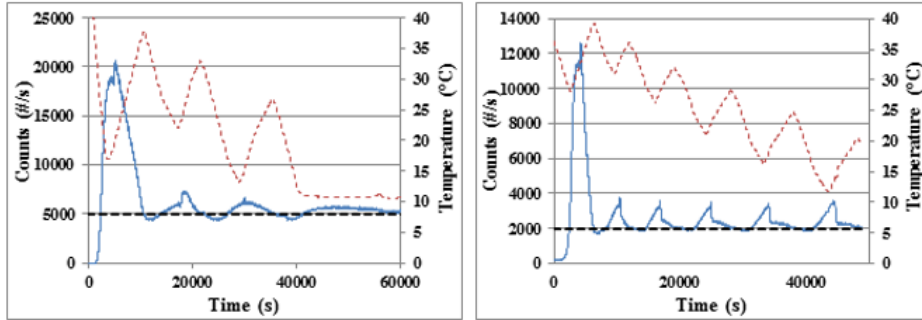
Figure 2.4: Performance of DNC in a conventional heated crystallizer with set point of 5,000 counts (left) and 2,000 counts (right). Solid line is the counts data and the dashed line is the crystallizer temperature. The stright dashed line is used as aid to show the counts set point.
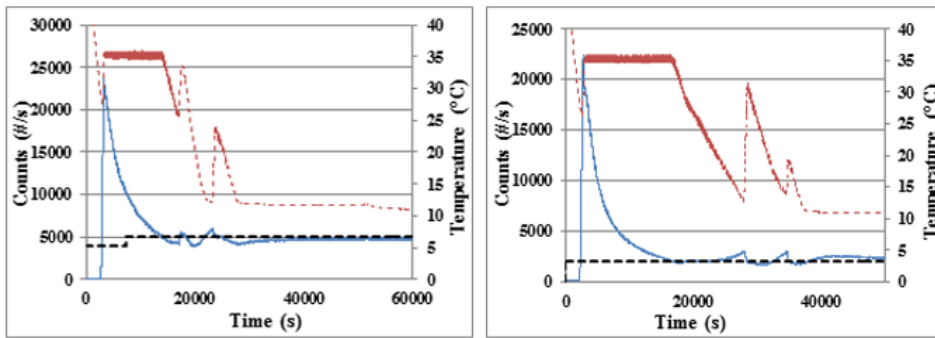
Figure 2.5: Performance of DNC with microwave assisted heating of the crystallizer with set point of counts at 5,000 (left figure) and 2,000 (right figure). Solid line is the counts data and the dashed line is the crystallizer temperature. The stright dashed line is used as aid to show the counts set point.

the initial primary nucleation event, the counts rose to a value larger then 20000, the time required to converge to the set point value was significantly shortened. Furthermore, the set point was maintained for at least about 6 to 7 additional hours as the deviation in counts was within the bounds, after which the experiment was ended.

The significant improvement in control performance was the result of the instantaneous response in heating actuation enabled by the microwaves combined with the restricted heating temperature. After primary nucleation, indicated by the first peak in the number of counts, a microwave heating cycle was able to rapidly raise the crystallizer temperature (to the maximum heating temperature). Thereby almost immediately mitigating the impact of excessive primary nucleation by triggering dissolution, as observed from the rapid decrease in counts. Whereas in the conventional experiments the heating response was comparatively gradual and hence the counts still rose slowly before starting to decrease. The gradual response of conventional

heating would also have allowed nuclei/fines to grow, thus imposing a greater demand on the dissolution cycle. Later in the dissolution/heating phase with the microwave heating, the rapid initial drop in counts decayed and leveled off near to the set point. The decay in the rate of count reduction was due to the depletion of the initially generated undersaturation, as the crystallizer temperature was maintained constant once it had reached the maximum. With the conventional heating experiments, the dissolution process approached the set point approximately linearly as the temperature of the crystallizer rose, creating undersaturation, until the number of counts was lowered to a value under the set point. Although the end temperatures after the first heating cycles are not very far apart, the gradual dissolution in microwave experiments avoided excessive dissolution, implying less supersaturation generation requirement in the subsequent growth cycle for maintaining the set point and hence limiting secondary nucleation. A few secondary nucleation peaks were observed subsequently, which were again suppressed rapidly by the microwave heating before the microwave experiments reached the end-point temperature. In this way, the use of microwave heating allowed to quickly shift from a nucleation dominated regime to a growth dominated regime. The final result is a significantly reduced batch time (by almost 50%) with fewer cycles.

Figure 2.6, shows the square weighted chord length distribution (SWCLD), obtained at the end of the experiments, which gives a qualitative idea about the crystal size distribution. The comparison shows that slightly larger mean sizes were obtained when the set point of counts was 2,000 as compared to the set point of 5,000. Similar size distributions were obtained when a comparison between the distribution from conventionally heated and microwave heated experiments is made, even though the batch times were drastically different in the two cases.
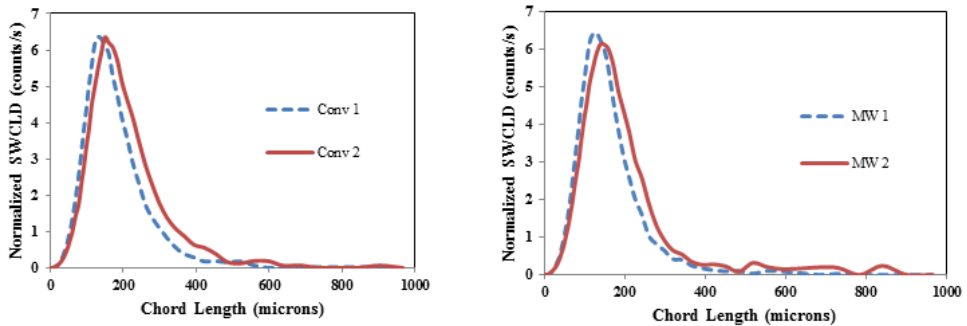
Figure 2.6: Normalized chord length distribution of the product crystals at the end experiments.

The size distribution of the product crystals, measured by laser diffraction, at the end of the experiments 'Conv2' and 'MW2' (see Table 3.1) is shown in Figure 2.7. The distributions obtained from experiments 'Conv2' and MW2' had comparable mean sizes, while a slightly narrower size distribution was observed in case of the microwave assisted experiment (MW2). The result from size distribution measurement confirms the trends that were measured with the FBRM probe.

Images of the product crystals from 'Conv2' and 'MW2' experiments were also taken using a microscope and are shown in Figure 2.8, respectively. In agreement with the CSD in figure 2.7 a small amount of fine crystals are present in the product crystals of both experiments. In addition some agglomeration can be observed explaining the rise at larger crystal sizes in the CSDs. Agglomeration may have occurred due to the sampling procedure of crystals which involved filtration. In both the images (Figure 2.8), the present particles seem to reflect the size distributions presented earlier in figure 2.7 quite well.
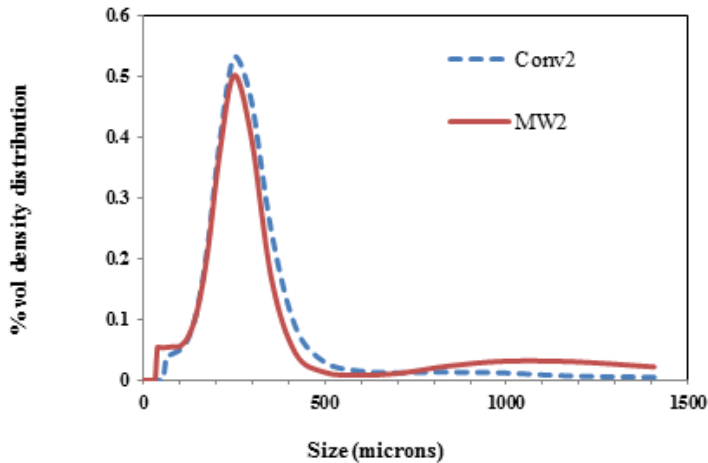
Figure 2.7: Volumetric crystal size density distribution of the product crystals obtained from the experiments.
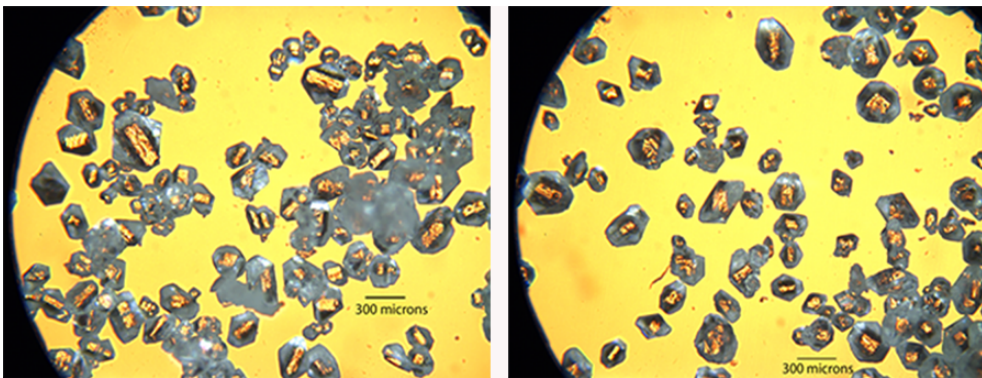
Figure 2.8: Image (magnification 5x) of the product crystals from experiment 'Conv2' (left) and Image (magnification 5x) of the product Crystals from experiment 'MW2'(right)

Compared to conventional fines removal system, where generally active particle count control is not employed and a cooling profile is continued to lower temperatures

2

despite occurrence of unwanted nucleation as a result of the sustained supersaturation in the crystallizer, DNC offers improved active control by directly restricting fines formation in the first place. By lowering the supersaturation in the crystallizer by raising the temperature, DNC acts against unwanted nucleation directly. Combined with microwaves, DNC offers a rapid response, resulting in faster reduction of fines in the crystallizer. Thus allowing for the achievement of products with narrow size distributions and desired size, which can be selected by choosing the appropriate set point values of the controller. The enhanced in-situ nucleation control efficiency also holds the potential to extend the approach for effective polymorphism or impurity control, by choosing an appropriate feed-back framework.

This study demonstrates the advantages of the use of microwaves to improve the efficiency of the direct nucleation control strategy for batch cooling crystallization processes. The introduction of microwave heating offers a fast and appropriate response to nucleation events of varying amplitude.

Batch-to-batch variability caused by the time variant driving forces in a batch process gives rise to varying secondary nucleation rates and hence varying fines production rate, which makes control based on heat transfer limited conventional approaches ineffective. This work forms a proof of concept of microwave assisted DNC and adds on to the examples of previously demonstrated synergistic approaches of microwaves in various crystallization processes.

Application of this concept in industrial crystallization processes however will require further research. First of all the direct application of the microwave heating in the crystallizer should be tested, avoiding the external loop which is in general undesirable and can cause operational problems. In addition, the extension of microwave assisted control, towards shape, polymorphism and impurity control, will be examined

2.4. Conclusions

Direct nucleation control in combination with microwave heating was successfully applied in a batch cooling crystallization process of paracetamol from iso-propyl alcohol. The direct heating capacity of microwaves provided a very rapid response to nucleation events measured by a rise in the particle counts, avoiding periods with high supersaturations during the batch. Consequently, the impact of nucleation could be strongly mitigated by quick dissolution of the generated fine particles, and resulted in a remarkable reduction in the number of heating cycles needed to keep the particle counts at their set-point value at the end of the batch. The fast microwave heating response, leading to a tight control over nucleation also resulted in a reduced number of heating/cooling cycles and therefore, a reduced batch time. In particular, at least for the tested cases, the batch time could be reduced with about 50% when using microwave heating compared to conventional heating. The effective removal of fines allowed for similar product crystal size distribution to be produced as compared to the conventional process.

References

2

[1] Z. K. Nagy and R. D. Braatz, *Advances and new directions in crystallization control,* Annual Review of Chemical and Biomolecular Engineering **3**, 55 (2012).

[2] Z. K. Nagy and R. D. Braatz, *Open-loop and closed-loop robust optimal control of batch processes using distributional and worst-case analysis,* Journal of Process Control **14**, 411 (2004).

[3] S. H. Chung, D. L. Ma, and R. D. Braatz, *Optimal seeding in batch crystallization,* The Canadian Journal of Chemical Engineering **77**, 590 (1999).

[4] A. N. Kalbasenka, L. C. Spierings, A. E. Huesman, and H. J. Kramer, *Application of seeding as a process actuator in a model predictive control framework for fedbatch crystallization of ammonium sulphate,* Particle & Particle Systems Characterization **24**, 40 (2007).

[5] M. Jiang, X. Zhu, M. C. Molaro, M. L. Rasche, H. Zhang, K. Chadwick, D. M. Raimondo, K.-K. K. Kim, L. Zhou, Z. Zhu, M. H. Wong, D. O'Grady, D. Hebrault, J. Tedesco, and R. D. Braatz, *Modification of crystal shape through deep temperature cycling,* Industrial & Engineering Chemistry Research **53**, 5325 (2014).

[6] M. R. Abu Bakar, Z. K. Nagy, A. N. Saleemi, and C. D. Rielly, *The impact of direct nucleation control on crystal size distribution in pharmaceutical crystallization processes,* Crystal Growth & Design **9**, 1378 (2009).

[7] G. L. Zipp and A. D. Randolph, *Selective fines destruction in batch crystallization,* Industrial & Engineering Chemistry Research **28**, 1446 (1989).

[8] S. Rohani, N. S. Tavare, and J. Garside, *Control of crystal size distribution in a batch cooling crystallizer,* The Canadian Journal of Chemical Engineering **68**, 260 (1990).

[9] R. D. Braatz and S. Hasebe, *Particle size and shape control in crystallization processes,* AIChE Symposium Series **98**, 307 (2002).

[10] H. Tong, W. Ma, L. Wang, P. Wan, J. Hu, and L. Cao, *Control over the crystal phase, shape, size and aggregation of calcium carbonate via a l-aspartic acid inducing process,* Biomaterials **25**, 3923 (2004).

[11] R. Lakerveld, J. J. H. van Krochten, and H. J. M. Kramer, *An air-lift crystallizer can suppress secondary nucleation at a higher supersaturation compared to a stirred crystallizer,* Crystal Growth & Design **14**, 3264 (2014).

[12] X. YiáWoo and B. Reginald, *Precise tailoring of the crystal size distribution by controlled growth and continuous seeding from impinging jet crystallizers,* CrystEngComm **13**, 2006 (2011).

[13] R. J. P. Eder, S. Schrank, M. O. Besenhard, E. Roblegg, H. Gruber-Woelfler, and J. G. Khinast, *Continuous sonocrystallization of acetylsalicylic acid (asa): Control of crystal size,* Crystal Growth & Design **12**, 4733 (2012).

[14] G. Shan, K. Igarashi, H. Noda, and H. Ooshima, *Production of large crystals with a narrow crystal size distribution by a novel wwdj batch crystallizer,* Chemical Engineering Journal **85**, 161 (2002).

[15] A. Soare, R. Dijkink, M. R. Pascual, C. Sun, P. W. Cains, D. Lohse, A. I. Stankiewicz, and H. J. M. Kramer, *Crystal nucleation by laser-induced cavitation,* Crystal Growth & Design **11**, 2311 (2011).

[16] Z. K. Nagy, G. Fevotte, H. Kramer, and L. L. Simon, *Recent advances in the monitoring, modelling and control of crystallization systems,* Chemical Engineering Research and Design **91**, 1903 (2013).

[17] J. W. Mullin and J. Nývlt, *Programmed cooling of batch crystallizers,* Chemical Engineering Science **26**, 369 (1971).

[18] M. Fujiwara, Z. K. Nagy, J. W. Chew, and R. D. Braatz, *First-principles and direct design approaches for the control of pharmaceutical crystallization,* Journal of Process Control **15**, 493 (2005).

[19] Z. Q. Yu, J. W. Chew, P. S. Chow, and R. B. H. Tan, *Recent advances in crystallization control: An industrial perspective,* Chemical Engineering Research and Design **85**, 893 (2007).

[20] F. Lewiner, G. Févotte, J. P. Klein, and F. Puel, *An Online Strategy To Increase the Average Crystal Size during Organic Batch Cooling Crystallization,* Industrial & Engineering Chemistry Research **41**, 1321-1328 (2002) .

[21] N. Doki, H. Seki, K. Takano, H. Asatani, M. Yokota, and N. Kubota, *Process control of seeded batch cooling crystallization of the metastable α-form glycine using an in-situ atr-ftir spectrometer and an in-situ fbrm particle counter,* Crystal Growth & Design **4**, 949 (2004).

[22] E. Simone, W. Zhang, and Z. K. Nagy, *Application of process analytical technology-based feedback control strategies to improve purity and size distribution in biopharmaceutical crystallization,* Crystal Growth & Design **15**, 2908 (2015).

[23] A. Saleemi, C. Rielly, and Z. K. Nagy, *Automated direct nucleation control for in situ dynamic fines removal in batch cooling crystallization,* CrystEngComm **14**, 2196 (2012).

[24] A. N. Saleemi, C. D. Rielly, and Z. K. Nagy, *Comparative investigation of supersaturation and automated direct nucleation control of crystal size distributions using atr-uv/vis spectroscopy and fbrm,* Crystal Growth & Design **12**, 1792 (2012).

[25] A. N. Saleemi, G. Steele, N. I. Pedge, A. Freeman, and Z. K. Nagy, *Enhancing crystalline properties of a cardiovascular active pharmaceutical ingredient using a process analytical technology based crystallization feedback control strategy,* International Journal of Pharmaceutics **430**, 56 (2012).

[26] N. Sanzida and Z. K. Nagy, *Iterative learning control for the systematic design of supersaturation controlled batch cooling crystallisation processes,* Computers & Chemical Engineering **59**, 111 (2013).

[27] C. O. Kappe, *Controlled microwave heating in modern organic synthesis,* Angewandte Chemie International Edition **43**, 6250 (2004).

[28] C. Leonelli and T. J. Mason, *Microwave and ultrasonic processing: Now a realistic option for industry,* Chemical Engineering and Processing: Process Intensification **49**, 885 (2010).

[29] D. Jones, T. Lelyveld, S. Mavrofidis, S. Kingman, and N. Miles, *Microwave heating applications in environmental engineering—a review,* Resources, conservation and recycling **34**, 75 (2002).

[30] I. Girnus, K. Jancke, R. Vetter, J. Richter-Mendau, and J. Caro, *Large alpo4-5 crystals by microwave heating,* Zeolites **15**, 33 (1995).

[31] J. N. Lee, Y. W. Choi, B. J. Lee, and B. T. Ahn, *Microwave-induced low-temperature crystallization of amorphous silicon thin films,* Journal of Applied Physics **82**, 2918 (1997).

[32] N. Radacsi, J. H. ter Horst, and G. D. Stefanidis, *Microwave-assisted evaporative crystallization of niflumic acid for particle size reduction,* Crystal Growth & Design **13**, 4186 (2013).

[33] A. Rizzuti and C. Leonelli, *Crystallization of aragonite particles from solution under microwave irradiation,* Powder Technology **186**, 255 (2008).

[34] *Cryprins home page* .

[35] G. S. J. Sturm, A. Q. Van Braam Houckgeest, M. D. Verweij, T. Van Gerven, A. I. Stankiewicz, and G. D. Stefanidis, *Exploration of rectangular waveguides as a basis for microwave enhanced continuous flow chemistries,* Chemical Engineering Science **89**, 196 (2013).

[36] SAIREM SAS, *Internal trasnmission line- microwave batch reactor* .

[37] M. Komorowska-Durka, M. Barmen't Loo, G. S. Sturm, M. Radoiu, M. Oudshoorn, T. Van Gerven, A. I. Stankiewicz, and G. D. Stefanidis, *Novel microwave reactor equipment using internal transmission line (intli) for efficient liquid phase chemistries: A study-case of polyester preparation,* Chemical Engineering and Processing: Process Intensification **69**, 83 (2013).

3

Novel Microwave Integrated Crystallizer: Implementation of Direct Nucleation Control for Crystal Size Control.

3

The control of nucleation in crystallization processes is a challenging task due to the often lacking knowledge on the process kinetics. Inflexible (predetermined) control strategies fail to grow the nucleated crystals to the desired quality because of the variability in the process conditions, disturbances and the stochastic nature of crystal nucleation. Previously, the concept of microwave assisted Direct Nucleation Control (DNC) was demonstrated in a laboratory setup to control the crystal size distribution in a batch crystallization process by manipulating the number of particles in the system. Rapid temperature cycling was used to manipulate the super(under)saturation and hence the number of crystals. The rapid heating response achieved with the microwave heating improved the DNC control efficiency, resulting in halving of the batch time. As an extension, this work presents a novel design in which the microwave applicator is integrated in the crystallizer, hence avoiding the external loop though the microwaves oven. DNC implemented in the 4 litre unseeded crystallizer, at various count set points, resulted in strong efficiency enhancement of DNC, when compared to the performance with slow responding system. The demonstrated crystallizer design is a basis for extending the enhanced process control opportunity to other applications.

3.1. Introduction

Specialty chemicals and high value molecules such as active pharmaceutical ingredients (APIs) usually pose high demands on product quality attributes and require also that the product quality is stringently met [1]. The desired quality attributes can often be difficult to achieve and hence the complexity of the production process and the production costs increase. Crystallization is one of the key unit operations involved in production of solid products by separating the solute from the solution [2]. Traditionally in the industry the crystallization is carried out in stirred tank reactors operating in batches with a predetermined recipe [3]. The batch approach, with fixed operation recipe often leads to variability in product quality. Additional downstream processes are required in order to treat the product after the crystallization step in order to achieve desired product quality [4].

During crystallization one of the typical quality attributes of concern, is to be able to produce a desirable and repeatable particle size distribution (PSD). To achieve this, a tight control over the nucleation rate is required to generate a sufficient number of nuclei initially in the batch. Under tight control, the nucleated nuclei grow out uniformly to the desired size by consuming the large part of the generated supersaturation in the remainder of the batch. Many control strategies have been employed to gain control over the crystal size distribution either based on models which require a priori knowledge of the crystallization kinetics to predict an optimum process trajectory or more popularly seeding based strategies to suppress primary nucleation have been employed [5–11]. Unfortunately many of these strategies are often unsuccessful due to model uncertainties resulting from poor estimation of the complex non-linear crystallization process and due to the unexpected process disturbances which often offset the process [12]. Direct nucleation control (DNC) is a model free feedback control strategy based on using PAT tools for process monitoring [13, 14]. Real time control over the process, based on in situ measurements of the state variables, is implemented in the DNC framework to recover the process from the deviations from the desired set point. The DNC approach fits well in the QbD approach, as not only strict control over the product quality can be ensured but also through process monitoring mapping of the operating conditions and the resulting product quality can be obtained.

Temperature cycling (heating and cooling) is yet another control strategy usually used for the crystal shape and size control and for the removal of fines during crystallization where the fine particles are expected to dissolve sooner compared to the larger particles, when the system temperature is increased [15–17]. Upon cooling, the generated supersaturation is ideally expected to be consumed by the larger particles remaining after the dissolution step. Since temperature cycles are in principle dissolution and growth/nucleation cycles the application of temperature cycling to serve various control objectives exists. Application of temperature cycling within the DNC framework is thus, not limited to size control of the crystalline product only. DNC has been applied or has potential to be applied to areas such as crystal shape manipulation, polymorphism control or chiral resolution, to name a few [18, 19]. However, the issue of limited heat transfer capacity can be limiting factor for the application of process control based on temperature cycling approach. Especially at

large scales, the heat transfer limitation worsens as the ratio of the cooling surface area to the crystallizer volume decreases at increasing crystallizer capacity. As an alternative for increasing the heat transfer surface area (which can be undesirable in context of controlling nucleation), the application of microwave heating can be one of the solutions to attain an enhanced heat transfer [20]. However, the limited penetration depth of the microwaves presents a challenge for large scale implementation. Careful design, probably utilizing multiple sources of microwaves in combination with efficient stirring, is needed to ensure uniform bulk heating. The improved process control opportunity achieved by implementation of microwave heating is not particularly restricted to high heating rates but also a faster switch to cooling can be made, saving time otherwise spent in changing the process stream from hot to cold and vice versa in case conventional heat transfer via the same jacket.

In a previous study, the concept of a microwave assisted DNC approach was demonstrated [21]. Manipulation of the crystal size distribution in a batch crystallization process was achieved by manipulating the number of particles in the system. The DNC approach was implemented via the feedback control based on the in situ measurement of the number of particles by FBRM. Temperature cycling was triggered upon the deviation of the particle count from the set point, resulting in heating for dissolving the excess particles and cooling for generating new particles via nucleation or to grow the particle for achieving the desired yield. The study concluded that the use of rapid heating achieved by applying microwaves in comparison to the slower heating response (limited by jacket heat transfer), leads to the improvement in the efficiency of the control by reducing the number of temperature cycles required to reach the desired set point. Overall, a reduction of the batch time by a factor two was achieved. At the same time, the size distribution of the end product obtained when microwave was used was narrower as better control over fines removal was achieved. The significant improvement in the control efficiency was due to the rapid response after the detection of a nucleation event. Due to the strong non-linear dependence of the nucleation rate on the supersaturation, a fast response on a nucleation burst is essential to prevent a large overshoot in the number of particles, which can only be counteracted by dissolution. The direct heating property of microwaves allowed the rapid response in terms of heating and eliminated the delay usually involved with switching between heating and cooling phases. Our study showed the need to have fast response to nucleation for controlling the number of particles during crystallization, which require special design consideration in order to not get limited by the heating rates usually restricted by the limited heat transfer surface in conventionally heated crystallizers.

The proof of concept study published earlier showing the enhanced DNC control, by combining microwave heating during crystallization, was carried out at a laboratory scale using an external loop which circulated the slurry from the crystallizer through a microwave cavity to introduce the microwave heating in the system. Such an external loop is not desired as the influence of circulating the crystals through the loop on the process is not clear and difficult to scale up. Therefore, in this paper we present the microwave assisted DNC in a novel crystallizer designed to apply the microwaves directly into the crystallizer, thus avoiding the implementation of an

external loop. Also, the scale of the crystallization process has been enhanced. The integrated microwave assisted crystallizer has been developed by Siarem SAS, based on internal transmission line technology, which directly integrates microwave heating in a jacketed crystallizer made of steel (Labrotron 4000, 4 L in capacity). Through the implementation of DNC approach for controlling the size of paracetamol crystals in iso-propyl alcohol (IPA) in the Labotron 4000 unit, we intend to further the novel crystallizer design and demonstrate the concept crystallizer which can serve as a base for industrial applications.

3.2. Experimental Section

3.2.1. Materials
Acetaminophen (Paracetamol, BioXtra ≥99%, Sigma Aldrich) and iso-propyl alcohol (IPA, 99%, VWR) has been used in this study.

3.2.2. Particle count measurement: FBRM
Focused Beam Reflectance Measurement (FBRM) probe (model G600) from Mettler Toledo was used to measure in situ the particle count and the chord length distributions (CLD). The iC FBRM software (version 4.4) was used for the data acquisition and analysis. The scan speed of the unit was set to 4 m/s with measurement interval of 5 seconds in all experiments. Both primary and macro modes are available to analyze the FBRM data. The count data reported here are based on primary mode which means that the count data has high sensitivity for the edges detected. Mean squared chord length data from FBRM is used for reporting the mean particle size as measured by the FBRM.

3.2.3. Particle size distribution: Laser Diffraction (LD)
Laser diffractometer (Mircotrac S3500) was used for particle size measurement using dry mode sample measurement. Samples for particle size distribution analysis were prepared by filtering the slurry. The residue containing the product crystals was washed with a small amount of IPA and left overnight for drying in an oven maintained at 30 °C. The samples have also been pictured under microscope.

3.2.4. In-situ concentration measurement
An ATR probe, model K1 Katana 6mm supplied by Hellma, connected to a Deuterium light source (model DH-2000-BAL) and to a spectrometer (HR2000+CG), both supplied by Ocean Optics, has been used to measure the absorption spectra of paracetamol in IPA. The concentration of paracetamol in IPA is estimated from the spectra collected by Spectrasuite software (Ocean Optics), by calculating the absorbance between the wavelengths of 255 up to 270 nm. Calibration was performed by measuring the absorbance spectrum of known concentration samples at temperatures ranging from 50 - 10 °C. The measurements always started at the highest temperature and were stopped when nucleation was detected or when the temperature reached the lower end. A model was then fit to relate the absorbance spectra to the concentration, in the form of Equation 3.1

$$c = a_1 Abs + a_2 Abs^2 + a_3 T + a_4 Abs T + a_5 \qquad (3.1)$$

3

Where c is the concentration (g paracetamol / g isopropanol), a_i are the coefficient to be adjusted, T is the temperature ($°C$) and Abs is the absorbance. In order to correct for the baseline fluctuations of the spectra the derivative of the absorption spectra from 255 to 270 nm is estimated. The derivate is then integrated between the desired wavelengths to retrieve the absorbance. The parameter estimation was done by a least squares optimization. The model parameters obtained are $a_1 = -0.398$, $a_2 = 0.214$, $a_3 = 1.55e - 5$, $a_4 = -2.89e - 3$ and $a_5 = 2.26e - 3$. The concentration measurement and the calibration procedure adopted here are as reported in the literature in a previous study [13]. Figure 3.1, shows the measured concentration of sample with known concentration of paracetamol in IPA against the saturation data reported in literature [22]. The measured values are in line with literature values. The error between the measured and the estimated concentration was ascertained using a validation set prepared separately. Validation experiments were performed to test the calibration by heating slurry of paracetamol IPA in steps in a temperature range similar to the calibration curve. As the slurry was heated, a part of the excess particles in the slurry dissolved to reach the new equilibrium concentration at the end of each step and the error in predicted concentration was estimated to be in the range of ±2%
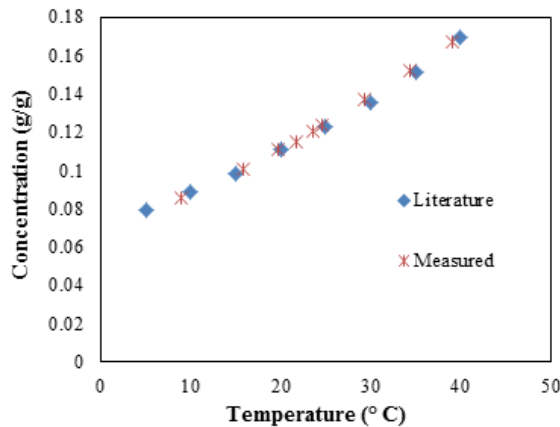
Figure 3.1: Concentration measurement using the model described by equation 1 vs saturation concentration as per literature. Saturation concentration data is from literature [23]

3.3. Experimental Conditions

3.3.1. Set-up

The unit, Labotron 4000, designed and manufactured by Siarem S.A.S, allows integration of the microwave heating within a jacketed reactor. It uses internal transmission line technology for transfer of microwave directly into the slurry for direct heating of the contents inside the reactor. Thus, the unit consists of a microwave generator (2 kW, 2.4 GHz) connected via the internal transmission line to a 4 L jacketed stainless steel reactor. The system is detailed in Figure 3.2
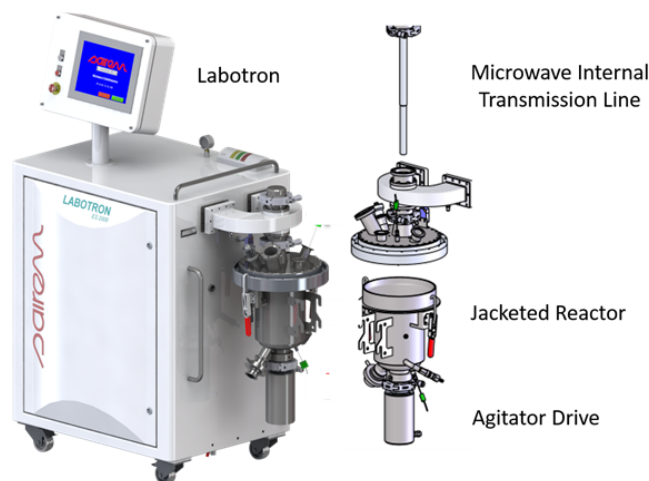
Figure 3.2: Labotron 4000, along with schematic of the essential constituents.

An agitation drive connected to a pitched blade propeller provides sufficient mixing in the crystallizer to keep the crystals in the crystallizer suspended. The FBRM has been introduced at the bottom of the reactor through the drain at the bottom of the crystallizer. Sufficient mixing is achieved in the system for FBRM to give a reliable indication of the change in particle count in the crystallizer.

Cooling crystallization was carried out in the jacketed reactor (as described above) which was connected to Lauda RE-310 (Ecoline Star edition) thermostat unit for regulating the temperature of the jacket. Pt100 temperature probe connected to the thermostat unit was used to measure the temperature inside the reactor and the measured temperature was conveyed to the main controller as feedback for the control. In case of experiments with microwave heating, the input power of the system was set to a maximum of 2kW, which was regulated internally by the PID controller in the Labotron unit to achieve the desired set temperature based on the difference from the current crystallizer temperature. The heating rates realized in the crystallizer depend on the dielectric properties of the liquid which dictate the amount of the microwave energy absorbed by the liquid solvent. Figure 3.3, provides the overview of the implementation of process monitoring and control.

Figure 3.3: Control overview of the setup, with CryPrins giving the temperature set point based on the particle count (FBRM) feedback and the Labview based Controller communicates the temperature set point to the thermostat bath and the microwave unit. TEMP has been used in short for temperature.

3.3.2. Microwave assisted Direct Nucleation Control structure

Figure 3.3, provides the overview of the implementation of process monitoring and control. CryPRINS (crystallization process informatics system) software which has the DNC approach implemented has been used to obtain the feedback of the particle count via the FBRM. For information about DNC using CryPRINS, literature can be referred [23]. The temperature set point output by CryPRINS is linked to a Labview program (developed in-house) which controls and communicates the temperature set point of the thermostat and the mi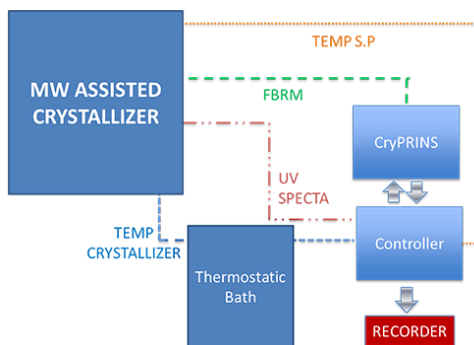crowave unit. Based on the temperature set point received by the microwave unit, an internal PID controller on the Labotron unit itself, switches the microwave on or off and regulates the power level (maximum 2 kW)

Primarily due to nucleation or dissolution events, the particle count deviates, which (detected via the FBRM) trigger heating or cooling response in form of a new temperature set point for the crystallizer. In case of no microwave heating, the controller simply regulates the thermostatic bath to achieve heating and cooling via the jacket in the crystallizer. When the microwave is used, only cooling is then carried out by the thermostatic bath. The use of microwave heating allows us to maintain the jacket at a lower temperature (approximately 6 $°C$ than the crystallizer temperature) during the microwave heating cycles, thereby obtaining a quicker switch to cooling. An overview on the microwave assisted DNC control structure implemented in this study can be found in our previous proof of concept work.

3.3.3. Experimental design

Experiments have been performed with and without microwave heating to demonstrate the enhancement in efficiency of DNC using rapid temperature cycling. In both the cases, the experimental configuration was kept the same. Saturated solution at 40 $°C$ was prepared by dissolving 0.18 grams of paracetamol per gram of the solvent (IPA). Then the solution was heated to 50 $°C$ and left for one hour to ensure complete dissolution. Direct nucleation control was switched on (count set point activated).

Table 3.1: Summary of experiments and associated experimental conditions. SP = Set Point

Experiment	Type Heating	Heating/Cooling Rate (°C/min)	Counts SP
Conv 1	Jacket/conventional	0.7/0.5	4500
Conv 2	Jacket/conventional	0.7/0.5	3500
Conv 3	Jacket/conventional	0.7/0.5	2250
MW 1	Microwave	2/0.5	4500
MW 2	Microwave	2/0.5	3500
MW 3	Microwave	2/0.5	2250

The rate of change in temperature set point in the crystallizer with microwave heating was set to 2 $°C/min$, while in the experiments with jacket/conventional heating (when no microwave heating is used) a value of 0.7 $°C/min$ is used. The lower heating rate in case of the conventional heating is due to the heat transfer limitations of the jacket. In case of IPA as solvent, heating rates of up to 5-6 $°C/min$ could be achieved at a full microwave output power of 2 kW. In case of conventional heating the heat transfer via the jacket was limiting. The maximum and minimum temperatures in the system were limited to 50 $°C$ and 5 $°C$ respectively. This was done to avoid excessive dissolution of the particles, which could lead to total loss of nucleated particles and hence will require new nucleation events repeatedly in order to generate the required number of particles. A cooling rate of 0.5 $°C/min$ was used in all experiments for gentle supersaturation generation to avoid excessive secondary nucleation during the cooling cycles. Experiments at different set points for the particle count were performed in order to analyze the effect of the set point values on the process dynamics and the product quality. In essence, by maintaining a lower number of crystals in the system larger crystals can be obtained. Whereas a high number of crystals will lead not only to relatively smaller crystals but will also possibly have lot more fine particles. On the other hand a batch process without any feedback control with a simple linear cooling profile (cooling a saturated solution at 40 $°C$ to 5 $°C$ at 0.5 $°C/min$), results in counts value in the order of 20000 and a broad particle size distribution (data not shown in the paper for brevity). The count set point chosen here, with a tight control bound of ± 250 counts, set a challenge for the controller to maintain the crystal count in the crystallizer at much lower values when compared to the count achieved by primary nucleation with same linear cooling rate but no control. The DNC control at various count set points should lead to different final size of the crystal product. Table 3.1 summarizes the experiments carried out at the various counts set point.

3.4. Results & Discussions

3.4.1. Microwave assisted DNC

Experiments have been carried out at different count set points with and without rapid temperature cycling (summarized in Table 3.1). These experiments evaluate the performance of DNC in the current crystallizer. Different count set points for the

DNC impose the growth of a different number of crystals in the process and thus a different product size. As shown before in our previous study, the low count values are the most demanding for the control especially when nucleation is dominating requiring large number of temperature cycles to reduce the count after nucleation and to maintain the desired set point value. Figure 3.4, shows the results of the DNC with conventional heating for a set point of 3500 (Conv 2). The figure shows the trends in the particle count, the temperature, the concentration and the mean particle size. The first peak in the count profile is due to the primary nucleation which occurs when the clear saturated solution is cooled down. The primary nucleation peak is the largest compared to the subsequent peaks which are due to the secondary nucleation. Upon deviation from the count set point, the controller switches to the heating/cooling cycles. Excess nuclei are dissolved when sufficient under saturation is created during the heating phase of the temperature cycles. Subsequently nuclei are generated by triggering nucleation during the cooling phase of the temperature cycles creating supersaturation in the system. The process control continues to cycle between heating and cooling phases till the end temperature is reached and the count set point is within the set bounds. Overall, about 6 to 7 cycles were required at this count set point value of 3500 before the target temperature (close to $5\,^\circ C$) and the desired count set point was reached. Figure 3.4 also shows (in the plot inset) the trend of the solute concentration which also varies with the process changes before reaching a constant value close to the saturation shortly after the temperature reached the target value. The plot inset in figure 3.4 also shows the evolution of the mean particle size which varies with the nucleation and the dissolution events and reaches a steady value at the end of the control process.

Figure 3.5, shows the particle count and the temperature profile from the experiment with the microwave heating at the same count set point of 3500 (MW 2). Concentration and the mean size are shown in the plot inset in Figure 3.5. The striking difference compared to experiment CONV 2 in Figure 3.5, is the reduction in the number of cycles needed before the control reaches the target temperature and the count set point value. In addition, the value of the first count peak due to primary nucleation is strongly reduced (approximately by 50%) in the experiment MW 2 due to the rapid heating and the reduced lag time between switching of temperature cycles. By avoiding the number of particles to drop far below the set point value during dissolution, the subsequent need of supersaturation generation for generation of new nuclei to recover the particle count is also lowered. Hence, gentle secondary nucleation cycles are observed. The consecutive dissolution and growth cycles continue till the set point is achieved. The count reaches approximately a value of 3000, in both experiments with conventional heating and with microwave heating, close to the lower bound of the set point. At the end of the cycles, the concentration data (plot inset in Figure 3.5) confirms that constant concentration close to saturation is achieved, signifying the end of process and a steady particle size. The batch time is dependent on the number of cycles before the control objective is achieved. Hence by the implementation of rapid heating a reduction in the number of temperature cycles and therefore a reduction in batch time is obtained. Overall the batch time is approximately lowered by a factor of two in case of the experiment MW 2 due to the

Figure 3.4: Count and temperature profile measured during DNC with conventional heated crystallizer, experiment Conv 2. The plot inset shows the evolution of the mean square weighted chord length of the crystals and the concentration of paracetamol in the crystallizer

lower numbers of temperature cycles.

Experiments have also been performed at other count set points. Figure 3.6 shows the temperature and counts profile for experiments at the counts set point of 2250 (experiments Conv 3 and MW 3). A larger number of temperature cycles are needed before the count set point is reached. Due to the low count set point and due to slow response in the conventionally heated/cooled system, a large under saturation is created after the primary nucleation event which almost completely dissolves the nucleated crystals. Thus, subsequent nucleation cycles are required for generating new nuclei to regain the count set point. Figure 3.8 (left) shows the concentration profiles for experiments Conv 3 and MW 3. A large drop in the concentration is seen during the crystallization phase (i.e. during nucleation events) followed by excess dissolution reinstating the starting concentration throughout the experiment Conv 3. Poor control due to the slow response in the experiment (Conv 3) results in the temperature cycles being stuck between dissolution and nucleation events and in no convergence to the desired set point. The almost complete dissolution of the nucleated crystals at the end of each temperature cycle results in the temperature of the system to be high, far from the desired end temperature and hence the solution concentration remains high.

In experiment MW 3, the fast response significantly lower the number of excess crystals after the cooling phases and the shortage in number of crystals after the heating phase, making the convergence to the set point value much easier. The
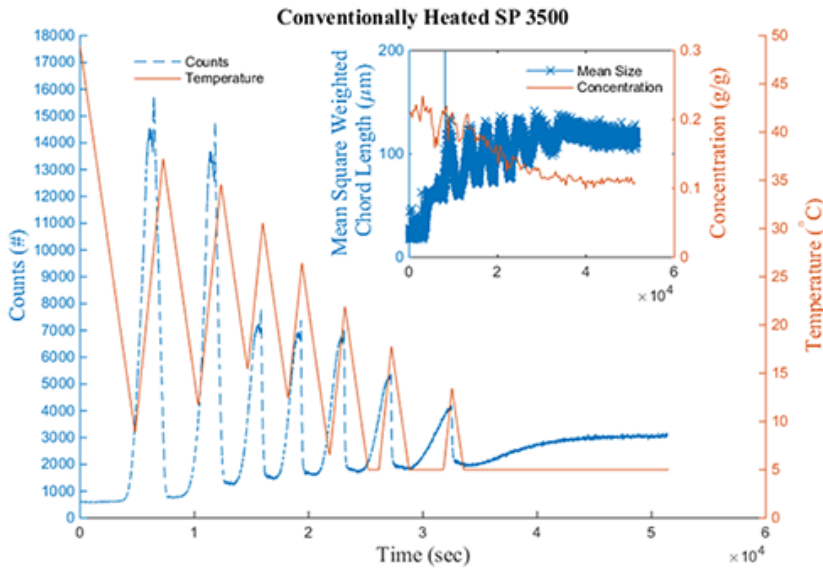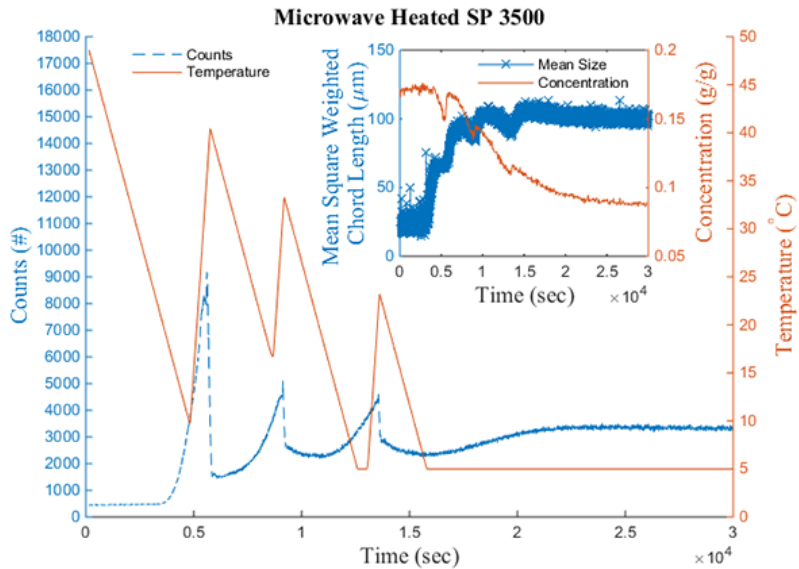
Figure 3.5: Count and temperature profile measured during DNC with microwave heated crystallizer, experiment MW 2. The plot inset shows the evolution of the mean square weighted chord length of the crystals and the concentration of paracetamol in the crystallizer.

smaller drops in the concentration during nucleation seen in concentration profile for experiment MW 3 (Figure 3.8 (left)), is because of the tight control achieved by rapid heating. As a result, the batch in experiment MW 3 reaches the targeted end temperature at the desired count set point. Overall the process with microwave heating converges towards the set point in a total of 5-6 cycles. Samples of crystals were taken at the end of the experiment MW 3 only as the experiment Conv 3 did not converge to the set point and had to be stopped.

The temperature and count profile for both experiments MW 1 and Conv 1, with the higher count set point of 4500, is shown in Figure 3.7. At this count set point of 4500, approximately the same number of cycles and comparable batch time is observed in both the experiments MW 1 and Conv 1. The low number of cycles observed is due to the high number of particle being maintained in the system which rapidly consumes the supersaturation. Figure 3.8 (right), shows the concentration profile for both the experiments Conv 1 and MW 1, respectively. Both the concentration profile approach saturation values expected at the end of the experiment. However, in the experiment MW 1 the count set point reached is closer to the set point value of 4500 ±250. Whereas the final count value in the experiment Conv 1 is much lower and the set point is not achieved. Even though the paracetamol IPA system exhibits dominant secondary nucleation, the high particle count allows rapid consumption of the supersaturation for the growth of the particles and hence helps to avoid secondary nucleation. Process dominated by growth rather than nucleation

Figure 3.6: Count and temperature profile measured during experiments Conv 3 (left) and during experiment MW 3 (right) at count set point of 2250.
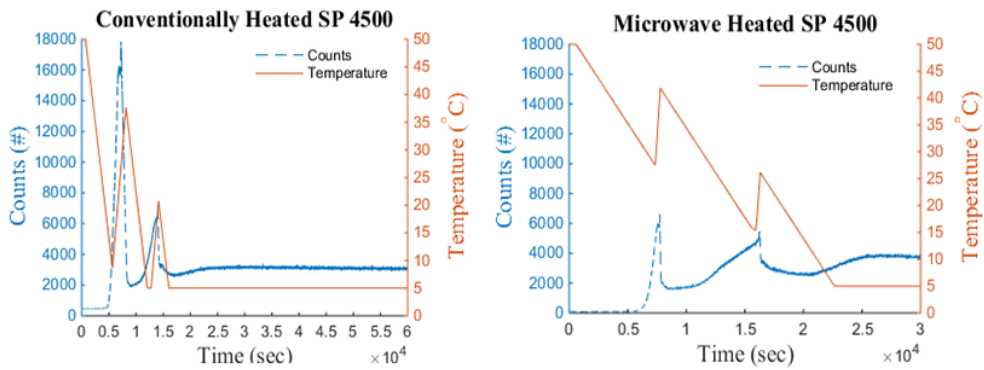
Figure 3.7: Count and temperature profile measured during experiments Conv 1 (left) and during experiment MW 1 (right) at count set point of 4500.

events makes it difficult for the control process to reach the count set point by triggering nucleation even as the supersaturation is generated during the cooling to the end tempera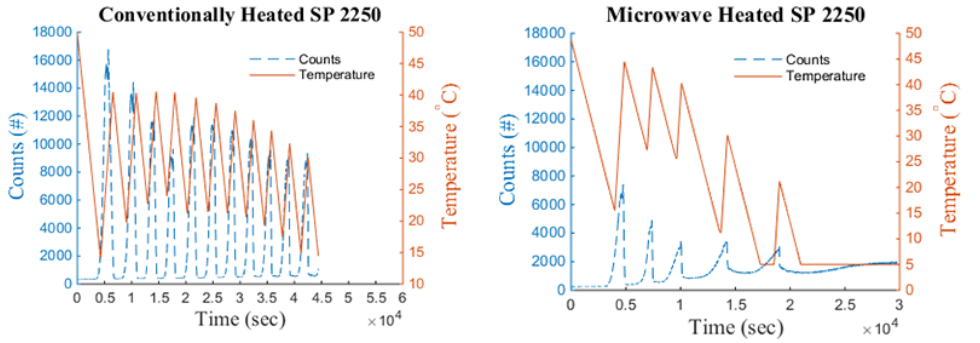ture. In experiment MW 1, the tight control over the number of particle during nucleation and dissolution allows for the batch to approach the desired count set point closely.
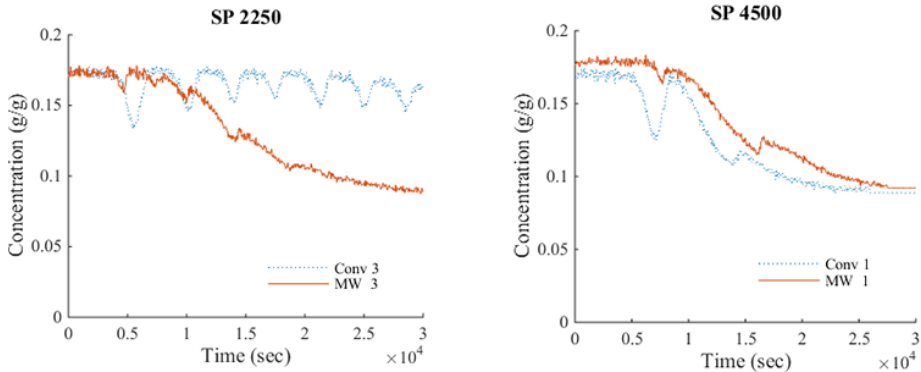
Figure 3.8: Concentration profile measured during DNC with conventional and microwave heated crystallizer at count set point of 2250 (left) and at count set point of 4500 (right).

3.4.2. Particle size distribution with rapid temperature cycling

To assess the final product crystals, the size distribution of crystals at the end of each experiment has been determined, by measuring the dried sample in a forward laser diffraction instrument. In addition, samples have been imaged under the microscope and the chord length distribution data measured by the FBRM is also available.

Figure 3.9, shows the normalized volume distribution for microwave assisted DNC experiments carried out at various count set points. Unimodal distribution is observed, with small shoulder at large sizes. The shoulder could be due to agglomerated crystals resulting during the sampling process which involves filtration and drying. The effect of the different count set points on crystal size is seen from the peaks in the size distribution (Figure 3.9). The enhanced control with microwave assisted DNC allowed the three count set points in our experimental design to be realized through strict regulation of the number of particle. As a result, increased particle size is observed as the count set point is decreased. However, at high count set point of 4500 a lot of fine particles still remain in the system and that is visible in the size distribution at small sizes around 50 μm.

Images of the product crystals from the above experiments were also taken under microscope. Figure 3.10 show the product crystals obtained from the experiments at count set point of 2250 and 4500 respectively. Larger crystals with fewer fines are seen in the case of count set point of 2250 in accordance with the measured particle size distribution. The large number of temperature cycles experienced at the low count set point ensures that fine particles dissolve and hence larger crystals are obtained. In the case of the count set point of 4500, a large number of fines
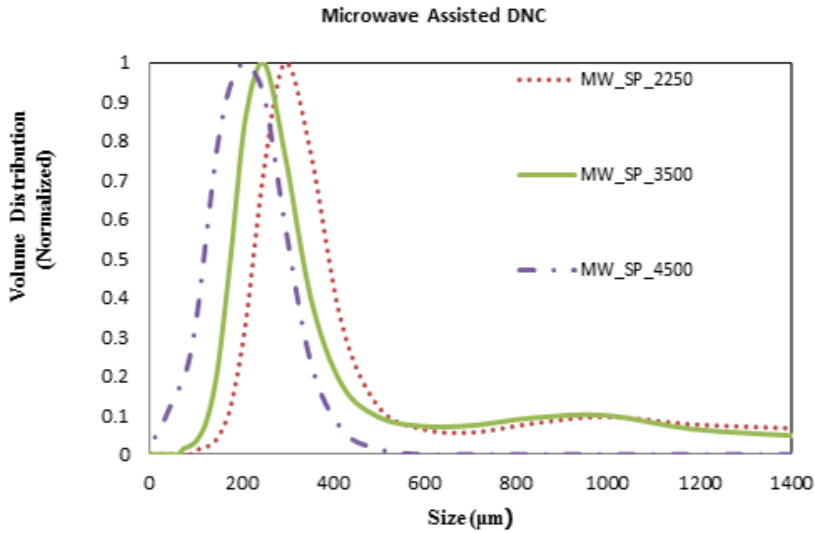
Figure 3.9: Volume based particle size distribution obtained at various count set points with microwave assisted heating.

are visible. The large crystals are surrounded by many smaller fine particles and agglomeration is also noticeable. The large count set point allows a large number of particles to be sustained in the process and due to the fewer temperature cycles a lot more fines are present.
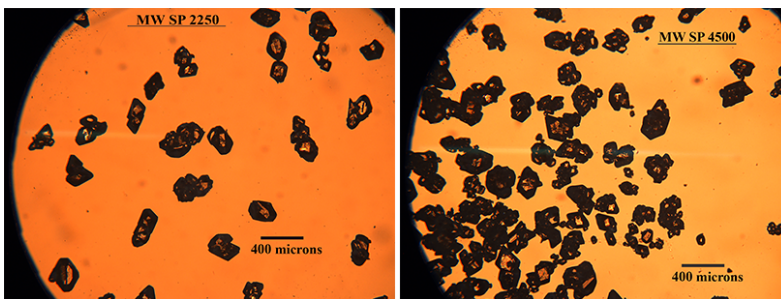
Figure 3.10: Images of samples taken at the end of experiment with count set point of 2250 (left) and 4500 (right). (All pictures are at 5x magnification).

3.4.3. Effect of design and scale on microwave assisted DNC

In comparison with our earlier study in which 1L scale glass reactor with external loop for microwave heating was used, the 4 L stainless steel design presented here integrates the microwave heating into the crystallizer vessel. With this design the use

of an external loop though the microwave oven is avoided which is known to cause problems, such as attrition of crystals due to pumping, poor temperature control and scaling. In the previous design high temperature of slurry in the loop was reached in order to achieve the required heating rate to respond to the nucleation event. The new integrated setup is an alternative design for rapid and flexible bulk heating of the crystallizer, utilizing microwave heating in combination with the already present convective dispersion due to the stirring. The Labotron unit allows high heating rates directly in the crystallizer without the need of increased heat transfer surface area or the use of external heat exchangers. Our design allowed rapid response against the onset of nucleation by creating undersaturation to tightly control the number of particles in the crystallizer, essential for efficient DNC control strategy.

At large scales, the limited penetration depth of the microwaves warrant the use of multiple power sources in combination of efficient stirring to ensure proper heat distribution. The integration of microwaves fields with the crystallizer however also restricts the use of PAT tools in vicinity of microwaves. Careful design based on the knowledge of attenuation of microwave field allowed the PAT tools to be placed near the bottom of our crystallizer, where the microwave fields if present are very weak. Positioning the FBRM probe at the bottom near the impeller is not the optimum positioning for efficient performance of the FBRM. Analogously for industrial implementations a draft tube crystallizer design could ensure safe introduction of the microwaves in the central annular region with the outer region isolated from microwaves for implementation of PAT tools.

The results obtained with the novel crystallizer presented in this study are in line with our previously reported proof of concept study. The process control response achieved with rapid heating in both these studies resulted in a significant enhancement in the direct nucleation control efficiency. In both setups the low count set points required larger number of cycles when compared to higher set points. Most importantly the tight control achieved with rapid heating resulted in the control process to converge for the low count set points in both the studies, which was more challenging for the control process. A direct comparison between the experiments done with the lab unit with external circulation loop and the Labotron unit is difficult due to the differences in the impeller design (mixing) and the PAT tool (FBRM) positioning which influence the detected particle count. In a separate experiment the control performance was also tested with higher heating rates (4-6 $°C/min$) with the Labotron unit. The result showed that the temperature cycle time was reduced but excessive dissolution occurs as the system was heated too fast to temperatures above the saturation level. The resulting excessive dissolution resulted in additional cycles to achieve the count set point. Additional tuning of the control is required to optimize the use of the higher heating rates and hence experiments with high heating rates were not reported here. A simple solution is to limit the maximum temperature and thus limit the under saturation which can be created by the controller.

3.5. Conclusions

In this study a novel microwave integrated crystallization unit is presented and successfully applied to demonstrate the enhancement in the efficiency of DNC using rapid heating. The Labotron 4000 unit (4 L in capacity) from Sairem with its internal transmission line technology was redesigned to enable integration of microwave heating directly into a crystallizer, avoiding the use of external dissolution loop.

By performing a DNC study on the paracetamol- isopropanol system it has been demonstrated that the application of rapid heating to counter the bulk nucleation directly in the crystallizer offers a much higher efficiency, resulting in significant reduction in batch time. The integration of microwave heating along with the PAT tools for process monitoring in a single crystallizer offers an alternative for designing and implementing advanced process control. Fast response to the deviations in the process resulted in a significant reduction in the number of control cycles and the best result was obtained for the experiments at the count set point of 3500, were the batch time with microwave heating was halved in comparison to slower response to nucleation. With rapid nucleation control, all the tested count set points were achieved and the particles size could be manipulated to different sizes accordingly. The results obtained with the microwave assisted DNC in the new crystallizer design were in line with our previous proof of concept study.

The novel crystallizer design with integrated microwave heating promises to be a convenient tool for optimizing processes based on temperature cycling. At lab/pilot scale, the microwave assisted crystallizer can be used for screening and for mapping the process space for gaining better control over nucleation and growth events. Such knowledge is valuable for rapid process development and design of crystallization processes. Our design thus, serves as a basis for advanced control opportunity to be realized in similar equipment or applications to meet stringent product quality standards.

References

[1] B. Y. Shekunov and P. York, *Crystallization processes in pharmaceutical technology and drug delivery design,* Journal of Crystal Growth **211**, 122 (2000).

[2] J. Chen, B. Sarma, J. M. B. Evans, and A. S. Myerson, *Pharmaceutical crystallization,* Crystal Growth & Design **11**, 887 (2011).

[3] J. W. Mullin and J. Nývlt, *Programmed cooling of batch crystallizers,* Chemical Engineering Science **26**, 369 (1971).

[4] P. A. Larsen, D. B. Patience, and J. B. Rawlings, *Industrial crystallization process control,* IEEE Control Systems **26**, 70 (2006).

[5] S. Rohani, N. S. Tavare, and J. Garside, *Control of crystal size distribution in a batch cooling crystallizer,* The Canadian Journal of Chemical Engineering **68**, 260 (1990).

[6] G. L. Zipp and A. D. Randolph, *Selective fines destruction in batch crystallization,* Industrial & Engineering Chemistry Research **28**, 1446 (1989).

[7] R. D. Braatz and S. Hasebe, *Particle size and shape control in crystallization processes,* AIChE Symposium Series **98**, 307 (2002).

[8] H. Tong, W. Ma, L. Wang, P. Wan, J. Hu, and L. Cao, *Control over the crystal phase, shape, size and aggregation of calcium carbonate via a l-aspartic acid inducing process,* Biomaterials **25**, 3923 (2004).

[9] A. N. Kalbasenka, L. C. Spierings, A. E. Huesman, and H. J. Kramer, *Application of seeding as a process actuator in a model predictive control framework for fed☐batch crystallization of ammonium sulphate,* Particle & Particle Systems Characterization **24**, 40 (2007).

[10] R. Lakerveld, J. J. H. van Krochten, and H. J. M. Kramer, *An air-lift crystallizer can suppress secondary nucleation at a higher supersaturation compared to a stirred crystallizer,* Crystal Growth & Design **14**, 3264 (2014).

[11] X. YiáWoo and B. Reginald, *Precise tailoring of the crystal size distribution by controlled growth and continuous seeding from impinging jet crystallizers,* CrystEngComm **13**, 2006 (2011).

[12] Z. K. Nagy, G. Fevotte, H. Kramer, and L. L. Simon, *Recent advances in the monitoring, modelling and control of crystallization systems,* Chemical Engineering Research and Design **91**, 1903 (2013).

[13] A. N. Saleemi, G. Steele, N. I. Pedge, A. Freeman, and Z. K. Nagy, *Enhancing crystalline properties of a cardiovascular active pharmaceutical ingredient using a process analytical technology based crystallization feedback control strategy,* International Journal of Pharmaceutics **430**, 56 (2012).

[14] M. R. Abu Bakar, Z. K. Nagy, A. N. Saleemi, and C. D. Rielly, *The impact of direct nucleation control on crystal size distribution in pharmaceutical crystallization processes,* Crystal Growth & Design **9**, 1378 (2009).

[15] A. G. Jones and A. Chianese, *Fines destruction during batch crystallization,* Chemical Engineering Communications **62**, 5 (1987).

[16] M. Jiang, X. Zhu, M. C. Molaro, M. L. Rasche, H. Zhang, K. Chadwick, D. M. Raimondo, K.-K. K. Kim, L. Zhou, Z. Zhu, M. H. Wong, D. O'Grady, D. Hebrault, J. Tedesco, and R. D. Braatz, *Modification of crystal shape through deep temperature cycling,* Industrial & Engineering Chemistry Research **53**, 5325 (2014).

[17] Z. Wu, S. Yang, and W. Wu, *Application of temperature cycling for crystal quality control during crystallization,* CrystEngComm **18**, 2222 (2016).

[18] M. R. A. Bakar, Z. K. Nagy, and C. D. Rielly, *Seeded batch cooling crystallization with temperature cycling for the control of size uniformity and polymorphic purity of sulfathiazole crystals,* Organic Process Research & Development **13**, 1343 (2009).

[19] K. Suwannasang, A. E. Flood, C. Rougeot, and G. Coquerel, *Using programmed heating–cooling cycles with racemization in solution for complete symmetry breaking of a conglomerate forming system,* Crystal Growth & Design **13**, 3498 (2013).

[20] C. Saltiel and A. K. Datta, *Heat and mass transfer in microwave processing,* in *Advances in Heat Transfer*, Vol. Volume 33, edited by T. F. I. Y. I. C. James P. Hartnett and A. G. George (Elsevier, 1999) pp. 1–94.

[21] R. Kacker, P. M. Salvador, G. S. Sturm, G. D. Stefanidis, R. Lakerveld, Z. K. Nagy, and H. J. Kramer, *Microwave assisted direct nucleation control for batch crystallization: Crystal size control with reduced batch time,* Crystal Growth & Design **16**, 440 (2015).

[22] H. Hojjati and S. Rohani, *Measurement and prediction of solubility of paracetamol in water−isopropanol solution. part 2. prediction,* Organic Process Research & Development **10**, 1110 (2006).

[23] Z. K. Nagy, E. Aamir, and C. D. Rielly, *Internal fines removal using population balance model based control of crystal size distribution under dissolution, growth and nucleation mechanisms,* Crystal Growth & Design **11**, 2205 (2011).

3

4

Residence Time Distribution of Dispersed Liquid and Solid Phase in a Continuous Oscillatory Flow Baffled Crystallizer

4

The use of a continuously operated oscillatory flow baffled crystallizer (COBC) has been promoted as a promising alternative crystallizer design for continuous crystallization because of the claim, based on dispersion of liquid, that plug flow can be achieved. Plug flow can lead to uniformity in product quality, if good control over nucleation and the growth of crystals is also achieved. In this study a residence time distribution (RTD) analysis was made for both homogeneous (methylene blue-water) and heterogeneous tracer system (melamine-water). In literature it is proposed, on the basis of homogeneous tracer experiments only, that the velocity ratio Ψ (the ratio between the oscillatory velocity and the superficial velocity of the imposed flow) is sufficient to identify optimal operating conditions for plug flow in COBC. Multiple combinations of amplitude and frequency result in the desired Ψ value. Our results show that operating at high amplitudes increases dispersion, reducing the plug flow like mixing. Thus Ψ alone is not sufficient for optimizing the mixing. Our study for the first time compares dispersion of homogenous and heterogeneous tracer in the commercially available DN15 system, addressing the knowledge gap in handling solids in COBC. Comparable responses were obtained with both the tracer systems for changes in the oscillatory flow variables. Operation at relative low amplitudes was optimal to obtain plug flow like behavior, even with 10 % (w/w) slurry with no problems of the particles settling. The optimal operating condition for minimal dispersion was clearly different for the homogenous and the heterogeneous system.

4.1. Introduction

Continuous production processes, especially in the pharmaceutical industry, are getting much attention in recent years due to their potential for cost reduction, improved process control and greater reliability [1]. Continuous operation in a stirred tank crystallizer is a popular choice, due to the advantage of utilizing the existent stirred tank equipment, infrastructure and operating knowledge [2]. However, challenges associated with the stirred tank systems, such as poor local mixing, low heat transfer rates and varying shear rates, result in non-uniform conditions in the crystallizer and as such in poor control of the crystal quality. Furthermore, a continuous crystallization process carried out in a single stirred tanks results in a broad residence time distribution (RTD), which is difficult to manipulate and leads to often undesired broad crystal size distributions, affecting the subsequent downstream processes in a production process. Especially the filtration and the tableting processes (in case of APIs) can be rendered inoperative, if the product specifications from the upstream processes are not met. To improve this situation, process flowsheets using cascades of mixed-suspension and mixed-product removal (MSMPR) crystallizers and recycle streams to boost the product yield have been investigated to achieve a better control over the product quality [3–7].

Alternatively, various configurations of the tubular crystallizer are being investigated in order to obtain a better control over the crystallization process, a few examples being the segmented or the slug flow crystallizers [8–11] and the oscillatory flow baffled crystallizer [12]. The continuous flow tubular crystallizers offer, improved heat transfer due to the large surface to volume ratio [13], homogeneous process conditions due to the controlled mixing as a result of the opportunity to operate in near plug flow regime and the ease of scalability through 'scale-out' approach [9]. Improved heat transfer under plug flow conditions enables a tight control over the local supersaturation in order to suppress unwanted nucleation and to achieve uniform growth conditions for the crystals [14]. The flexibility to vary the operating conditions over multiple segments, for example by multiple solvent addition points [14, 15] or tubular segments at different temperatures [16], offers additional degrees of freedom for process control. However, there are various challenges associated with tubular crystallizers. The most obvious being limited residence time and the high risk of scaling and unwanted nucleation due to the large surface area [17].

In a continuous oscillatory flow baffled crystallizer (COBC), mixing in radial and axial direction is achieved by interaction of the oscillating flow with the baffles. Interaction of the oscillating flow with the baffles generate eddies, inducing local turbulence and radial motion which results in uniform mixing in each inter-baffle region. Overall in a COBC, plug flow like behavior can be achieved at low superficial flow velocity by choosing the right operating amplitude and the frequency of oscillations [18]. Since it is claimed that the control over mixing in a COBC can be optimized independent of the flow rate, large residence times can be realized in relatively short tubes under proper oscillatory conditions avoiding poor mass transfer, settling of crystals and high dispersion [19]. These advantages make COBC an attractive option to carry out continuous crystallization; however optimal flow and oscillatory conditions for particulate systems still need to be investigated further.

The fluid dynamics in the COBC is characterized by a number of dimensionless numbers, namely the oscillatory Reynolds number (Re_o) based on maximum (peak) oscillation velocity giving a measure of the oscillatory mixing intensity, the Strouhal number (St), the Reynolds number (Re) based on the superficial velocity of the imposed flow and the velocity ratio Ψ (the ratio of Re_o to Re). A detailed discussion on the use of dimensionless numbers to characterize the flow in COBC along with their definitions can be found in the various communications [20–22]. The above mentioned dimensionless numbers are defined in set of equations in equation 4.1,4.2,4.3 & 4.4.

$$Re_o = \frac{2\pi f x_o \rho D}{\mu} \tag{4.1}$$

$$St = \frac{D}{4\pi x_o} \tag{4.2}$$

$$Re = \frac{D v \rho}{\mu} \tag{4.3}$$

$$\Psi = \frac{Re_o}{Re} \tag{4.4}$$

Where f is the frequency of oscillations (Hz), x_o is the center to peak oscillation amplitude (mm), D is the inner tube diameter (m), ρ is the fluid density ($kg/m3$), v is the superficial fluid velocity (m/s) and μ is the fluid viscosity ($kg/m.s$).

Many studies over several years, have characterized mixing in systems involving oscillatory flow in combinations with baffles, in batch or in continuous mode. Mostly the RTD using homogeneous tracers dispersed in the liquid continuous phase has been studied as a function of the operating conditions, parameterized in the form of dimensionless numbers Re, Re_o, St, Ψ and the dispersion number [21–29]. Various equipment configurations utilizing, vertical or horizontal baffled tubes of different internal diameters (ranging from 1.6 mm to 150 mm), multiple pistons or configurations with different baffle kinds [30], such as fixed or moving baffles and baffles with single or multiple orifices have been studied. A number of computational fluid dynamics studies on characterizing the radial velocity, the axial velocity and the dispersion as a result of the prevalent oscillatory flow conditions have also been reported [31–33]. The focus of the computational studies has been more on validating the model and limited links to the experimental results have been made. A study on simulating the effect of viscosity on axial dispersion showed that both radial and axial mixing are dominant at low viscosities and only axial mixing is dominant with a highly viscous fluid. The study concluded that an increase in the oscillation intensity can lead both to increased or decreased dispersion, depending on the viscosity [33].

Predominantly most of the studies have focused on dispersion of the liquid tracers injected in a liquid continuous phase, with conductivity measurements being popular choice to study the RTD by injecting a pulse of tracer. The studies have shown that a net Re number below 250 is preferred in order to avoid axial (back) mixing due to predominance of chaotic turbulence instead of the symmetric eddy generation across the baffles [34]. The ratio Ψ has been shown to be important for COBC operation

[35]. Minimized dispersion has been reported for values of Ψ in the range of 1.8-10 [34, 36, 37]. A fixed net flowrate (based on the desired residence time), fixes the corresponding Re number and depending on the chosen value of the ratio Ψ, the required Re_o becomes known. Based on this required Re_o, multiple combinations of the oscillation amplitude and the frequency can be chosen. From the literature, high oscillation amplitudes have been shown to be detrimental for maintaining low dispersion and changes in the frequency is relatively insignificant when compared to effect on dispersion due to the variation of the fluid oscillation amplitude [36]. Since a range of operational conditions can be chosen, depending on the application, and also the fact that various design configurations of the oscillatory flow baffled systems exist, a rapid determination of RTDs using a design of experiments of approach has been reported to facilitate the design of operation [38]. Based on a central composite design comprising of 20 experiment (at amplitudes ranging from 0.6-3.6 mm, frequency from 0.49-2.29 and flowrate from 86-304 ml/min) the RTD was determined using pH measurements and a second order model was fit to correlate the RTD with the operating parameters. The ratio Ψ equal to 1.9 was shown to minimize dispersion. Since the crystallization process involves slurries of varying density,studying liquid phase RTD alone is not sufficient. In a recent publication the same concern has been highlighted by the authors, and it is the only publication showing plug flow behavior of slurry in continuously operated down-scaled system called the meso-scale oscillatory flow reactor (having internal diameter ranging from 1-10 mm). Different geometrical designs (i.e. different baffle spacing, orifice diameter and smooth baffle or sharped edged baffle design) were tested and dispersion number calculated from dispersion model showed that plug flow was achieved with the slurry (10% w/w) [39]. Whereas in a COBC with 15 mm internal tube diameter, recently a demonstration of continuous seeded cooling crystallization of L-glutamic acid is demonstrated where a value of 20 for the ratio Ψ was used, which is high when compared to the recommended values of Ψ [40]. Efforts have been made to study, for example, the effect of tracer density on dispersion [41] with the conclusion that an increase in dispersion with higher densities of the liquid tracer was only predominant at low oscillatory mixing intensities. Moreover, handling of slurries in a COBC presents further challenges as highlighted in a comprehensive review on the application of COBC for crystallization processes [36]. A number of process parameters, especially high viscosity and solid content are identified to be critical and limiting for the performance of a crystallization process in the COBC. Apart from crystallization, COBC has also been investigated for other applications [42] and some learning on handling and dispersion of solids can be derived from there [43]. From a study on suspending polyamide particles (15 % w/w) in a novel oscillatory flow meso-reactor with smooth periodic constriction it was concluded, that a combination of a high frequency and low amplitude is best suited to suspend the particles. Operation of the oscillatory flow meso-reactor at high frequencies required the oscillation velocity to be not very high but comparable in magnitude with the settling velocity of the particles, for uniformly suspending the particles. Therefore significantly low amplitude of oscillations could be used [44]. On the contrary, in another study with a vertically oriented batch oscillatory baffle reactor, an increase in the oscillation velocity (irrespective of the combination of fre-

quency or amplitude) compared to the settling velocity of the particles, resulted in a more homogenous suspension of particles along the tube [45]. Nevertheless, an investigation of the dispersion of the solids in a crystallization process in a COBC and its consequence on crystallization kinetics is lacking.

In this study we have characterized the mixing and the dispersion in the commercially available DN15 COBC system from Nitech Solutions, using a homogeneous (liquid) and a heterogeneous (slurry) tracer, at various operating conditions. The details of the equipment are available in the section 4.2.1. As to our knowledge many research groups are investigating the application of COBC using DN 15 or similar set ups, but still a detailed characterization of the system in terms of the appropriate operating conditions for slurry handling is not reported, making this study a valuable contribution in understanding mixing behavior of solids/crystals which is directly relevant for continuous crystallization processes. Absorbance spectrometry was used to estimate the concentration of the homogenous tracer in the liquid continuous phase. A focused beam reflectance measurement (FBRM) was used to measure the heterogeneous tracer system through the counts of particles detected by FBRM. The effect of varying the net flow rate without any oscillation, the effect of change in frequency at fixed amplitude and vice versa and the effect of increasing COBC length on the dispersion of the homogenous tracer system was studied. Dispersion of the heterogeneous tracer was studied at different slurry concentrations (0.5%, 1%, 5% and 10% w/w). The operating conditions have been identified where dispersion can be minimized to achieve homogenous mixing which enables better control over supersaturation and particle concentrations and thus better control over the crystallization process.

4.2. Experimental methods and materials

4.2.1. COBC set-up

The COBC setup used in this study is DN15 LITE from NiTech Solutions, which consists of baffled glass straights (15 mm inner diameter) with jackets for heat exchange. The baffles are spaced at a distance of 1.5 times the inner diameter and the baffle orifice is measured to be 9 mm in diameter. In our system, the total volume of the setup is approximately 1 l. A PEEK piston, connected to a linear motor, generates the oscillations by coming in contact with the process fluid or slurry. The frequency of oscillations ranges from 0 to 5 Hz and the amplitude of the strokes of the piston from 0-70 mm. The residence time of the system depends on the flowrate. At a flowrate of 100 ml/min, typical residence time of around 10 minutes can be achieved.

The COBC startup procedure involved, filling the COBC with demineralized water which is the bulk phase in our study. Vigorous agitation was required to make the system air free. After this startup procedure, the desired oscillation amplitude and frequency was set and the setup was left to stabilize for at least 4-5 residence time. The feeding of water was achieved by a peristaltic pump (520s/REM, Watson Marlow). The jackets of the COBC tubes were connected to a water bath in order to maintain a constant temperature.
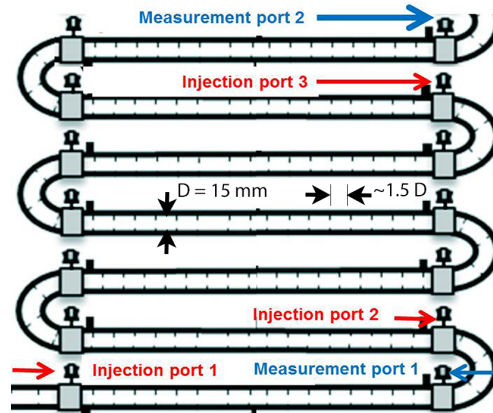
Figure 4.1: Schematic representation of the COBC setup showing the injections ports and the measurement ports used in the study.

4.2.2. Homogenous tracer system

Methylene blue (Sigma-Aldrich) was used as the homogeneous tracer system. A 1 ml pulse of 0.75 mg/ml of methylene blue in water was injected in a few seconds using a disposable 5 ml plastic syringe. Various tracer concentrations with density close to the density of water were tried before finalizing the concentration used. Low concentrations didn't give reliable RTD results as they were quickly dispersed and to dilute to measure. Very high concentrations close to the saturation/solubility of the methylene blue at 25 $°C$ results in a density of around 1.1 g/l. Therefore an intermediate concentration was chosen with density similar to water. To study the dispersion of the injected pulse as a function of the COBC length, injection was made at different locations in the COBC. The Figure 4.1 shows the schematic diagram of the COBC setup with the all injection and the measurement ports. Injection port 3 was used to achieve a short travel path for the tracer and the injection port 2 was used to achieve a longer path. Measurement port 2 was used to measure the tracer concentration for both the long and the short travel path for the tracer. The concentration was measured using in-situ absorbance spectrophotometry. The details of the method are given in the next section.

4.2.3. Absorbance spectrometry

In line spectrometry system from Ocean Optics consisting of a transmission probe (T300), a visible light source (DH-2000-BAL) and a spectrophotometer (HR2000+CG-UV-NIR) connected to the SpectraSuite software, was used to measure the absorbance spectra of methylene blue dye. The transmission probe was installed through a sampling joint which provided access to the flow within the COBC. Calibration was performed by correlating the measured absorbance with the dye concentration, by the preparing various concentrations of methylene blue in water. The peak height corresponding to 665 nm wavelength in the measured absorption spectra was linearly correlated to the dye concentration. This calibration was used to inter-

polate the concentration of the injected tracer in the COBC. The fit of the calibration curve is shown, in Figure 4.2.
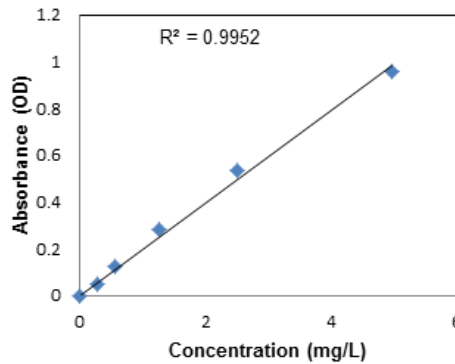
Figure 4.2: Calibration plot used for absorbance spectrometry; correlation of the measured absorbance with methylene blue concentration.

4.2.4. Heterogeneous tracer experiments

A suspension of melamine (mean particle size of 100 μm), supplied by DSM B.V., in water was chosen as the heterogeneous tracer system. The melamine slurry was prepared by adding 5 g, 10 g, 50 g and 100 g of melamine to 1 l of saturated solution of melamine in water at 30 °C to obtain different concentrations of the tracer system, 0.5 %, 1%, 5% and 10% (w/w) respectively. For the RTD study, a pulse of the melamine slurry was injected by pumping the prepared slurry through the injection port 1 (as shown in figure 4.1) using a peristaltic pump operating at a flowrate of 360 l/min for 15 seconds. Pumping for a short interval at comparatively high flowrate, ensured that a pulse with sufficient amount of melamine crystals was introduced into the COBC for clear detection by the FBRM probe as described in the next section 4.2.5. In separate experiments, measurement port 1 was used to measure and characterize the injected tracer pulse near the inlet and measurement port 2 was used to measure the tracer pulse at the exit. The choice of melamine crystals (elliptical and rounded particles) as the heterogeneous tracer, with an intermediate density value of 1.57 g/cm^3 is a good representation of crystals in a crystallization process. The settling velocity of the particles based on Newtonian drag regime is calculated to be 0.033 m/s.

4.2.5. Focused Beam Reflectance Measurement (FBRM)

FBRM has been used for measuring the counts of the melamine crystals, which allowed for tracking the melamine pulse and hence study the mixing and the dispersion of the injected heterogeneous tracer directly. The iC FBRM software provided by Mettler was used to record the data from the probe. Due to limited availability of the FBRM instrument the RTD study with slurry having the concentration of 0.5% and 1% (w/w) was carried by using FBRM, G400 unit (Metler Toledo). Whereas FBRM

G600 unit (Metler Toledo), was used when experiments with slurries having 5% and 10% (w/w) concentrations were carried out. In principle, both the unit use the same models for evaluating the signal obtained by FBRM and by ensuring the same positioning of the two systems, no difference due to the use of the two different FBRM units is expected. The measurement interval for the FBRM was set to 2 seconds in all experiments. The G400 unit with 9 mm tip diameter and the G600 unit with 18 mm tip diameter but with an active area having the measurement window of 11 mm in diameter were placed through a sampling port that allowed access to the flow inside the COBC. In principle, FBRM is a calibration free tool which directly gives a quantitative measure of the number of particles in the system. However, the dynamics of the particle, affected by the prevalent mixing conditions, influences the detected back scatter. For example, it is observed in a stirred reactor an increase in stirring intensity increases the counts which were being detected with the previous setting. This could be due to more number of particles passing through the focus of FBRM as a result of change in local particle concentration or the same particles are detected multiple times. In our case since a constant net flow ensured that the pulse of the tracer particles passed across the small focus region of the FBRM probe, a clear detection of the pulse from the start to the end could be made. The background noise which is usually present in FBRM has been subtracted by processing the counts data obtained from the FBRM in the commercial software package MATLAB (R2014b, MathWorks).

4.2.6. Analysis of the pulse (concentration and the count data)

Since our injection procedure lasts only for 2-3 seconds compared to the average residence time of 10 minutes in the COBC, the tracer injection can be assumed to be a pulse. Because, the shot of tracer injected is immediately dispersed by the flow oscillation present at the time of injection, the dispersion of the RTD measured downstream (spanning over 100 seconds) compared to the dispersion due to the injection process can be been assumed to be insignificant, justifying the assumption of the pulse injection. In general, the measured tracer concentration profiles can be used to estimate the dispersion coefficient or the vessel dispersion number, by using various models, for example dispersion or tank in series model. E-curve which is the normalized concentration profile is preferred over the F-curves (the integral of E-curves which smooth outs the data/signal) to model dispersion. Since the COBC in principle has open boundaries, E-curve cannot be obtained by simply dividing the concentration profiles by the initial pulse concentration [46]. Especially, in case of the heterogeneous tracer where we measure the particle counts and not directly the concentration of the tracer, hence application of E-curve is not justified.

Nevertheless, each pulse can be evaluated independently and the simplest way to study dispersion of the injected pulse at the exit of the COBC is to analyze the standard deviation σ (s) of the measured signal X $(mg/lor\#)$ from the mean residence time $\bar{t}$ (s), for both the studied tracer systems. The expressions used to calculate $\bar{t}$ and σ are expressed in set of equations, equation 4.5, 4.6, 4.7, 4.8.

$$\tau = \frac{V}{Q} \tag{4.5}$$

$$X_o = \int_0^{\text{inf}} X(t)dt \tag{4.6}$$

$$\bar{t} = \frac{\int_0^{\text{inf}} X(t)dt}{X_o} \tag{4.7}$$

$$\sigma = \sqrt{\frac{\int_0^{\text{inf}} (t - \bar{t})^2 X(t)dt}{X_o}} \tag{4.8}$$

4

Where X_o ($mg/lor\#$) is the area under the signal curve. τ (s) is the expected residence time in case of an ideal plug flow, calculated as shown in equation 4.5, where V (m^3) is total volume of the COBC and Q (m^3/s) is the flowrate of the bulk phase maintained through the COBC. Thus by evaluation of σ (s), the spread of the signal/tracer can be obtained, which can be used as an indication of dispersion as in ideal case $\bar{t}$ and σ^2 is directly linked to the dispersion theory [46]. A convenient approach to estimate the dispersion number ($D/\mu L$) is to match the experimental σ^2 to the analytical solution based on dispersion model for the ideal case of open-open boundary conditions as shown in equation 4.9 [47]. Alternatively the dispersion number can be obtained by direct fitting of the E-curve to the analytical solution for dispersion model with open-open boundaries. The trends reported by estimating dispersion number based on equation 4.3 are similar to the results obtained by fitting the E-curves directly. Care has been taken and the model is not applied to highly skewed profiles (Figure 4.6: heterogeneous tracer profile near the inlet). The dispersion numbers have been obtained by least square minimization using Microsoft Excel.

$$\frac{\sigma^2}{\bar{t}^2} = 2\frac{D}{\mu L} + 8(\frac{D}{\mu L})^2 \tag{4.9}$$

Where D (m^2/s) is the dispersion coefficient, u (m/s) is the superficial velocity due to the net flow and L (m) is the length of the COBC (path travelled by the tracer). In order to compare the results for experiments with different expected residence times the standard deviation σ (s) can be scaled by dividing by τ (s). The value σ/τ so obtained is the similar if ideally E-curves plotted against dimensionless time were used to calculate the standard deviations. Thus ratio σ/τ has been used to compare the spread of the RTD across experiments with different expected residence time. Moreover the dispersion number ($D/\mu L$) is used to quantify dispersion and can be directly compared across all experiments. Ratio of $\bar{t}/\tau$ can also be used as a measure of deviation from ideal plug flow. Non idealities in flow conditions such as back mixing or dispersion will result in the deviation of the ratio $\bar{t}/\tau$ from the ideal value of 1.

4.3. Results & Discussions

The results from the RTD study carried out with the two tracer systems are presented in this section. The effect of operating at different flowrates, fixed at 100, 200 and 400 ml/min (without any oscillation) on the mixing and dispersion of the homogenous tracer system has been studied. As in most crystallization processes the residence time is an important process variable for achieving crystals of the desired size and quality. In a COBC setup variations in residence times can easily be achieved by variation of the length of the crystallizer without altering the required throughput. Therefore, the effect of COBC length on tracer dispersion is studied by injecting the homogenous tracer at locations close to and far from the measurement port. The effect of operating the COBC at different frequencies and amplitudes of fluid oscillations has been studied in detail at the fixed flowrate of 100 ml/min. The discussion on choosing the best operating conditions to achieve the optimal turbulence with minimal dispersion is also presented in this section. A minimum of two, if not three, repeats for each operating condition has been carried out and the average values are reported.

4.3.1. Effect of flowrate without oscillatory mixing

The baffled design of the COBC facilitates mixing even in the absence of flow oscillation. This is due to the presence of the baffles which induce the expansion and contraction of the flow, as it passes through the baffle orifice. A pulse of methylene blue (homogeneous tracer system as described in section 4.2.4) was injected at the injection port 3 and measured near the exit at the measurement port 2 (refer Figure 4.1). Thus the tracer covered a distance comprising of two baffled tubes and a U-bend connector (in total 1.65 m in length). The tested flow rates of 100, 200 to 400 ml/min corresponded to the expected residence times of 175, 87.5 and 43.75 seconds respectively. The results in Figure 4.3, shows the dimensionless E-curve against the dimensionless time and the effect of flowrate on RTD is quantified in Table 4.1. The table 4.1 summarizes the tested flowrates, the corresponding Reynolds number (based on tube diameter), the calculated ratios $\bar{t}/\tau$, σ/τ and the dispersion number. The Reynolds numbers were 141, 283 and 565, which in a tube without baffles would represent laminar flow regime. The calculated σ/τ values and the dispersion number in Table 4.1 ranging from 0.29 to 0.19 and 0.033 to 0.019 respectively confirmed the decreased dispersion at the high flowrates. The interactions with baffles promote turbulence and radial mixing, especially at high flow rate of 400 ml/min where the least dispersion of the tracer is observed. At lower flowrates, the wider spread is due to the longer hold-up of the tracer in the COBC. The wider RTD could be the result of the radial mixing by the eddies being more significant than the advection by the axial flow through the baffle orifice.

4.3.2. Effect of amplitude: fixed frequencies and fixed flowrate of 100 ml/min

Similar to previous experiments, a pulse of methylene blue (homogeneous tracer system) was injected at the injection port 3 and measured near the exit at the mea-
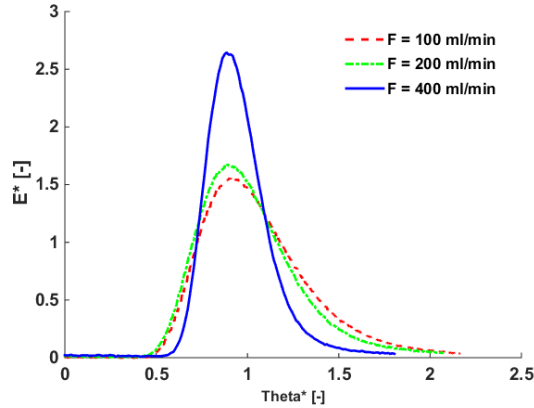
Figure 4.3: Dimensionless E-curve of the homogeneous tracer injected at the injection port 3 and measured at the measurement port 2 without any fluid oscillations, by varying the flowrates with corresponding $Re = 141, 283\ and\ 565$ respectively.

Table 4.1: Operating flowrates, Re, $\bar{t}/\tau$, σ/τ and dispersion number for experiments performed with homogeneous tracer and without any oscillations at various flow rates. Tracer was injected at injection port 3 and measured at measurement port 2.

Flowrate (ml/min)	Re	$\bar{t}/\tau$	σ/τ	$D/\mu L$
100	141	1.06	0.29	0.033
200	283	1.01	0.28	0.034
400	565	0.95	0.19	0.019

surement port 2 (refer Figure 4.1). At fixed frequencies of 1, 2 and 4 Hz, the amplitude of flow oscillations was varied. The measured tracer concentration profiles are shown in figure 4.4 for the frequencies 1, 2 and 4 Hz respectively.

Figure 4.4 shows that the dispersion of the tracer changes significantly with changes in amplitude. The effect of the different amplitudes on the concentration profiles was different for the three frequencies. The concentration profiles measured at the frequency of 2 Hz shows only small effect of the change in amplitude. The experiments performed at the frequency of 1 and 4 Hz show a clear increase in the dispersion on increasing the operating amplitude. Further, there is no common amplitude at which the dispersion is minimized at all the three frequencies studied. A range of amplitudes can be determined for each frequency, where minimal dispersion can be achieved. The concentration profiles are also not symmetric, which could be due to back mixing or due to the injection procedure which can cause local disturbance to the mixing during the short injection time. Table 4.2, summarizes the experimental conditions and the tracer dispersion, giving the operating amplitude, Re_o, the ratios Ψ, $\bar{t}/\tau$, σ/τ and the dispersion number.

On comparing the values of σ/τ and dispersion numbers, for at least the frequencies of 1 and 2 Hz, multiple operating amplitude can be identified which results in
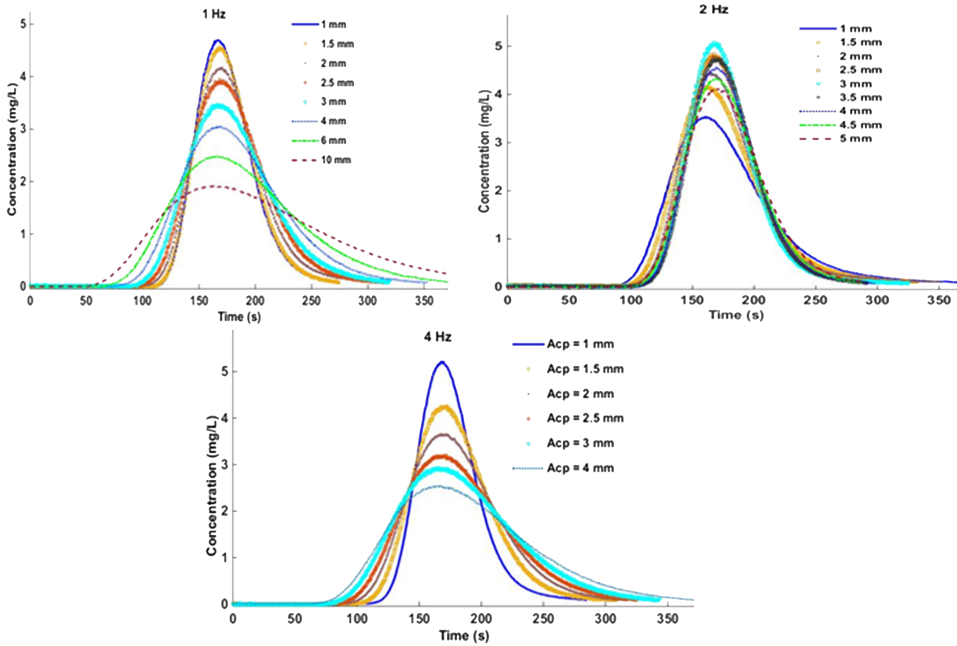
Figure 4.4: Concentration profile of the homogeneous tracer injected at the injection port 3 and measured at the measurement port 2, as a result of varying the amplitude at fixed oscillation frequency of 1, 2 and 4 Hz respectively and a fixed flow rate of 100 ml/min ($Re = 141$).

values of σ/τ within ±5% of the minimum value. Deviations from the optimum amplitude range results in enhanced dispersion of tracer concentration profile. Values of ratio Ψ corresponding to the minimal dispersion can be identified to be 0.67, 5.33 and 2.66, for the operating frequency of 1, 2 and 4 Hz, respectively. Clearly the optimum value of Ψ is a function of the frequency. Values of Ψ in the range of 2-10 are reported in literature for achieving plug flow behavior with minimized dispersion, but we observed minimized dispersion at Ψ equal to 0.67 outside the optimal range and a very high dispersion at value of Ψ equal to 6.66 inside this optimal range. Therefore no generalization based on the values of ratio Ψ could be made. Overall, the results show the benefits of the flow oscillation on controlling the dispersion of the tracer, especially when comparison is made with operation without any oscillatory mixing at the same flowrate of 100 ml/min flowrate (Table 4.1). The condition for minimizing dispersion is lost when operation is outside the optimal combination of the frequency and the amplitude, especially when operating at high amplitudes. For example, for operation with 1 Hz and 10 mm as the flow oscillation frequency and amplitude, the value of σ/τ is 0.43, which is worse than the case of having no oscillation at the same flowrate of 100 ml/min, where the value of σ/τ was calculated to be 0.29.

Operating at suboptimal operating configurations, probably leads to an imbalance between radial and axial mixing, leading chaotic behavior of the flow which increases

Table 4.2: Operating amplitude, Re_o, Ψ, $\bar{t}/\tau$, σ/τ and dispersion number corresponding to RTDs at measurement port 2 for homogeneous tracer injected at injection port 3 at frequencies of 1,2 and 4 Hz respectively. At a constant flow rate of 100 ml/min.

Amplitude (mm)	Re_o	Ψ	$\bar{t}/\tau$	σ/τ	$D/\mu L$
Fixed frequency of 1 Hz					
1	94	0.67	0.99	0.146	0.010
1.5	141	1.00	1.00	0.149	0.011
2.0	188	1.33	1.02	0.201	0.018
2.5	236	1.67	1.03	0.205	0.018
3.0	283	2.01	1.04	0.238	0.024
4	377	2.66	1.06	0.268	0.028
6	565	4.00	1.09	0.322	0.037
10	942	6.66	1.16	0.429	0.056
Fixed frequency of 2 Hz					
1.0	188	1.33	1.03	0.286	0.034
1.5	283	1.99	1.02	0.241	0.025
2.0	377	2.66	1.05	0.281	0.032
2.5	471	3.33	1.01	0.205	0.019
3.0	565	3.99	1.01	0.197	0.018
3.5	660	4.66	1.02	0.172	0.014
4.0	754	5.33	1.02	0.172	0.014
4.5	848	5.99	1.02	0.175	0.014
5.0	942	6.66	1.03	0.185	0.016
Fixed frequency of 4 Hz					
1.0	377	2.66	1.01	0.164	0.013
1.5	565	3.99	1.03	0.190	0.016
2.0	754	5.33	1.04	0.217	0.020
2.5	942	6.66	1.05	0.245	0.025
3.0	1131	7.99	1.06	0.276	0.030
4.0	1508	10.66	1.09	0.323	0.038

dispersion. The same effect, increased dispersion upon increasing the amplitude to 8, 12 and 16 mm was observed, when the tracer was injected at injection port 2 and measured at the measurement port 2, thus allowed to travel a longer path in the COBC (5.4 m, see Figure 4.1). Table 4.3 summarizes the operating conditions and the calculated value of the ratio $\bar{t}/\tau$, σ/τ and dispersion number resulting from the variation of the amplitude for the case of longer COBC configuration. We observe from the values of σ/τ and the dispersion numbers, that the dispersion of the tracer concentration profile increases as the amplitude of fluid oscillation is increased. This is in line with our observation with previous experiments at the frequency of 2 Hz and various amplitudes, where also increasing amplitude above 4 mm lead to increased dispersion.

Table 4.3: Frequency, Amplitude, Re_o, Ψ, $\bar{t}/\tau$,σ/τ and dispersion number for experiments performed at fixed frequency of 2 Hz and at various operating amplitudes, with tracer injected at injection port 2 and measured at measurement port 2, at fixed flow rate of 100 ml/min.

Frequency (Hz)	Amplitude (mm)	Re_o	Ψ	$\bar{t}/\tau$	σ/τ	$D/\mu L$
2	8	1508	10.66	1.10	0.236	0.021
2	12	2262	15.99	1.19	0.329	0.033
2	16	3016	21.32	1.29	0.421	0.045

4.3.3. Effect of frequency: Fixed center to peak Amplitude of 1 mm and Flow rate of 100 ml/min

Experiments were performed in which the amplitude was fixed at 1 mm and the frequency was varied. The tracer was injected at injection port 3 and measured at measurement port 2. Table 4.4 lists the operating conditions and the calculated value of the ratio $\bar{t}/\tau$, σ/τ and dispersion number. Based on a deviation range of approximately ±5% from the minimum value of σ/τ , multiple operating frequencies can be chosen. Figure 5, shows the tracer concentration profiles for multiple operating frequencies at fixed amplitude of 1 mm. It can be seen that changing the operating frequency from 1 Hz to 1.5 and from 2 or 2.5 Hz, the tracer dispersion increases. Operating with frequencies ranging from 3 to 5 Hz minimized the dispersion. We suspect since operation frequency is responsible for rate of eddy generation, depending of the geometry of the OFR (baffle spacing, l/D ratio and the baffle constriction opening area) there could be an imbalance between eddy generation and propagation at the intermediate frequencies. However it is a possible hypothesis and requires a more fundamental approach to study the dynamics of the mixing at different frequencies. Interestingly, for minimizing dispersion for operation at 1 mm as the flow oscillation amplitude, both a high and a low operating frequency can be chosen, 1 and 5 Hz. With respect to the design of the operation conditions of the COBC, choosing a low or a high frequency results in different Re_o numbers (Table 4.4). Higher Re_o numbers corresponds to a higher local mixing intensity and hence higher local fluid velocities. Variation of local mixing intensities at different choices of the operating conditions, could in turn, lead to varying kinetics of the crystallization process i.e. impacting the growth or the secondary nucleation process.

4.3.4. Effect of COBC length on dispersion for operation at optimal settings

By injecting the tracer at injection port 2 and measuring the tracer at the measurement port 2, the distance travelled by the tracer was increased to approximately 5.4 m in length. The flowrate was kept the same at 100 ml/min for the two optimal configurations, 2 Hz & 4 mm and 4 Hz & 1 mm, which minimized dispersion of the tracer in the previously discussed experiments. The two tracer concentration profiles look similar, in agreement with the previous experiments at the two optimal operating configuration of the COBC. Table 4.5, summarizes the operating conditions and the calculated values of the ratio $\bar{t}/\tau$, σ/τ and dispersion number. The σ/τ values

Table 4.4: Operating frequency, Re_o, Ψ, $\bar{t}/\tau$, σ/τ and dispersion number corresponding to RTDs at measurement port 2 for homogeneous tracer injected at injection port 3 at various frequencies at a fixed amplitude of 1 mm and a flow rate of 100 ml/min.

Frequency (Hz)	Re_o	Ψ	$\bar{t}/\tau$	σ/τ	$D/\mu L$
1.0	94	0.67	0.99	0.146	0.010
1.5	141	1.00	1.01	0.201	0.018
2.0	188	1.33	1.03	0.289	0.034
2.5	236	1.67	1.00	0.206	0.019
3.0	283	2.00	0.99	0.157	0.012
3.5	330	2.33	1.00	0.149	0.011
4.0	377	2.66	1.01	0.164	0.013
5.0	471	3.33	0.99	0.144	0.010

4
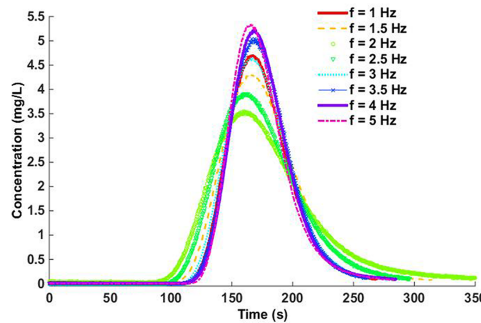
Figure 4.5: Concentration profile of the homogeneous tracer injected at the injection port 3 and measured at the measurement port 2, as a result of varying the frequency at fixed oscillation amplitude of 1 mm and a fixed flow rate of 100 ml/min (Re141).

are in the same order of magnitude when compared to the values of σ/τ with the shorter COBC configuration, even though the absolute numbers are slightly lower. The disturbance of the flow momentarily due to the tracer injection process could be a reason for the somewhat larger values of σ/τ in the shorter COBC configuration. Increasing the distance of the injection port from the measurement port will dampen the disturbance related to the pulse injection. Therefore it can be concluded that longer residence times can be realized by extending the length of the COBC without consequences to the dispersion behavior, which should be the case unless the fluid dynamics/mixing changes.

4.3.5. Dispersion of heterogeneous tracer system

A pulse of the heterogeneous tracer system (slurry of melamine in water) was introduced by pumping the slurry in at the injection port 1 for a short duration and the tracer pulse was measured at the measurement port 1 (see fig. 4.1). Experiments were designed around the previously observed optimal configuration of 2 Hz and 4 mm for the homogeneous tracer system. The flow rate of the continuous phase

Table 4.5: Frequency, Amplitude, Re_o , Ψ, $\bar{t}/\tau$, σ/τ and dispersion number corresponding to RTDs from the experiments performed at two optimum operating configuration using homogeneous tracer injected at injection port 2 and measured at measurement port 2 and at a fixed flow rate of 100 ml/min.

Frequency (Hz)	Amplitude (mm)	Re_o	Ψ	$\bar{t}/\tau$	σ/τ	$D/\mu L$
2	4	754	5.33	1.04	0.117	0.006
4	1	377	2.66	1.03	0.138	0.008

(water) was maintained to be 100 ml/min and the local concentration of the injected tracer particles was estimated in terms of the number of particles measured by the FBRM, placed at the measurement port 1. In a separate set of experiments, the tracer was injected at injection port 1 and measured by FBRM at measurement port 2 (see fig.4.1). Measuring the tracer particles at measurements port 1 and 2 allowed us to characterize the injected pulse of the tracer, shortly after injection as well as at the exit of the COBC. Ideally measuring the same pulse at the two locations is preferred but due to availability of only one FBRM probe, two independent sets of experiments at each operating conditions, were carried out. Figure 4.6 shows the counts of the injected tracer particles measured by the FBRM at measurement port 1, for two different tracer concentrations of 0.5 and 1 % (w/w). At the used frequency of 2 Hz, high amplitudes result in broader distributions of the particle counts and hence increased dispersion. Especially at the operating amplitude of 8 mm, for both the tracer concentrations, a long tail in the particle counts distribution is visible. The long tail in the concentration profiles could be caused by the holdup in the inter baffle compartments due to the increased turbulence as the amplitude is increased. Most likely the asymmetric nature of profile with the long tail is caused by the injection procedure which causes disturbance to the flow, due to pumping, during the injection period of 15 seconds. Approximately 70% of the volume in the first tube is replaced by the tracer and pulse is smeared out by the oscillations especially at the higher amplitudes, which explains the strong effect of amplitude on the dispersion of the tracer profiles and the skewed nature of the profiles.
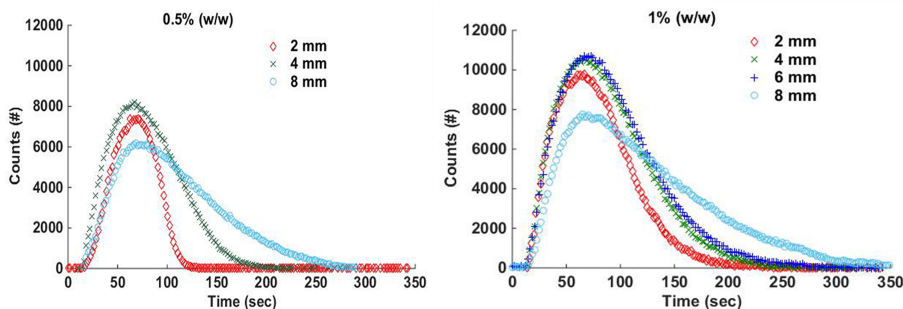

Figure 4.6: Particle counts distribution, measured by FBRM at the end of first baffled tube (injected at injection port 1 and measured at measurement port 1), at various operating amplitudes with operating frequency fixed at 2 Hz and fixed flowrate of 100 ml/min ($Re141$).

Figure 4.7, shows the counts distribution measured at measurement port 2 for the tracer concentrations of 0.5%, 1% and 5% (w/w) respectively, injected at injection port 1 (longer COBC configuration). Due to the longer residence time spent by the tracer in the COBC, the counts profiles shown in Figure 4.7 is not specifically skewed when compared to the counts profiles of the tracer measured near the inlet (shown in Figure 4.6). The disturbance during the injection of the tracer is not visible anymore due to the dispersion of the pulse in the long tube. A clear rise in the number of counts can be seen with the increase in tracer concentrations. However at high concentrations of 5% (Figure 4.7), the difference in the peak counts at different operating amplitudes is not large. The same is observed when tracer concentration of 10% (w/w) was used (not shown in figure for brevity). Due to the optical properties of melamine at the high concentrations of 5% and 10% (w/w), the change in particle counts detected by FBRM is much less, and not linear with the change in concentration of the tracer. This explains the relatively low change in peak values of counts profiles observed with tracer having a concentration of 5% (w/w). Separately in a batch stirred vessel with ideal FBRM positioning, the number of counts has been recorded at increasing melamine concentrations (up to 15% w/w), and the same loss in the linearity in the number of counts as function of the concentration of melamine has been observed (data not shown). No settling of crystals at these high concentrations was observed and the results clearly show that an increase in the operating amplitude results in an increase in the spread of the concentration profile. Table 4.6, summarizes the operating conditions, the calculated ratios Ψ, $\bar{t}/\tau$, σ/τ and dispersion number for the four tracer concentrations studied. Increase in the amplitude of operation, leads to a larger axial dispersion due to the increased turbulence, changing the balance between the radial and the axial mixing. This is confirmed by the trends in the dispersion number and the mean residence time. The values of σ/τ (Table 4.6), based on the counts profile of the longer COBC configuration are in line with the observation made from the homogenous tracer study. Interestingly, $\bar{t}/\tau$ values (Table 4.6) obtained with the heterogeneous tracer system is larger when compared to the values observed with the homogenous tracer. The observation of larger $\bar{t}/\tau$ values suggests that solids spend a longer time in the COBC system. This observation is in line with the similar conclusion drawn in a recent publication [39]. Most importantly, our observation suggest that mixing intensity achieved at low amplitudes of operation is sufficient to suspend the four slurry concentrations tested and to obtain plug flow like mixing of the solid particles. Operation at 2 Hz and 2 mm gave minimal dispersion which is different from the optimal values observed with the homogenous tracer. Operation at high amplitudes lead to larger dispersion, similar to the homogeneous tracer, which suggests that melamine crystals in our case flow in phase with the fluid streamlines. The dispersion numbers reported in Table 4.5 for homogeneous tracer at optimal operation of COBC are comparable to dispersion numbers observed with heterogeneous system at optimal operating condition.

Our results show that there are many similarities between the mixing behavior of the homogenous and the heterogeneous tracer system. On the other hand the optimal conditions for the two systems were clearly different, and a warning must be issued not to translate directly the results of the homogeneous tracer experiment
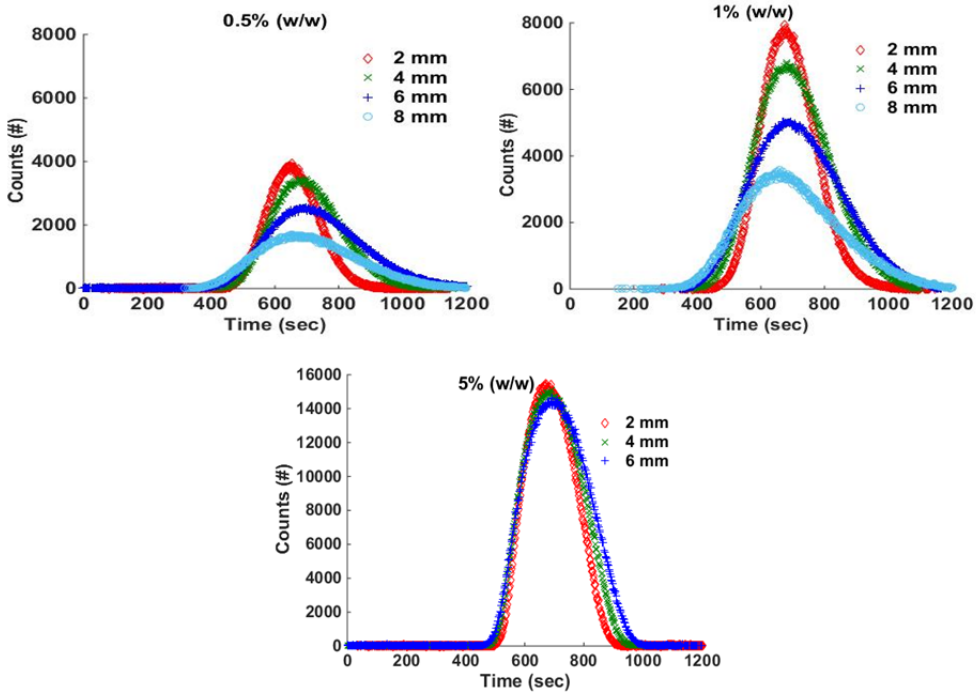
Figure 4.7: Particle counts distribution, measured by FBRM at the exit of COBC for tracer injected at injection port 1, at various operating amplitudes with operating frequency fixed at 2 Hz and fixed flowrate of 100 ml/min (Re141).

to a heterogeneous system. In addition one has to realize that in this study we have not been able to examine the influence of the whole spectrum of operating conditions and the properties of the suspension on the flow behavior. We have limited our research to relative low frequencies and have not examined the influence of wettability, shape and size of the particles In addition more research should be done, multiple optimum operating points that were discovered in the homogeneous tracer experiments, which are not discovered yet for the heterogeneous system.

4

Table 4.6: Frequency, Amplitude, Re_o , Ψ, $\bar{t}/\tau$ and σ/τ for experiments performed with heterogeneous tracer inject at injection port 1 and measured at measurement port 2 by varying amplitude at fixed frequency of 2 Hz and at fixed flow rate of 100 ml/min.

Frequency(Hz)	Amplitude(mm)	Re_o	Ψ	$\bar{t}/\tau$	σ/τ	$D/\mu L$
Tracer concentration 0.5% (w/w)						
2	2	377	2.67	1.14	0.125	0.005
2	4	754	5.34	1.23	0.151	0.007
2	6	1131	8.02	1.28	0.239	0.016
2	8	1508	10.69	1.26	0.245	0.018
Tracer concentration 1% (w/w)						
2	2	377	2.67	1.21	0.102	0.003
2	4	754	5.34	1.24	0.154	0.007
2	6	1131	8.02	1.26	0.184	0.010
2	8	1508	10.69	1.23	0.228	0.017
Tracer concentration 5% (w/w)						
2	2	377	2.67	1.21	0.139	0.006
2	4	754	5.34	1.22	0.160	0.008
2	6	1131	8.02	1.24	0.184	0.011
Tracer concentration 10% (w/w)						
2	2	377	2.67	1.22	0.164	0.009
2	4	754	5.34	1.24	0.179	0.010
2	6	1131	8.02	1.28	0.226	0.015

4.4. Conclusions

The results of the RTD study carried out using both homogeneous and heterogeneous tracer systems with DN15 COBC system have been discussed. The experiments using homogeneous tracer system showed that the dispersion can be minimized by operating at optimal oscillatory conditions. The parameter Ψ often reported in literature is not sufficient to choose the optimum operation condition of the COBC, as we observed multiple conditions (with different values of Ψ) where dispersion was minimized. Each optimal condition represented a different mixing intensity which could in turn affect the local crystallization kinetics and result in different product quality. We have reported optimum velocity ratio outside the range of 1.8 to 10 reported in literature and have also observed sub-optimal operation (high dispersion) within the suggested velocity ratio range. In general, operating with high amplitudes of fluid oscillations resulted in increased dispersion, which is in agreement with the knowledge in literature. Whereas both high and low frequencies were identified to be optimal for minimizing dispersion, from experiments carried out at fixed amplitude of $1\ mm$. The results with longer COBC configuration showed that extending the COBC has no consequence on the mixing and hence dispersion of the dispersed phase. Good control over dispersion with longer COBC configurations allows for longer residence time to be realized and hence make COBC available for processes with relatively slower kinetics. The gap in knowledge on handling solids in a COBC is addressed by showing that operation at $2\ Hz$ and $2\ mm$ was optimal to suspend the melamine crystals and obtain a plug flow like residence time distribution at four different slurry concentrations. The optimal settings for the oscillatory flow parameters are different from the optimal operation point observed with the homogenous tracer. The mean residence time shows that heterogeneous tracer has longer residence time in the system, which is in agreement in the only literature where RTD with solid tracer was studied. For processes with fast kinetics precise knowledge on residence time helps in having a good control over the end of the process and hence the product quality. Overall, with respect to crystallization process, the two systems studied show that careful characterization of the dispersed phase is required in order to effectively operate the COBC.

References

[1] S. Mascia, P. L. Heider, H. Zhang, R. Lakerveld, B. Benyahia, P. I. Barton, R. D. Braatz, C. L. Cooney, J. M. B. Evans, T. F. Jamison, K. F. Jensen, A. S. Myerson, and B. L. Trout, *End-to-end continuous manufacturing of pharmaceuticals: Integrated synthesis, purification, and final dosage formation,* Angewandte Chemie International Edition **52**, 12359 (2013).

[2] Q. Su, Z. K. Nagy, and C. D. Rielly, *Pharmaceutical crystallisation processes from batch to continuous operation using msmpr stages: Modelling, design, and control,* Chemical Engineering and Processing: Process Intensification **89**, 41 (2015).

[3] S. Ferguson, F. Ortner, J. Quon, L. Peeva, A. Livingston, B. L. Trout, and A. S. Myerson, *Use of continuous msmpr crystallization with integrated nanofiltration membrane recycle for enhanced yield and purity in api crystallization,* Crystal Growth and Design **14**, 617 (2014).

[4] G. Power, G. Hou, V. K. Kamaraju, G. Morris, Y. Zhao, and B. Glennon, *Design and optimization of a multistage continuous cooling mixed suspension, mixed product removal crystallizer,* Chemical Engineering Science **133**, 125 (2015).

[5] J. L. Quon, H. Zhang, A. Alvarez, J. Evans, A. S. Myerson, and B. L. Trout, *Continuous crystallization of aliskiren hemifumarate,* Crystal Growth and Design **12**, 3036 (2012).

[6] J. S.-I. Kwon, M. Nayhouse, P. D. Christofides, and G. Orkoulas, *Modeling and control of crystal shape in continuous protein crystallization,* Chemical Engineering Science **107**, 47 (2014).

[7] S. Y. Wong, A. P. Tatusko, B. L. Trout, and A. S. Myerson, *Development of continuous crystallization processes using a single-stage mixed-suspension, mixed-product removal crystallizer with recycle,* Crystal Growth and Design **12**, 5701 (2012).

[8] S. Guillemet-Fritsch, M. Aoun-Habbache, J. Sarrias, A. Rousset, N. Jongen, M. Donnet, P. Bowen, and J. Lemaître, *High-quality nickel manganese oxalate powders synthesized in a new segmented flow tubular reactor,* Solid State Ionics **171**, 135 (2004).

[9] R. Vacassy, J. Lemaitre, H. Hofmann, and J. Gerlings, *Calcium carbonate precipitation using new segmented flow tubular reactor,* AIChE Journal **46**, 1241 (2000).

[10] N. Jongen, M. Donnet, P. Bowen, J. Lemaître, H. Hofmann, R. Schenk, C. Hofmann, M. Aoun-Habbache, S. Guillemet-Fritsch, J. Sarrias, A. Rousset, M. Viviani, M. T. Buscaglia, V. Buscaglia, P. Nanni, A. Testino, and J. R. Herguijuela, *Development of a continuous segmented flow tubular reactor and the "scale-out" concept – in search of perfect powders,* Chemical Engineering and Technology **26**, 303 (2003).

[11] R. J. P. Eder, S. Schrank, M. O. Besenhard, E. Roblegg, H. Gruber-Woelfler, and J. G. Khinast, *Continuous sonocrystallization of acetylsalicylic acid (asa): Control of crystal size,* Crystal Growth and Design **12**, 4733 (2012).

[12] S. Lawton, G. Steele, P. Shering, L. Zhao, I. Laird, and X.-W. Ni, *Continuous crystallization of pharmaceuticals using a continuous oscillatory baffled crystallizer,* Organic Process Research and Development **13**, 1357 (2009).

[13] R. J. P. Eder, S. Radl, E. Schmitt, S. Innerhofer, M. Maier, H. Gruber-Woelfler, and J. G. Khinast, *Continuously seeded, continuously operated tubular crystallizer for the production of active pharmaceutical ingredients,* Crystal Growth and Design **10**, 2247 (2010).

[14] A. J. Alvarez and A. S. Myerson, *Continuous plug flow crystallization of pharmaceutical compounds,* Crystal Growth and Design **10**, 2219 (2010).

[15] B. J. Ridder, A. Majumder, and Z. K. Nagy, *Population balance model-based multiobjective optimization of a multisegment multiaddition (msma) continuous plug-flow antisolvent crystallizer,* Industrial and Engineering Chemistry Research **53**, 4387 (2014), cited By :5 Export Date: 20 October 2015.

[16] A. Majumder and Z. K. Nagy, *Fines removal in a continuous plug flow crystallizer by optimal spatial temperature profiles with controlled dissolution,* AIChE Journal **59**, 4582 (2013).

[17] G. Cogoni, B. P. de Souza, and P. J. Frawley, *Particle size distribution and yield control in continuous plug flow crystallizers with recycle,* Chemical Engineering Science **138**, 592 (2015).

[18] T. Howes and M. R. Mackley, *Experimental axial dispersion for oscillatory flow through a baffled tube,* Chemical Engineering Science **45**, 1349 (1990).

[19] X. Ni, M. R. Mackley, A. P. Harvey, P. Stonestreet, M. H. I. Baird, and N. V. Rama Rao, *Mixing through oscillations and pulsations—a guide to achieving process enhancements in the chemical and process industries,* Chemical Engineering Research and Design **81**, 373 (2003).

[20] X. Ni and P. Gough, *On the discussion of the dimensionless groups governing oscillatory flow in a baffled tube,* Chemical Engineering Science **52**, 3209 (1997).

[21] A. W. Fitch and X. Ni, *On the determination of axial dispersion coefficient in a batch oscillatory baffled column using laser induced fluorescence,* Chemical Engineering Journal **92**, 243 (2003).

[22] M. R. Mackley and X. Ni, *Mixing and dispersion in a baffled tube for steady laminar and pulsatile flow,* Chemical Engineering Science **46**, 3139 (1991).

[23] X. Ni, *Residence time distribution measurements in a pulsed baffled tube bundle,* Journal of Chemical Technology and Biotechnology **59**, 213 (1994).

[24] P. Gough, X. Ni, and K. C. Symes, *Experimental flow visualisation in a modified pulsed baffled reactor,* Journal of Chemical Technology and Biotechnology **69**, 321 (1997).

[25] X. Ni and N. E. Pereira, *Parameters affecting fluid dispersion in a continuous oscillatory baffled tube,* AIChE journal **46**, 37 (2000).

[26] M. Palma and R. Giudici, *Analysis of axial dispersion in an oscillatory-flow continuous reactor,* Chemical Engineering Journal **94**, 189 (2003).

[27] A. W. Dickens, M. R. Mackley, and H. R. Williams, *Experimental residence time distribution measurements for unsteady flow in baffled tubes,* Chemical Engineering Science **44**, 1471 (1989).

[28] N. Reis, A. A. Vicente, J. A. Teixeira, and M. R. Mackley, *Residence times and mixing of a novel continuous oscillatory flow screening reactor,* Chemical Engineering Science **59**, 4967 (2004).

[29] G. Vilar, R. A. Williams, M. Wang, and R. J. Tweedie, *On line analysis of structure of dispersions in an oscillatory baffled reactor using electrical impedance tomography,* Chemical Engineering Journal **141**, 58 (2008).

[30] J. R. McDonough, A. N. Phan, and A. P. Harvey, *Rapid process development using oscillatory baffled mesoreactors – a state-of-the-art review,* Chemical Engineering Journal **265**, 110 (2015).

[31] X. Ni, H. Jian, and A. W. Fitch, *Computational fluid dynamic modelling of flow patterns in an oscillatory baffled column,* Chemical Engineering Science **57**, 2849 (2002).

[32] X. Ni, H. Jian, and A. Fitch, *Evaluation of turbulent integral length scale in an oscillatory baffled column using large eddy simulation and digital particle image velocimetry,* Chemical Engineering Research and Design **81**, 842 (2003).

[33] M. Manninen, E. Gorshkova, K. Immonen, and X.-W. Ni, *Evaluation of axial dispersion and mixing performance in oscillatory baffled reactors using cfd,* Journal of Chemical Technology and Biotechnology **88**, 553 (2013).

[34] P. Stonestreet and P. M. J. Van Der Veeken, *The effects of oscillatory flow and bulk flow components on residence time distribution in baffled tube reactors,* Chemical Engineering Research and Design **77**, 671 (1999).

[35] P. Stonestreet and A. P. Harvey, *A mixing-based design methodology for continuous oscillatory flow reactors,* Chemical Engineering Research and Design **80**, 31 (2002).

[36] T. McGlone, N. E. B. Briggs, C. A. Clark, C. J. Brown, J. Sefcik, and A. J. Florence, *Oscillatory flow reactors (ofrs) for continuous manufacturing and crystallization,* Organic Process Research and Development **19**, 1186 (2015).

[37] A. Harvey, M. Mackley, and P. Stonestreet, *Operation and optimization of an oscillatory flow continuous reactor,* Industrial and engineering chemistry research **40**, 5371 (2001).

[38] A. M. Stanley, R. Adam, H. A. P., and I. Morrison Michelle, *Rapid determination of the residence time distribution (rtd) function in an oscillatory baffled reactor (obr) using a design of experiments (doe) approach,* International Journal of Chemical Reactor Engineering **12**, 575 (2014).

[39] L. N. Ejim, S. Yerdelen, T. McGlone, I. Onyemelukwe, B. Johnston, A. J. Florence, and N. M. Reis, *A factorial approach to understanding the effect of inner geometry of baffled meso-scale tubes on solids suspension and axial dispersion in continuous, oscillatory liquid–solid plug flows,* Chemical Engineering Journal **308**, 669 (2017).

[40] N. E. B. Briggs, U. Schacht, V. Raval, T. McGlone, J. Sefcik, and A. J. Florence, *Seeded crystallization of β-l-glutamic acid in a continuous oscillatory baffled crystallizer,* Organic Process Research and Development (2015), 10.1021/acs.oprd.5b00206.

[41] X. Ni, Y. S. d. Gélicourt, J. Neil, and T. Howes, *On the effect of tracer density on axial dispersion in a batch oscillatory baffled column,* Chemical Engineering Journal **85**, 17 (2002).

[42] M. S. Lucas, N. M. Reis, and G. Li Puma, *Intensification of ozonation processes in a novel, compact, multi-orifice oscillatory baffled column,* Chemical Engineering Journal **296**, 335 (2016).

[43] E. Lobry, T. Lasuye, C. Gourdon, and C. Xuereb, *Liquid–liquid dispersion in a continuous oscillatory baffled reactor – application to suspension polymerization,* Chemical Engineering Journal **259**, 505 (2015).

[44] N. Reis, A. P. Harvey, M. R. Mackley, A. A. Vicente, and J. A. Teixeira, *Fluid mechanics and design aspects of a novel oscillatory flow screening mesoreactor,* Chemical Engineering Research and Design **83**, 357 (2005).

[45] M. R. Mackley, K. B. Smith, and N. Wise, *The mixing and separation of particle suspensions using oscillatory flow in baffled tubes,* Chemical Engineering Research and Design **71a**, 649 (1993).

[46] O. Levenspiel, *Chemical Reaction Engineering*, 3rd ed. (Wiley, 1999) p. 688.

[47] O. Levenspiel, *Tracer Technology*, Fluid Mechanics and Its Applications, Vol. 96 (Springer-Verlag New York, 2012) pp. XII, 148.

5

Application of inline imaging for monitoring crystallization process in a continuous oscillatory baffled crystallizer (COBC)

5

In this study, an in-situ imaging system has been analysed to characterize the crystal size, the shape and the number of particles during a continuous crystallization process in a COBC. Two image analysis approaches were examined for particle characterization in the suspension containing both small nuclei and larger grown crystals (non-spherical and irregular in shape). The pattern matching approach, in which the particles are approximated to be spherical, did result in an overestimation of the size. Alternatively, a segmentation based algorithm resulted in reliable crystal size and shape characteristics. The laser diffraction analysis in comparison to the image analysis overestimated the particle sizes due to the agglomeration of particles upon filtration and drying. The trend in the particle counts during the start of crystallization process, including nucleation, determined by the image analysis probe was comparable with the one measured by FBRM, highlighting the potential of in-situ imaging for process monitoring.

5.1. Introduction

Control over the product quality in the crystallization process is crucial for obtaining the right solid product. In bio, pharma and food industry, stringent guidelines apply for quality control. Especially products designed for human use (for direct or indirect consumption) must meet the required criteria to be marked safe for use. Safe product is ensured through consistent and reproducible production of the pre-approved product quality. Various methods are employed to ensure the product quality and currently Quality by Design (QbD) is one of the governing philosophies in the industry. The QbD approach dictates that the product quality control should be an integral part of the design procedure. Hence the quality should be in-built in the process [1].

In the production process of active pharmaceutical ingredients (APIs), crystallization is one of the important separation operations carried out for obtaining the API from the solution in solid form. Control over the properties of the solid API obtained during crystallization is quintessential for guaranteeing further downstream processing and the desired drug efficacy. API properties, such as the shape, size, polymorphism and purity, needs to be controlled during the crystallization process. For process monitoring and control, Process Analytics Tools (PAT) are used under the QbD philosophy [2]. The use of PAT facilitates, precise monitoring and control of the formation and growth of the crystals. Use of PAT also facilitates identification of the critical operating parameters for process optimization, thereby mapping the critical operating parameter with the desired product attributes for optimal operation.

Over the on and off line techniques, inline techniques are preferred as sampling or operations to separate solids from liquids in the case of the crystallization process can introduce large errors and be non-representative of the actual state of the particles. In addition, inline measurement techniques offer the potential of real time process control without disturbing the process. Spectroscopic techniques like Raman and FTIR as well as particle characterization techniques like focused beam reflectance measurement (FBRM) and the particle vision and measurement probe (PVM) for inline microscopy are the popular choices. The latter techniques, the FBRM and the PVM, directly characterize the solid phase. Process vision: the ability to visualize and quantify the product quality directly based on the physical form of the crystals has immense potential for control of the crystallization process. Since particle size and shape characterization are important for quality control, a number of size and shape characterization systems have been developed and employed. A brief overview of the state of the art on/off/inline particle measurement techniques is provided in the following paragraphs.

Most commonly used particle characterization techniques are based on laser diffraction (LD), dynamic light scattering (DLS), ultrasound wave attenuation and light backscattering. The DLS method utilizes the measured fluctuation in the intensity of the light scattered by dispersed sub-micron particles due to the Brownian motion of those particles. In LD measurements, the angular dependence of the light scattered by the particles is used to estimate the particle size distribution. Several models, all based on the assumption that the particles are spherical, are used to correlate the diffraction pattern with the particle size (size range in μm to a few mm). The Lorentz-Mie theory is widely used for particle size estimation from the scatter

pattern [3]. The scattering based techniques are most commonly used for particle size characterization as distribution of spherical particles can be fairly ascertained; while a loss in accuracy is experienced for non-spherical particles [4]. Analysis of irregularly shaped particles such as elongated needles or plate like structure by LD technique leads to underestimation of the volume equivalent diameter as the predicted PSD is based on the area of the projected light intensity [5, 6]. No shape or morphology information is made directly available by the DLS technique [7]. The FBRM on the other hand measures the back scatter of the incident light reflected by single particle as the focussed beam passes over it. The laser in the FBRM constantly rotates with a fixed speed and based on the duration of the signal disruption the size of the particle is measured. The FBRM generates particle counts and size statistics based on chord lengths, as the measurement by FBRM is dependent on the particle shape and the spatial orientations.

Imaging techniques provide, through direct visualization, information on the evolution of the crystal size as well as the morphology. Optical or video based microscopy is preferred for process control where projections of the crystals can be relatively quickly analysed to ascertain shape and size characteristics. Shape descriptors such as roundness, elongation, aspect ratio, convexity or form factor are used. Whereas size can be characterized from projections by estimating Sauter mean diameter, Feret diameter, equivalent diameter of a circle, or the axis lengths (major and minor) of an ellipse fitted to the projection, which results in 1D or 2D size distribution. Non-intrusive observers based on bulk video imaging offer a low resolution PAT opportunity [8]. Techniques like hot stage microscopy offer online solution by circulating the slurry from the crystallizer to the sampling cell and back. *in-situ* imaging based on stroboscopic endoscope include a number of high resolution systems for example, Particle Imaging System (PARIS) of Dupont, PVM from Mettler Toledo, Process Image Analyzer (PIA) of MessTechnik Schwartz GmbH, In-Situ Particle Viewer (ISPV) of Perdix Analytical Systems and the more recently introduced imaging system from SOPAT GmbH [9]. Needless to say, the result of the image analysis depends on the quality of the images captured which in turn depends on factors like distribution of the light intensity, focussing or the depth of view of the optics and the optical properties of the particles. The concentration of the particles is preferred to be low to obtain good image in which overlap or shielding of the particles by other particles can be avoided. Many studies have demonstrated the implementation of imaging and the subsequent analysis of the captured images to ascertain the particle size distribution (PSD) [10–13] (The references are in no way exhaustive).

The image analysis process involves usually, the enhancement and segmentation of the images. The enhancement step is carried out to smoothen and sharpen the images. The segmentation step is aimed at distinguishing the object in an image from the background. Various techniques have been reported in the literature for different operations during image analysis. For example, subtracting the background as a simple thresholding operation or use of multi variate analysis to differentiate the object pixels from the background pixels. The multi segmented Canny method has been shown to result in enhanced segmentation by accounting for the variation of the pixel intensity across the objects in the images [4]. The utilization of multi variate

principle component analysis has also been used for segmentation process during image processing [14]. The step following the object detection focuses on refining the detected boundaries or filling in the gaps in the object boundaries and rejecting the unwanted objects by classification method. Thus depending on the complexity of the application, various techniques have been applied and the commercially available software use combination of readily available and proprietary algorithms to carry out the various stages during image processing. The final pool of identified objects are then characterized to determine the shape and the size descriptors [11].

Some of the recent studies applying image processing for particle characterization include but are not limited to the studies like that of Eggers et. al., which used the axis length distributions (ALD) of ellipses fitted to the projections of carbon fibres (imaged in a flow cell) to predict the 2D PSD through an optimization process correlating the ALD to PSD [15]. Schorsch et. al., demonstrated the implementation of stereo imaging in a new on-line sampling setup with direct circulation and controlled dilution of the slurry from the crystallizer to obtain high quality images. Stereo microscopy allowed estimation of 3D PSD based on multi 2D projections through classification of crystals into generic geometric shapes like circle, cylinder or cuboid [16]. Recently Agimelen et. al. used the aspect ratio distribution, sampled over the crystal population from *in-situ* imaging, as a constraint in combination with the FBRM's CLD data to predict accurately the PSD [17]. Ochsenbein et. al. segregated agglomerates from primary particles using image analysis by utilizing a pre-generated training set to classify the particles as agglomerates or primary particles based on a number of descriptors [18]. Ferreira et. al., have also combined image analysis with discreet factorial analysis to quantify the degree of agglomeration and growth rates of sucrose crystals by online monitoring of the crystallization process [19]. Efforts have also been made to use the 2D PSD data to estimate the crystal habit and to follow the evolution of the various facets of the crystal, mostly in combination with morphological population balance [20–24].

Therefore, techniques which avoid the sampling and transfer of slurry are being preferred for process monitoring and control, as the process is not disturbed and sampling induced errors can be avoided. In this paper, we present the implementation of the inline imaging system from SOPAT GmbH for monitoring the continuous crystallization process in a continuous oscillatory flow baffled crystallizer (COBC). In a COBC system image analysis based on external video imaging has been applied to ascertain the onset of nucleation, metastable zone width, crystal size distribution and estimation of crystallization kinetics [25–27]. Since application of COBC for continuous crystallization is an area of ongoing development, the use of an inline imaging tool provides an the additional advantage that more qualitative information is obtained which helps to get a better insight in the crystallization process in this flow crystallizer. The SOPAT-VI-industrial probe provides an opportunity to capture and analyse the particle images even at relatively high concentrations for monitoring and can have potential for real time control. The user interface of the image analysis tool from SOPAT allows generation of a search pattern through selection of particles as a training set by the user. The generated pattern is then used to process the image series to find objects matching the characteristics in the pattern. Since the pattern

generation from the training set is based on assumption of spherical particles, it may not be the best for application in the case of crystallization process where irregular shaped particles or complex shapes are observed. Therefore, a segmentation algorithm allowing a flexible boundary detection for irregularly shaped particles (made available by SOPAT) was tested to ascertain particle size and shape information from the image analysis. In this paper the outcome of the image analysis process using the pattern matching and the segmentation based algorithm is compared. The particle size and shape results from the image analyses are elaborated. A comparison of the results from image analysis is made with the results from sampled particles analysed using the LD technique. A comparison of the trend in number of particles as detected by FBRM is also made with the particle counts trend ascertained from images taken during various time points in the experiment.

In the subsequent sections, the setup and the systems used in the study are explained followed by a section on the image analysis procedures used. Lastly, the results and discussion are presented followed by the conclusions from this study.

5.2. Materials and methods

5.2.1. Experimental setup and operation

The continuous oscillatory baffled crystallizer (COBC) setup used in this study consists of jacketed tubes with periodically spaced baffles. Enhanced control over mixing with relatively large residence time and opportunity to have enhanced process control has promoted the COBC to be an alternative tool for implementing continuous crystallization in a tubular design. The details on the operation of an oscillatory flow baffled reactor/crystallizer can be found in details in literature [28].

DN15 LITE from NiTech Solutions, has been used in this study, which consists of 7 baffled glass straights (15 mm inner diameter) with jackets for heat exchange. The baffles are spaced at a distance of 1.5 times the inner diameter and the baffle orifice is measured to be 9 mm in diameter. The total volume of the set-up is approximately 1 L. A PEEK piston connected to a linear motor brings the oscillations to the flow by coming in contact with the process fluid or slurry. A detailed description of the optimum operation of the COBC with respect to the mixing resulting from the fluid oscillations can be found in our recent work [28]. The schematic of the COBC setup is shown in Figure 5.1. The residence time of the system depends on the flowrate. With a flowrate of 100 ml/min, typical residence time of around 10 minutes is achieved. Cooling crystallization of melamine from a clear saturated solution at 50 $°C$ was carried out in the COBC. Except the first tube, whose jacket temperature was maintained at 50 °C, the rest of the tubes in the COBC were maintained at 40 °C. The COBC start up procedure involved, filling the COBC with demineralized water followed by vigorous internal mixing/agitation to remove the air from the system. After the start up procedure, the desired operation amplitude and frequency of the fluid oscillations in the COBC was set and the setup was left to stabilize for at least 4-5 residence. The feeding of the clear solutions was achieved by a peristaltic pump (520s/REM, Watson Marlow). The jackets of the COBC tubes were connected to a thermostatic bath to maintain the desired temperature. The cooling of the tubes (except the first tube of

the COBC) was started after waiting for 2 residence time to ensure that the water in the COBC tubes was replaced by melamine solution. Visually, the nucleation was observed in the third tube and the fourth tube of the COBC. FBRM probe was placed at the end of the third tube in order to facilitate nucleation detection. The SOPAT-VI-industrial probe placed at the exit was used for *in-situ* imaging of the outgoing crystals. Samples of the crystals were also collected by filtering at the exit of the COBC at the end of the process for offline analysis using laser diffraction technique.
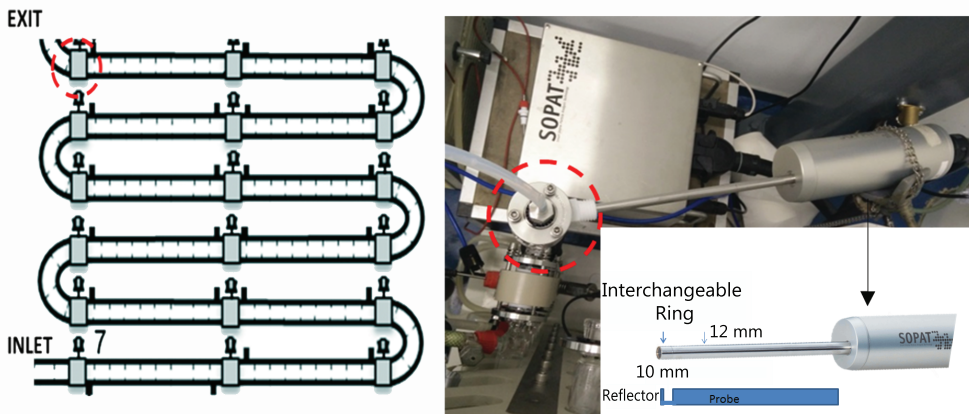

Figure 5.1: The schematic representation of the COBC setup with position of the image probe at the exit highlighted (left) and the top view of the connection port with the imaging probe. Inset is the schematic showing the dimensions of the probe with an interchangeable tip to connect a reflector plane(right. The slurry flows through the gap between the reflector plane and the probe tip.

5.2.2. Offline size measurement- laser diffraction (LD)

Particle size measurement using dry crystal sample were carried out using the Microtrac (model S3500) laser diffractometer. Samples were collected by filtering the slurry at the exit of the COBC. The residue comprising of crystals in the filter paper was washed with a small amount of water and dried overnight in an oven maintained at 30 $°C$. Volume based particle size distribution was obtained from the analysis. The collected crystals were also imaged under the microscope to visually verify the crystals.

5.2.3. Inline particle detection- FBRM

FBRM probe (model G400) from Mettler Toledo provided in situ measurements of the particle count. The iC FBRM software (version 4.4) coupled to the FBRM hardware acquires the data and allows for the data analysis. The scan speed of the unit was set to 2 m/s with measurement interval of 3 seconds. Two modes of data analysis called the Primary and Macro mode respectively are provided in the iC FBRM software. The count data reported here are based on Primary mode. The Macro mode neglects slight disturbances in the detected signal due to surface aberrations for example due to breakage or at interfaces of clusters of crystals and counts the particles as a single

particle. The FBRM in this study was solely used for nucleation detection and the chord length distribution statistics is not used for particle sizing. For further reading on the operating principle of the FBRM for particle characterization the literature should be referred [29].

5.2.4. Imaging system

The SOPAT imaging system (SOPAT –VI-industrial probe) consists of a probe with the tip diameter of 12 mm. The probe acts as an endoscope which is connected to a detector and the probe has integrated fiber optics for illumination by strobe flash. The objective in the probe enables objects from 2 μm till 250 μm to be imaged, based on the assumption that a minimum of five pixels is required as the minimum length (2 m) for a particle and 1/3rd of the image diagonal (750 m) is required for the maximum length. The high definition lens system in the image probe allow for the following specs; such as Field of view in the range 700-850 µm, particle size range 3-250µm, depth of field 200µm and a resolution 228 cpmm. The SOPAT system allows for imaging at frame rates varying from 1 to 20 Hz. The illumination intensity can also be controlled and a reflection plane can be easily attached to the end of the probe to allow improved illumination.

The SOPAT system allows for imaging at frame rates varying from 1 to 20 Hz. The illumination intensity can also be controlled and a reflection plane can be easily attached to the end of the probe to allow improved illumination. The probe is connected to a work station where the images captured by the camera are quickly transferred and saved in the workstations memory. The workstation has the SOPAT GUI installed for image acquisition and analysis.

In our study, the frame rate of 5 Hz was sufficient to capture clear images of the crystal. The chosen frame rate was not too fast so as to capture the same particle in multiple consecutive frames. Focus point was set between 400 to 600 μm from the probe window as better focusing of the particles was observed. In total 500 to 1000 images were captured during each trigger (lasting for 100-200 seconds). The images were later analyzed for the estimation of particle size and shape distribution. Illumination plays an important role in getting sharp and clear images of the particles. Various reflecting planes can be attached to the SOPAT probe for obtaining the right illumination [30]. A reflector plane with rhodium plated mirror was used to enhance illumination in the system and obtain a better contrast between the background and the crystals.

5.3. Image analysis

Various commercial software packages are available that analyze images automatically and measure the size of droplets or particles. The quality of the results from these packages differs and depends on a number of variables, including the quality of the initial images. Custom software can be written to incorporate previously validated image processing algorithms. Software is also available that allows manual selection of particles on the images, which are then measured by the computer. The process of manual counting is not only time consuming but also introduces human bias. Box-

all *et. al.*, showed the influence of human bias and the variance of manually counted drop size distributions and additionally reported about the repeatability of drop measuring experiments [31]. Automated quantification avoids the bias introduced by different observers and the errors which still arise are systematic. However manual selection of particles as training sets are essential for producing accurate results as well as checking the performance of automatic software [32]. Two approaches have been implemented in the SOPAT image analysis systems. One approach uses specific pattern generated based on the user identified objects to search for particles. The other approach uses segmentation algorithms to search for structures in the images. The image analysis algorithms used in this study was implemented in MATLAB® to count and measure, fully automatically, the crystals forming the multiphase systems. The general principle of the image analysis steps are shown in Figure 5.2 and more details of the methods are described in a previous publication [33]. In order to ensure the robust and accurate object detection, a series of images is first pre-filtered to remove irrelevant and misleading image information. This is done with image subtraction using the integrated sequence as difference image. The noise in the pictures is reduced by the self-quotient image method [34]. These operation norms the intensity of every local pixel based on the local environment. The procedure is carried out by division of the processed image by a smoothed version of itself. The self-quotient image emphasizes the changes of the intensities from the original image. This results into an independency on any illumination or process variation. The image enhancement process described above is common to both the approaches implemented in this study.
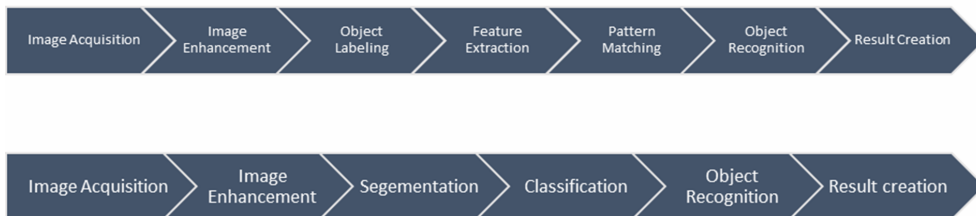

Figure 5.2: Overview of the principle steps employed in the two image analysis procedures followed in this study for particle characterization. Pattern matching approach (top) and segmentation based processing (bottom).

5.3.1. Pattern matching – user defined spherical particles

If the particles have similar characteristics and boundary features, for example oil droplets or air bubbles in a multiphase system, typical features can be extracted and be correlated during pattern matching to identify similar objects in a series of images. The pattern matching algorithm in the SOPAT analysis system allows user defined object labelling. Thus from the preprocessed images (Image Enhancement) the user can choose relevant particles by encircling them as samples for generating a pattern (Object Labeling). The encircled particle is assumed to be spherical and

typical features are extracted (Feature Extraction), such as radial intensity distribution etc., from the chosen particle candidates. The image series is processed to identify particles which match the characteristics contained in the generated pattern (Pattern Matching). The same principle of pattern based searching can be extended to other shapes as well. The pattern matching approach from SOPAT has been shown to work very precisely even on overlapping particles and for characterization of the size for air bubbles and dispersed droplets [35–41].

The object recognition consists of three steps: Pattern recognition by correlation of pre-filtered gradients with search patterns, the pre-selection of plausible circles and the classification of each of those circles by an exact edge examination. The software employs a normalized cross correlation procedure algorithm to evaluate possible object matches [42]. The automatic object recognition is most effective when objects appear in high contrast to the background and reasonable concentration of particles on the image. High contrast between the object and the background is preferred to ensure a good hit rate and low error quotient, while the reasonable concentration ensures that the computation renders more objects recognized per minute. The SOPAT software for spherical particle analysis has been proven to be very robust and able to compete with the human eye in processing complex images [33]. The computation time is nearly proportional to the pixel quantity being processed and depending on the images the processing time is twice to fifty times faster than manual counting. The user is also able to define thresholds for the error quotient and the hit rate to force the program into further parameter optimization. Threshold decides how close a match of the object to the user defined pattern is acceptable. For every detected particle the circle geometry (x, y, r) are created and saved into csv file for further processing (Result Creation).

The selection of the user defined particle samples influence the outcome of the automated image analysis. The small crystals which appear shortly after nucleation appear differently than the crystals that have grown to larger sizes. The small crystals due to the limited resolution do not present sharp edges or clear shapes. Therefore, the object features quantified for pattern generation can differ considerably for small and large crystals. Patterns based on incorrect particle features lead to higher fractions of false positives, structures that are detected but are not the target object. Therefore, in our approach we included both small and large particles to make the pattern robust. However, using a single pattern to search for crystals resulted in a lot overlapping detections. Especially multi areas were identified on the surface of large crystals as small particles. A refinement in pattern generation was achieved by dividing the particles into two pools: one for small and the other for large crystals. Figure 5.3, shows a selection of the crystals chosen as particle candidates. The pattern from the small crystals was defined separately from the one with the larger crystals. Analysis was performed separately with the two patterns. Size restrictions was placed to ensure that particle below 50 m are identified with the pattern searching for small particles and the other pattern searches particles above this size limit. Additionally, the results from the two search patterns were merged. In the merged results, to avoid calculations of the small particles inside the area covered by big particles, the small particles were only accepted as true results if the center point

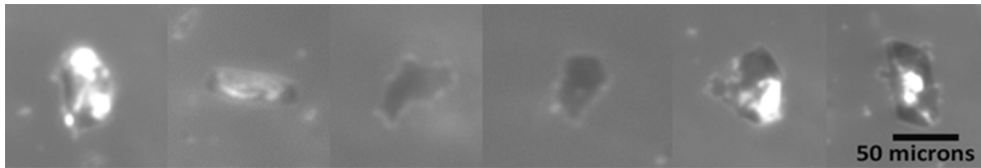was outside the already calculated larger particles in the vicinity.

Figure 5.3: A selection of crystals chosen as user defined particle candidates for generation of the search pattern. Images of single particles at different magnifications are shown to emphasize the shape of the particles.

As visible in figure 5.3 the shape of the observed crystals is irregular; the irregular shape makes generation of a generic pattern which matches most of the objects difficult. The feature of the crystal edges cannot be captured precisely as shapes such as a circle cannot be made to correspond exactly with crystal edges. For example, if there would be needle shaped crystals then it may be possible to carry out analysis via pattern matching using a rectangular approximation. Hence pattern matching approach may not be a good method to apply for a crystallization system resulting in complex structures.

5.3.2. Segmentation based image processing – flexible boundary detection

The segmentation technique is used in image processing to identify structures in an image. Flexibility in detection, unconstrained by search for a regular shape, allows structures with complex boundaries to be detected. Usually a refinement of the result is then required to only identify object of interest. Panckow textitet. al. (2015) did investigations of irregular objects using image analysis by increasing the shape complexity starting from spheres [30]. An improved version of the irregular shape analysis used by Panckow *et. al.* in their study is implemented in the SOPAT software. The pre-filters as well as the image pre-processing techniques (Image Enhancement) are the same as described previously. As seen from the bottom schematic in Figure 5.2 after the initial image pre-processing, segmentation is carried out to identify the structures in the images (Segmentation). To decrease the noise, single pixels which are surrounded by white pixels are deleted, while also the particles as small as one pixel are neglected. The algorithm employed in this study is as follows; , prefiltering with series mean filter, median filter, then conversion to binary images with locally adaptive image thresholding, overlay of resulting images and double thresholding with morphological reconstruction or more general: Canny, double thresholding, morphological operations.

From the identified segments 2D information, for example area and the full pixel by pixel boundary information, is captured for a precise shape analysis. The identified particles then need to be classified (for example crystals, bubbles, droplets, sharp and blurred, undefined objects etc.). The number of different classifications can be chosen and is usually three to five. In this study just one classifications was made (1-clear crystals). Rejection of air bubbles or blurred or unclear objects, by labelling the

objects manually or through a training set, was not done. For each of the particles a feature vector is created. The feature vector (i.e. sphericity, min. intensity, convexity, etc.) is then compared and adjusted to the labelled target particles. After this training procedure segmented particles are compared and only particles with the accepted feature values are retained (Classification). The results of the analysis are saved in a similar way to the results from the spherical analysis algorithm. Due to the flexible boundary detection the irregularly shaped objects can be analyzed to ascertain a number of particle properties. The Feret diameter (also called "caliper diameter") can be calculated based on the distance between two parallel planes that restrict the particle projection. To calculate the Feret diameters the measuring plane vector is rotated in 16 steps through 180 °by default for each particle.

5.4. Results & Discussions

5.4.1. Pattern matching

In case of the crystallization process, the interplay of various phenomena such as growth, attrition or agglomeration of crystals affects the appearance of the crystals and introduces complexities in identifying a generic shape based characteristics which fits most of the crystals. Additionally, due to the simultaneous occurrence of both the nucleation and the growth process during the crystallization process in our study, a variety of crystals sizes are observed. Two different training sets were generated and used to characterize separately the larger crystals which appeared to have well defined edges and the smaller crystal whose appearance was less sharp due to the limitation in the resolution. Figure 5.4, shows the crystals (encircled) which are identified during the analysis carried out using the pattern matching algorithm. The three identical images in Figure 4 show the results based on the pattern generated with a training set comprising of small crystals(left), large crystals (middle) and combined results of small and large crystal detections (right). In the case of the combined results, the small particles inside of big particles are rejected, although they are still visible in the right figure. The small particles are only accepted as true results when the center point was outside the already calculated particles.
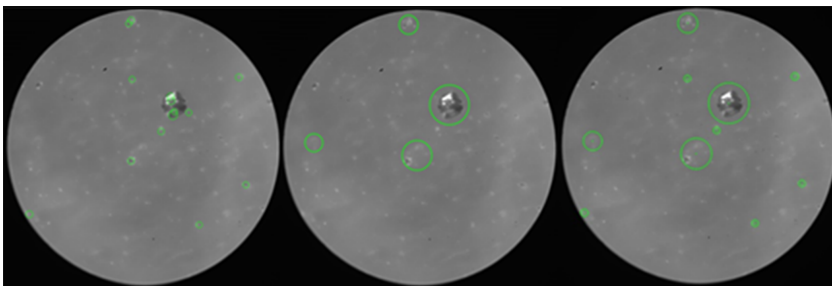

Figure 5.4: Results of pattern matching approach with pattern based on relatively small crystals (left), with pattern based on relatively large crystals (middle) and the resulting combination of both the separately detected large and small crystals(right).

As detailed in the section 5.3.1 the pattern matching algorithm is based on the

spherical approximation of the crystals. Pattern matching can be extended to irregular particles, however the parameter search scope for spherical obejcts (position, radius) is far smaller compared to irregular shaped objects. If only pattern recognition would be applied for the presented irregular particles, the search scope of the irregular pattern (rotation of the objects) would be far larger and the analysis time very time consuming. Thus a few shortcomings can be immediately identified. As seen from the large crystal in the middle of the images in Figure 5.4, the patterns matching for the small size range results in multiple areas on the large crystals being identified as separate particles. This is overcome by the pattern matching based on the large particles which detect the large crystal as a single particle, but on the other hand a compromise should be made as regions with small crystals close to each other can also be identified as a single large particle. Given the complex shapes of the crystals, the circular approximation during user defined training set selection only captures a part of the crystal features as the crystal edges do not corresponds to the drawn circle. In principle, the pattern matching process searches for a matching corona around the object. As seen in case of the larger particles the detected area is often larger than the particle and does not correspond closely to the crystal edges, leading to an overestimation of the particle size. It is clear that the circular approximation cannot provide any shape characteristics relevant to the non-circular particles. However, the result shows the importance of a relevant set of particle candidates for pattern matching based recognition of different kind of particles.

The procedure resulting in the particle detections as shown in Figure 5.4, was applied to a set of images. Figure 5a shows the cumulative number based size distribution as a result from the image analysis. The size data is based on the Feret diameter which in case of a circle is the same as the circle diameter. During the image analysis, the algorithm searches for particles with characteristic's matching the pattern generated based on the corona around the particles used for the training sets. The use of different sets of candidates for pattern generation thus creates different size distributions. Figure 5.5 b shows the number based density and the cumulative particle size distributions by combining the results of the two approaches. The bimodal nature of the distribution in the combined results is clearly seen. Based on the density distribution, the mode of the small particles is around 20 μm whereas the mode of the large particles is around 60 μm. The cumulative distribution from the results with the combined patterns has a prominent shoulder at sub 40 μm range as a result of the small particles and a inflection point around 60 μm because of the larger particles. The combination allows elimination of the overlapping detection of the same particles by the two different patterns. Overall through choosing the right set of candidates for generating the search pattern meaningful results are obtained.

Table 5.1 shows the parameters $xn10$, $xn50$ and $xn90$ which highlight that 50% of the total number of particles detected with the combined pattern are below the size of 21.29 μm. The measured size distribution characterizes the diversity in the crystal sizes observed due to the simultaneous presence of the nucleation and the growth process. Also, the mixing conditions in the COBC leading to a specific residence time distribution impacts the size distribution. Presence of baffles can result in crystal attrition due to collisions. Also, the oscillatory nature of flow can enhance crystal-

Table 5.1: Size distribution parameterized in terms of $xn10, xn50 and xn90$ (number based) base on the results of the image analysis using the combined pattern for the small and the large particles.

Size Parameter	Maximum Feret Diameter (μm)
xn10	19.20
xn50	21.29
xn90	76.03

crystal collisions. But the strong presence of nucleation is possibly the dominant factor behind the large number of smaller particles observed throughout the image processing.
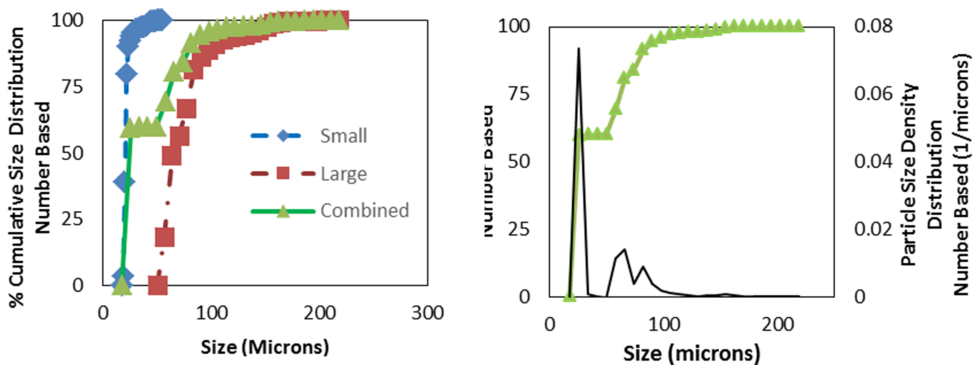

Figure 5.5: Cumulative number based particle size distributions determined by image analysis using the two different approaches (a) and the combined result (b)

5.4.2. Segmentation

Figure 5.6, shows the result from the image analysis using the segmentation algorithm designed to identify closely the non-circular or irregularly shaped objects. A number of images are shown in the Figure 6 which covers the performance of the image analysis as a result of flexible boundary identification the particle edges are detected very closely, leading to improved particle recognition. The majority of the large and the small particles are detected. The particle border identified by the analysis is a better approximation of the particle edges. Thus, shape information can also be ascertained which was not an option based on the circular area detection. However, with larger crystals some deviation in the detection of the crystals is also observed as sometimes only a part of the crystal is recognized or crystals close to the image boundaries are not recognized at all. The boxed areas in the top two pictures in Figure 5.6 highlight the deviations. These deviations in general can be overcome by processing a large number of objects which makes the data statistically robust.

Table 5.2 shows the distribution of the particle size in terms of the size parameters
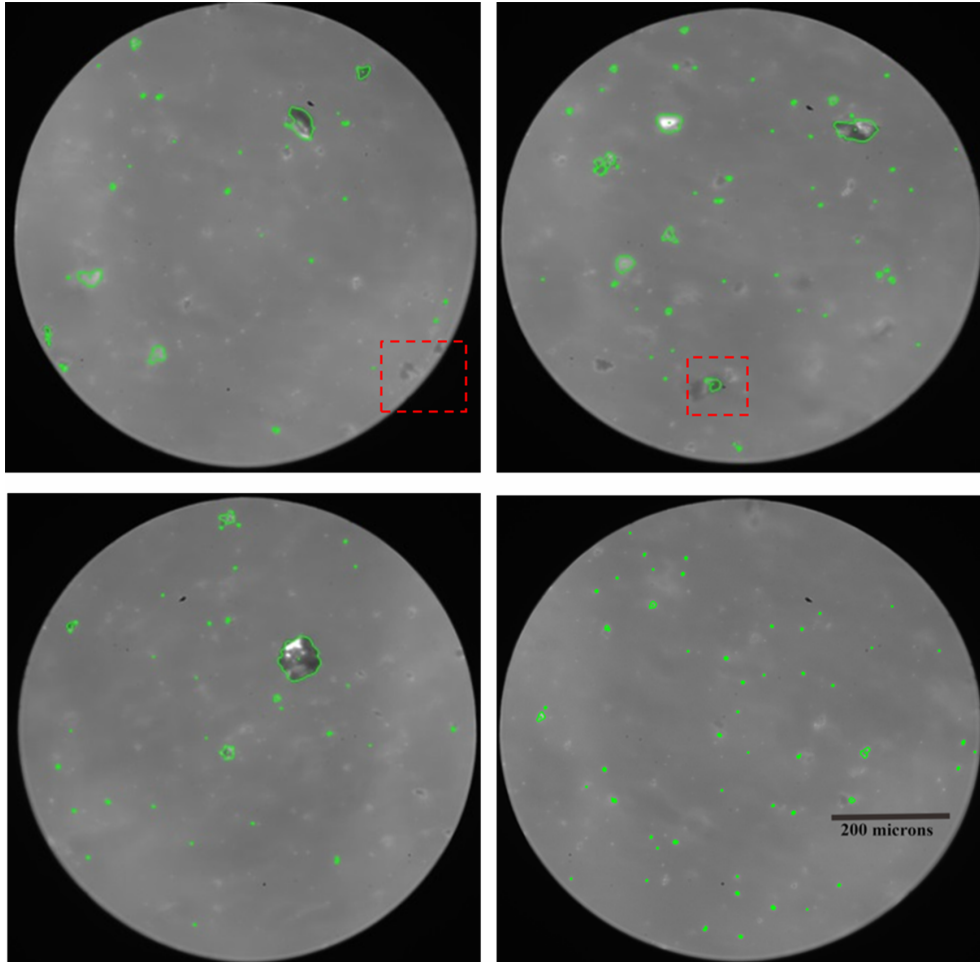
Figure 5.6: Identified crystals as a results of image analysis using the segmentation algorithm with the flexibility in boundary identification for irregular shape detection.

$xn10$, $xn50$ and $xn90$. 50% of the total number of the particles ($xn50$) lies below the size of 5.21 μm. Figure 5.7, shows the number based size distribution (maximum Ferret diameter) calculated by the image analysis. Maximum Ferret diameter essentially reflects the farthest distance between two opposite edges of the crystal. The bias of the distribution towards the small size range captures the fact that in the nucleation dominant process a large number of small particles are generated. The same is confirmed visually through the captured images where larger presence of small particles is observed. The cumulative distribution in Figure 5.7 shows the presence of a few large crystals above the 40 micron size. In contrast to the results obtained with the pattern matching approach in Table 5.1 the $xn50$ value in Table 5.2 is much smaller. Comparison of size distributions in Figure 5.5 b with the distribution

in Figure 5.7 shows that much smaller particle sizes are estimated by the segmentation based image analysis. In a crystallization process like studied here, the presence of both nucleation and growth process will make the dispersion in sizes of the particle inevitable. The automated analysis routine, systematically detects objects and a much larger number of objects are taken into account, resulting in representation of both the fines and the large crystals. This is required to have sensitivity for the fine crystals from nucleation as well as for the larger grown crystals.

In the images captured during the study, there is not a large concentration and rarely overlapping particles. Generally non-spherical particles may be far larger in size in the third dimension than predicted from the visible two dimensions. Therefore, a fair representation of the process is achieved in this methodology with a systematic error which is present as well in other methodologies. A comparison of the results from the automated segmentation analysis has been made with results from manual analysis of the image, which gives a pragmatic perspective to the automated imaged analysis. Due to simplicity, the relatively larger particles which appear sharply have been marked in 500 images out of the 1000 images acquired originally during the experiments. In total about 672 particles were manually identified and marked. The $xn50$ value with the manual analysis is calculated to be 23.87 and $xn90$ close to 40 m. However, there is bias introduced towards large size by not having representation of the fine particles, which are definitely generated due to the nucleation. The fine particles are tedious to mark and it should also be noted that with manual analysis only about 672 crystals could be marked from half of the total the images. Hence, definitely a large population of particle much large than the manual determined $xn90$ is not expected. With the systematic analysis of the automated process a large number of particles are analysed, especially the fines which dominate the process and hence smaller sizes are estimated. In comparison, the pattern matching approach with the circular approximations, leads to overestimation of the crystal sizes due to poor fit of the pattern with the crystal edges. The detection of the particle boundaries with the segmentation process offers more representative and consistent size estimation of the process.

Figure 5.8, shows the number based distribution of the aspect ratios ascertained from the image analysis. The aspect ratio has been calculated as the ratio between the minimum and the maximum Feret diameter. For example, a rectangle with length and width as 5 and 7 (arbitrary units) respectively will have the diagonal as the maximum Feret diameters and hence the resulting aspect ratio of 0.58. The mode of the aspect ratio distribution is seen to be around 0.8, which suggests that the majority of the detected particles have close to circular projections. From the images, the small particles do appear to have closely circular projections, however the crystals are not circular in practice. This can be due to multiple factors, out of which limitations in the resolution to observe small particles is most likely. Analysis based on relatively larger particles, where the crystal edges are better resolved could be employed to improve the results.

As mentioned earlier, the accuracy of the results from the image analysis is improved by making sure that a large number of objects are processed. Figure 5.9, shows the variation of the parameter $xn50$, the $x1,2$ (area weighted mean size) and

Table 5.2: Size distribution parameterized in terms of xn10, xn50 and xn90 (number based) base on the results of the image analysis using the segmentation algorithm.

Size Parameter	Maximum Feret Diameter (μm)
xn10	2.27
xn50	5.21
xn90	17.47

the corresponding average values against the number of particles analyzed during the image analysis. As the image analysis processes around 1000 images a high of number of particles are included to make the results statistically robust. If low number of particles are used to estimate the averaged size values a large variation in the statistical size parameters $xn50$ and $x1,2$ is observed. As a result a few thousands of particles analyzed in our study helped in estimating a stable value. Since the parameter $x1,2$ is weighted with the area of the detected particles (approx. square of the size) the variation with the number of particles is also amplified and more than 10,000 particles are needed to reach a stable average value.

In our nucleation dominated system with mostly small particles, it can be argued that a few large particles which are observed can be neglected by rejecting the objects above a certain size (particles above 100 μm). Given the limited field of view of the endoscope the chances are generally high that the few large particles in the system (200-250 μm) appear in partial on the image frame, which would result in the rejection of the particles. Nevertheless high number of particle processed in our study ensured reliable statistics and it was not necessary to remove the few outliers.

5.4.3. Comparison of results from image analysis with FBRM and LD

The crystals exiting the COBC (around steady state) were collected by filtering the crystals from the mother liquor and analysed using LD. The samples were also imaged under the microscope. Figure 5.10, shows the comparison of cumulative volumetric crystal size distribution obtained from the LD measurements with the results from the two image analysis approaches respectively. The volumetric distribution are obtained from the number distribution by multiplying the number in each class with Pi/6 and the cube of the class size. The LD results show a much broader distribution with shoulders around the 100 μm size range and around 250-300 μm range approximately. The broad size distribution suggests the varying sizes of crystals as observed from inline images with the SOPAT imaging system. Since only a few large crystals are required for the volumetric distribution to get biased towards the larger size class, the filtering process or sample preparation can easily influence the results from the offline LD analysis. Especially, if agglomerates form due to caking during the filtration process. Figure 5.11 shows the dried crystals sampled at the exit of the COBC, imaged under the microscope at two different magnification of 20x and 50x respectively. Many small particles at size below 100 μm along with a few larger crystals and a certain degree of agglomeration can be clearly observed in both the
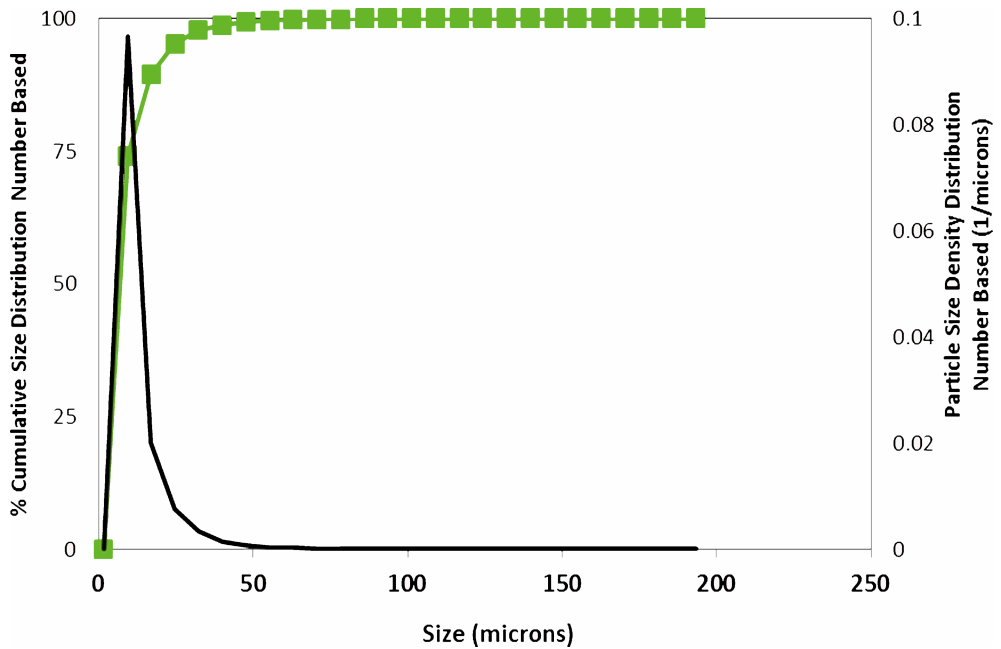
Figure 5.7: Crystal size distribution based on maximun Feret diameter calculated by the segemtation based image analysis algorithm.

images. The results with LD overestimated the particle sizes due to the sticking of the particles together during sampling and the analysis process. The comparison, thus highlight the advantage of using a reliable *in-situ* particle characterization technique whereby ambiguity due to sampling procedures can be avoided.

The inline imaging with the SOPAT system also provides an alternate for an FBRM instrument for *in-situ* monitoring and characterization of the particle concentration in a suspension . In our experiments the image capturing was triggered at several time points during the course of the experiment. Figure 5.12 presents a comparison of the normalised number of particles estimated by the image analysis and by the FBRM. With the large amount of images captured during the trigger interval of $3\ mins$, the image analysis requires considerable time to characterize the particles. While the FBRM measurement is rapid and resolution in order of seconds can be achieved. We observe that the trend in the normalized particle counts obtained by analyzing the images captured at several time points is comparable with the FBRM measurement. Around the onset of the nucleation (30 minutes mark in Figure 5.12) the change in the normalized count estimated by image analysis is larger in comparison to the measurement by FBRM. This observations indicates that imaging is more sensitive and detects a large number of small particles. On the other hand, for real time control the image processing as is done here is too slow to keep up with the process dynamics. Alternative image analysis could be used, like for example tracking changes in the mean image intensity in a series of images to achieve a fast nucleation detection.
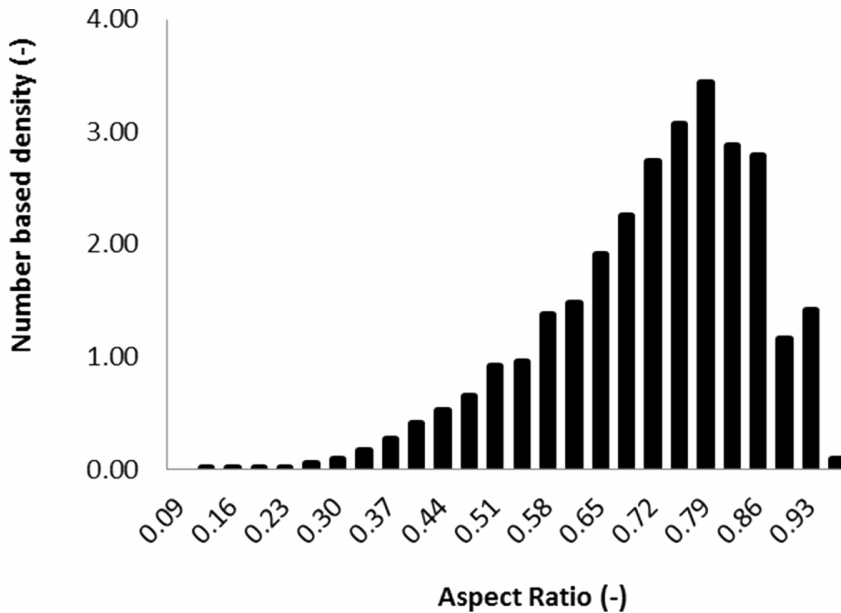
Figure 5.8: Number based density distribution of the aspect ratio of the crystals measured during image analysis.

However the FBRM is suitable for a large range of particle concentrations in comparison to imaging based detection and a comparison on absolute number of particles in not warranted

In terms of the crystallization process, the trend in particle counts indicates that the nucleation continues over several residence times and is thus distributed over the length of the COBC. The trend in particle counts implies that the nucleation is not limited to the first part of the COBC. As estimated from the image analysis the paticle counts at the exit of COBC increases during the process which implies that nucleation occurs also futher in the crystallizer where the susperaturation will be much lower due to the nucleation and growth of the crystals. Apparently secondary nucleation occurs possibly due to the particle-baffle and particle-particle collisions. The backmixing due to the oscillating flow would also contribute to some extent to the particle dispersion.

Figure 5.13 shows the evolution of the cumulative volumetric size distribution (%) measured at different time points (results are from the segmentation approach). The Trigger 1 represents the intimal stage of supersaturation generation during the cooling process. Trigger 2 captured the moment around the nucleation event as indicated by the rise in counts in the FBRM. Triggers 3 and 4 represents the process after several residence times, where the system would be expected to approach a steady state. Each trigger captures the process for about 3 minutes, producing the the high number of particles required to ascertain statistically robust size data
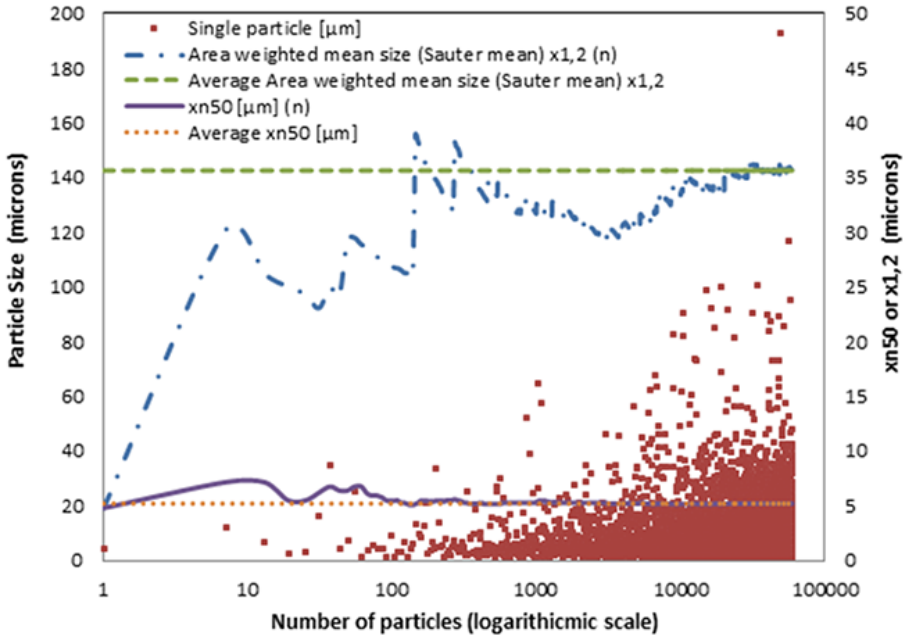
Figure 5.9: Sensitivity plot showing the variation of $xn50$ and $x1,2$ (Sauter mean size) over the number of particles analyzed by the image analysis.

from image analysis. The size distribution from Trigger 1 show very small particles which is mostly likely the impurities present in the system or it can also be the onset of nucleation with very fine particles which were not detected by the FBRM. However nucleation is not expected as supersaturation is very low during the initial cooling period. The size distribution data from trigger 2, 3 and 4 show a shift in the size distribution towards large particle size as the nucleated crystals grow. Also the presence of nucleation throughout the COBC tubes accounts for the similarity in the size distribution at the small size range (the distribution till the 50% mark is similar in all data points).
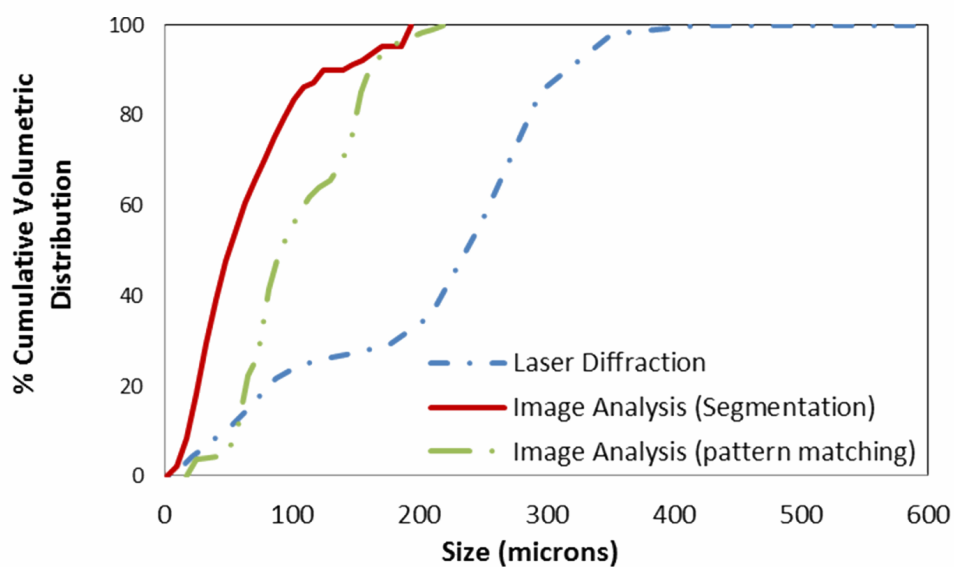
Figure 5.10: Crystal size distribution of the the crystals sampled at the exit of the COBC. Comparison of results using laser diffraction and image analysis.
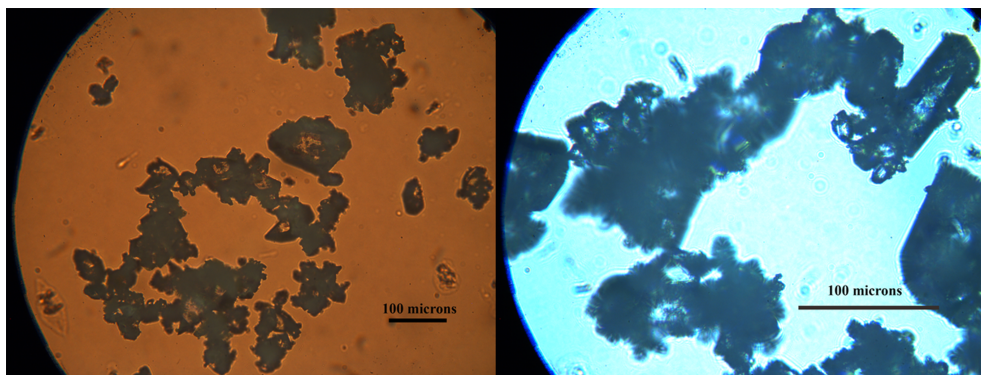
Figure 5.11: Sampled crystals imaged using microscope at magnification of 20x (left) and 50x (right).
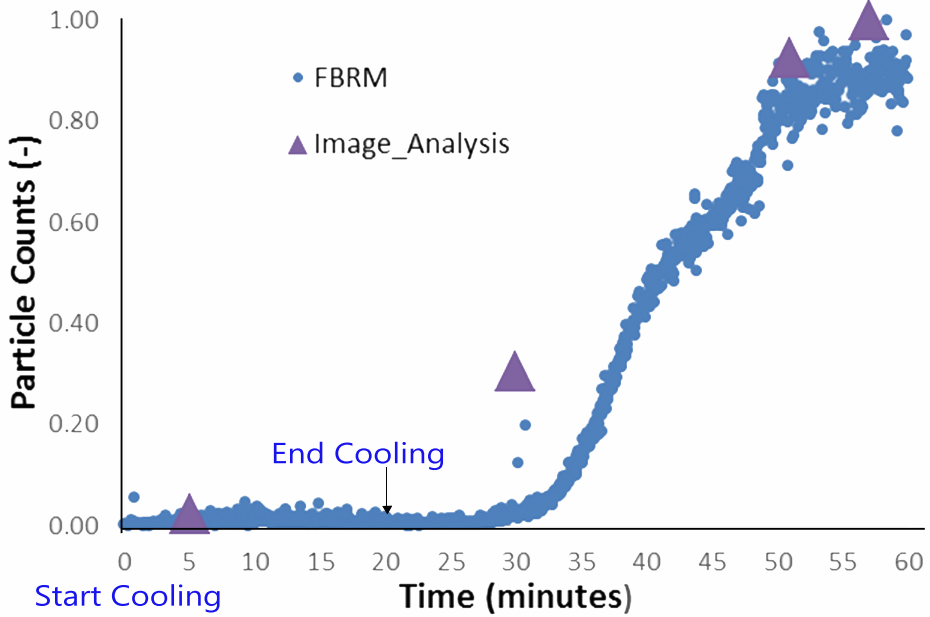
Figure 5.12: Evolution of the normalized number of particles based on images captured at select intervals of time during the experiment in comparison with the counts measured by FBRM over the period of the experiment. Average residence time in the crystallizer is 10 minutes.

Figure 5.13: Evolution of the cumulative number distribution at different process time during the experiment.

5.5. Conclusions

in-situ monitoring of shape and size distribution of melamine crystals nucleated in a COBC was accomplished using the SOPAT imaging system. The pattern matching algorithm based on the user defined training set and a segmentation based object 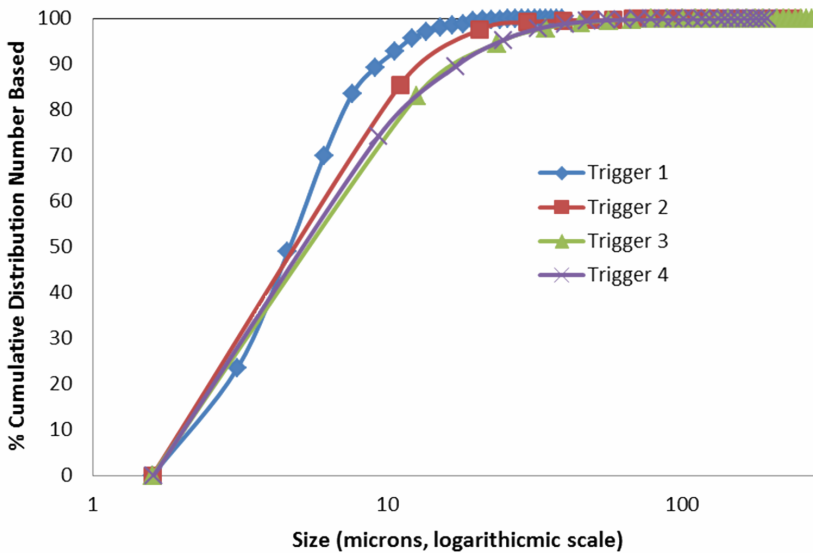recognition algorithm were compared. Due to simultaneous presence of both nucleation and growth both smaller and larger crystals were observed to be present in the COBC. Thus the difference in appearance of the smaller particles (limited by the resolution) from the large particles required separate patterns for reliable particle detection and analysis. A single pattern with sets of features which covered universally both the nucleated and the larger grown crystals could not be generated; highlighting the importance of the user defined training set for pattern matching based image analysis. The mismatch of the estimated circular boundary with boundaries of the non-circular crystals was the limitation Circular approximation of the crystal projections lead to the overestimation of the particle sizes and no accurate estimate could be derived.

The segmentation based algorithm having the flexibility in edge detection was better in identifying the irregular structures (crystals). Shape and size information on the crystals could be reliably estimated using the segmentation approach. The dominance of small particle in the estimated size distributions was due to the strong presence of nucleation during the crystallization process. The aspect ratios estimated from the projections of the particles suggested close to circular particles. The skewness of the aspect ratio toward the circular shape was attributed to the large amount of fine particles which due to the small size were limited by resolution and presented no clear shape. The robustness of the size distribution statistics was backed by the large number of particles detected during the image analysis process.

A comparison of the size distribution obtained from image analysis was also made with the offline measurement using the laser diffraction technique. Due to the influencing of sampling during the sample collection (filtration and drying), a broad size distribution with a bias towards large sizes was observed with the laser diffraction analysis. The collected samples when observed under microscope lend evidence to presence of agglomerates as a result of the sampling process and the hence the results from the laser diffraction. The comparison highlighted the benefit of using the *in-situ* imaging system over offline characterization which can be influenced by the sampling procedures.

Particle counts trend obtained from the imaging analysis were comparable to the trend obtained using the FBRM. The trend in particle counts implied that the nucleation was not localized but occurred over the length of the tubes before being detected by FBRM over a few residence times. Backmixing due to the oscillatory mixing and the presence of secondary nucleation cannot be ruled as factors contributing to distribution of the particles and the trend in the particle counts.

The *in-situ* imaging system offers to be a convenient and a reliable tool for inline characterization of the crystals during the cooling crystallization process in the COBC. The ability to measure *in-situ* without the need for the disturbing the process is need of the hour for continuous manufacturing operations.

References

[1] R. M. Haleem, M. Y. Salem, F. A. Fatahallah, and L. E. Abdelfattah, *Quality in the pharmaceutical industry – a literature review,* Saudi Pharmaceutical Journal **23**, 463 (2015).

[2] J. N. Sangshetti, M. Deshpande, Z. Zaheer, D. B. Shinde, and R. Arote, *Quality by design approach: Regulatory need,* Arabian Journal of Chemistry **10**, S3412 (2017).

[3] D. Lee Black, M. Q. McQuay, and M. P. Bonin, *Laser-based techniques for particle-size measurement: A review of sizing methods and their industrial applications,* Progress in Energy and Combustion Science **22**, 267 (1996).

[4] J. Calderon De Anda, X. Z. Wang, X. Lai, and K. J. Roberts, *Classifying organic crystals via in-process image analysis and the use of monitoring charts to follow polymorphic and morphological changes,* Journal of Process Control **15**, 785 (2005).

[5] B. Y. Shekunov, P. Chattopadhyay, H. H. Y. Tong, and A. H. L. Chow, *Particle size analysis in pharmaceutics: Principles, methods and applications,* Pharmaceutical Research **24**, 203 (2007).

[6] A. Califice, F. Michel, G. Dislaire, and E. Pirard, *Influence of particle shape on size distribution measurements by 3d and 2d image analyses and laser diffraction,* Powder Technology **237**, 67 (2013).

[7] R. Pecora, *Dynamic light scattering measurement of nanometer particles in liquids,* Journal of Nanoparticle Research **2**, 123 (2000).

[8] L. L. Simon, Z. K. Nagy, and K. Hungerbuhler, *Endoscopy-based in situ bulk video imaging of batch crystallization processes,* Organic Process Research & Development **13**, 1254 (2009).

[9] R. F. Li, R. Penchev, V. Ramachandran, K. J. Roberts, X. Z. Wang, R. J. Tweedie, A. Prior, J. W. Gerritsen, and F. M. Hugen, *Particle shape characterisation via image analysis: from laboratory studies to in-process measurements using an in situ particle viewer system,* Organic Process Research & Development **12**, 837 (2008).

[10] Y. Zhou, X.-T. Doan, and R. Srinivasan, *Real-time imaging and product quality characterization for control of particulate processes,* in *16th European Symposium on Computer Aided Process Engineering and 9th International Symposium on Process Systems Engineering*, Computer Aided Chemical Engineering, Vol. 21, edited by W. Marquardt and C. Pantelides (Elsevier, 2006) pp. 775 – 780.

[11] Y. Zhou, R. Srinivasan, and S. Lakshminarayanan, *Critical evaluation of image processing approaches for real-time crystal size measurements,* Computers & Chemical Engineering **33**, 1022 (2009).

[12] S. Maaß, J. Emmerich, J. Rojahn, S. Junne, and P. Neubauer, *Smart imaging analysis for the on line observation of bioprocesses at the example of the microalgae crypteconinium cohnii,* in *2013 AIChE Annual Meeting* (2013).

[13] S. Maaß, J. Rojahn, and S. H. ans M. Kraume, *On-line monitoring of fluid particle size distributions using image analysis.* in *1st international symposium on Multiscale Multiphase Process Engineering* (2011).

[14] D. Sarkar, X.-T. Doan, Z. Ying, and R. Srinivasan, *In situ particle size estimation for crystallization processes by multivariate image analysis,* Chemical Engineering Science **64**, 9 (2009).

[15] J. Eggers, M. Kempkes, and M. Mazzotti, *Measurement of size and shape distributions of particles through image analysis,* Chemical Engineering Science **63**, 5513 (2008).

[16] S. Schorsch, D. R. Ochsenbein, T. Vetter, M. Morari, and M. Mazzotti, *High accuracy online measurement of multidimensional particle size distributions during crystallization,* Chemical Engineering Science **105**, 155 (2014).

[17] O. S. Agimelen, A. Jawor-Baczynska, J. McGinty, J. Dziewierz, C. Tachtatzis, A. Cleary, I. Haley, C. Michie, I. Andonovic, J. Sefcik, and A. J. Mulholland, *Integration of in situ imaging and chord length distribution measurements for estimation of particle size and shape,* Chemical Engineering Science **144**, 87 (2016).

[18] D. R. Ochsenbein, T. Vetter, S. Schorsch, M. Morari, and M. Mazzotti, *Agglomeration of needle-like crystals in suspension: I. measurements,* Crystal Growth & Design **15**, 1923 (2015).

[19] A. Ferreira, N. Faria, F. Rocha, and J. A. Teixeira, *Using an online image analysis technique to characterize sucrose crystal morphology during a crystallization run,* Industrial & Engineering Chemistry Research **50**, 6990 (2011).

[20] X. Z. Wang, K. J. Roberts, and C. Ma, *Crystal growth measurement using 2d and 3d imaging and the perspectives for shape control,* Chemical Engineering Science **63**, 1173 (2008).

[21] R. F. Li, G. B. Thomson, G. White, X. Z. Wang, J. C. De Anda, and K. J. Roberts, *Integration of crystal morphology modeling and on-line shape measurement,* AIChE Journal **52**, 2297 (2006).

[22] S. Le Borne, H. Eisenschmidt, and K. Sundmacher, *Image-based analytical crystal shape computation exemplified for potassium dihydrogen phosphate (kdp),* Chemical Engineering Science **139**, 61 (2016).

[23] P. A. Larsen, J. B. Rawlings, and N. J. Ferrier, *Model-based object recognition to measure crystal size and shape distributions from in situ video images,* Chemical Engineering Science **62**, 1430 (2007).

5

[24] R. Zhang, C. Y. Ma, J. J. Liu, Y. Zhang, Y. J. Liu, and X. Z. Wang, *Stereo imaging camera model for 3d shape reconstruction of complex crystals and estimation of facet growth kinetics,* Chemical Engineering Science **160**, 171 (2017).

[25] C. J. Brown and X. Ni, *Online evaluation of paracetamol antisolvent crystallization growth rate with video imaging in an oscillatory baffled crystallizer,* Crystal Growth & Design **11**, 719 (2011).

[26] C. J. Brown and X.-W. Ni, *Evaluation of growth kinetics of antisolvent crystallization of paracetamol in an oscillatory baffled crystallizer utilizing video imaging,* Crystal Growth & Design **11**, 3994 (2011).

[27] C. J. Brown, Y. C. Lee, Z. K. Nagy, and X. Ni, *Evaluation of crystallization kinetics of adipic acid in an oscillatory baffled crystallizer,* CrystEngComm **16**, 8008 (2014).

[28] R. Kacker, S. I. Regensburg, and H. J. M. Kramer, *Residence time distribution of dispersed liquid and solid phase in a continuous oscillatory flow baffled crystallizer,* Chemical Engineering Journal **317**, 413 (2017).

[29] P. Barrett and B. Glennon, *In-line fbrm monitoring of particle size in dilute agitated suspensions,* Particle & Particle Systems Characterization **16**, 207 (1999).

[30] R. P. Panckow, G. Comandè, S. Maaß, and M. Kraume, *Determination of particle size distributions in multiphase systems containing nonspherical fluid particles,* Chemical Engineering & Technology **38**, 2011 (2015).

[31] J. A. Boxall, C. A. Koh, E. D. Sloan, A. K. Sum, and D. T. Wu, *Measurement and calibration of droplet size distributions in water-in-oil emulsions by particle video microscope and a focused beam reflectance method,* Industrial & Engineering Chemistry Research **49**, 1412 (2010), http://dx.doi.org/10.1021/ie901228e .

[32] D. A. R. Brown, P. N. Jones, and J. C. Middleton, *Handbook of Industrial Mixing: Science and Practice*, edited by E. Paul, V. Atiemo-Obeng, and S. Kresta (Wiley-Interscience, 2004).

[33] S. Maaß, J. Rojahn, R. Hänsch, and M. Kraume, *Automated drop detection using image analysis for online particle size monitoring in multiphase systems,* Computers & Chemical Engineering **45**, 27 (2012).

[34] R. Gopalan and D. Jacobs, *Comparing and combining lighting insensitive approaches for face recognition,* Computer Vision and Image Understanding **114**, 135 (2010).

[35] A. Amokrane, S. Maaß, F. Lamadie, F. Puel, and S. Charton, *On droplets size distribution in a pulsed column. part i: In-situ measurements and corresponding cfd–pbe simulations,* Chemical Engineering Journal **296**, 366 (2016).

[36] A. Grafschafter and M. Siebenhofer, *Design rules for the taylor-couette disc contactor,* Chemie Ingenieur Technik **89**, 409 (2017).

5

[37] A. S. Heeres, K. Schroën, J. J. Heijnen, L. A. M. van der Wielen, and M. C. Cuellar, *Fermentation broth components influence droplet coalescence and hinder advanced biofuel recovery during fermentation,* Biotechnology Journal **10**, 1206 (2015).

[38] L. Hohl, N. Paul, and M. Kraume, *Dispersion conditions and drop size distributions in stirred micellar multiphase systems,* Chemical Engineering and Processing: Process Intensification **99**, 149 (2016).

[39] A.-M. Marbà-Ardébol, J. Emmerich, P. Neubauer, and S. Junne, *Single-cell-based monitoring of fatty acid accumulation in crypthecodinium cohnii with three-dimensional holographic and in situ microscopy,* Process Biochemistry **52**, 223 (2017).

[40] S. Maaß, F. Metz, T. Rehm, and M. Kraume, *Prediction of drop sizes for liquid–liquid systems in stirred slim reactors—part i: Single stage impellers,* Chemical Engineering Journal **162**, 792 (2010).

[41] S. Maaß, T. Rehm, and M. Kraume, *Prediction of drop sizes for liquid–liquid systems in stirred slim reactors—part ii: Multi stage impellers,* Chemical Engineering Journal **168**, 827 (2011).

[42] J. P. Lewis, *Fast normalized cross-correlation,* in *Vision interface*, Vol. 10, pp. 120–123.

5

6

Ultrasound Assisted Seed Generation for Continuous Processes

6

In the study, the use of ultrasound (US) as process actuator for nucleation under moderate supersaturation condition has been investigated for continuous seed generation for the oscillatory flow baffled crystallizer. The US assisted seeding is envisaged to maintain and control the number of crystals in the continuous crystallizer for avoiding unwanted nucleation on the surface of the tubes of the COBC. As a consequence of the consistent seeding of the COBC, product crystals with narrow size distribution is targeted. To realize the US seed generation system, efficient mechanisms for applying ultrasound assisted nucleation has been studied. Nucleation at low supersaturation well within the MSZW is targeted to avoid excessive nucleation which leads to fines formation and hence poor size distribution. Therefore, identification of the supersaturation regime at which nucleation can be induced by application of US has been carried out, as well as the commonly used designs for application of US have been tested in their capability for in-situ seed generation, i.e. to provide a continuously supply of seeds with optimal quality. Two different US configurations have been used; one for batch application in which the US horn was inserted directly in a 1 L batch crystallizer and the other configuration, consisting of the US horn attached to a flow through cell, for continuous seed generation. Finally, the application of the US assisted flow through cell for seeding the COBC has been evaluated in its capacity to provide sufficient nuclei in the process to suppress unwanted nucleation on the walls of the COBC tubes.

6.1. Introduction

Continuous operation in general is attracting interest due to the potential benefits such as low operation cost, reduction in operating volume and improved safety and controllability. Design based on continuously operated stirred crystallizer or use of tubular flow systems with plug flow like mixing regime are being developed for continuous crystallization processes. With respect to the crystallization process, plug flow systems offer enhanced process control opportunities due to superior temperature control and the narrow residence time distribution that can be obtained. Plug flow systems can also be potentially attractive in terms of the flexibility to scale-out instead of scale-up. Tubular crystallizer employing interaction of the oscillating fluid flow with the baffles in the tubes to achieve plug flow like mixing conditions is a promising design. Since the mixing conditions mostly depend on the generation of the vortices from the interaction of the oscillating flow with the baffles, a flowrate independent control over mixing is achieved. Thus, the oscillatory flow baffled crystallizer allows for large residence times to be realized in relative short tube lengths. However, the reliability and the operation know-how of the stirred tank systems have favored the implementation of such systems for continuous operation at industrial scale [1]. A number of challenges are associated with the stirred tank systems which include among others, poor control over mixing leading to broad residence time distributions, low heat transfer rates, and varying shear rates which results in non-uniform conditions in the crystallizer and hence in poor control over the quality of the crystals.

Control of nucleation is important, irrespective of the type of the crystallizer, as the onset of the crystallization process is critical for controlling the end product quality. Gaining precise control over primary nucleation is however a challenge due to the stochastic nature of the nucleation process and its strong nonlinear dependence on the supersaturation, making it sensitive to small spatial inhomogeneity in the supersaturation. Nucleation outbursts causes issues, such as broad multi-modal size distribution and changes in crystal structure which needs to be avoided.

Several strategies have been proposed and implemented to control the nucleation. Seeding the batch or continuous operation is a popular choice as it eliminates the need for nucleation to generate the required number of crystals in the process. Avoiding the primary nucleation through seeding, allows the process to be operated at low supersaturations where growth is dominant. Seeding is often applied even in continuous mixed-suspension mixed-product removal (MSMPR) crystallization to ensure quick and reliable start-up. However, due to large residence time and dominance of secondary nucleation in MSMPR no additional seeding is needed. On the other hand, in the case of airlift crystallizer for example, where secondary nucleation is strongly suppressed, seeding might be required to ensure that no primary nucleation outbursts occur [2]. In case of continuous plug flow tubular crystallizers, seeding is continuously required as there is no back mixing of nuclei formed by attrition. In tubular crystallizers, the larger surface area can stimulate heterogeneous nucleation and presents risk of fouling of the walls, thus seeding must provide sufficient nuclei to consume the supersaturation through growth and avoid the unwanted nucleation. Various studies have focused on optimizing the seeding strategy by studying the influence of parameters such as the seed mass, the seed size distri-

bution or the ratio of the crystallized mass to the seeded mass on the crystallization process [3–7].

However, addition of an optimal number of seeds narrowly distributed around a specific mean size is challenging, especially during continuous operation. Agglomeration of the seed crystal is a problem which is often encountered and the seed crystal characteristics change due to aging during hold up. As a result of the agglomeration and growth of the seed crystals, the available surface area is reduced, leading to poor process control. Transferring of the seeds from the hold-up vessel to the crystallizer is also critical, as correct supersaturation needs to be ensured otherwise secondary nucleation occurs, which causes excessive fines production. Recycling the product as seed crystal is the most common solution, but it is costly as additional processing steps and control is required to ensure the optimum amount and quality of the seeds. Thus, an efficient process which ensures continuous supply of the optimum seed crystals is required.

The complexities and the challenges involved with the seeding process and with the recirculation of the product crystals as seeds, can be avoided by having a dedicated system where seeds can be generated through controlled nucleation. One of the potential nucleation control approaches is the use of external energy fields to control the nucleation rates. Application of external energy fields like ultrasound and laser pulses have been shown to be promising tools for gaining control over the nucleation rate for manipulating the number of crystals to obtain the desired size distribution and the crystal structure. Especially, US as a potential tool for seed generation, has been studied and demonstrated to produce crystals with narrow size distribution [8]. This approach needs to be further developed by identifying the optimum process conditions, like supersaturation, mixing and the energy of external fields required to gain the desired manipulability of the nucleation rates. Both process design and equipment configurations for controlled application of external energy fields require development to enable application of the technology to industrial processes. Ideally a multistage process is envisaged, where the use of external fields allows optimum seeding through direct generation of the seeds in the process, which can then be grown to the desired characteristics under controlled growth conditions.

6.1.1. Overview of application of ultrasound(US) in the crystallization process

Use of US in crystallization (sono-crystallization) has continued to be an area of active research. Application of US has been targeted to achieve a reduction in MSZW, increased productivity due to the increased nucleation rates, control over purity and polymorph of the crystals, inhibition of agglomeration, improved micro-mixing to enhance diffusion limited mass transport and most commonly for manipulating the particle size distribution [9–12]. It has been shown that the application of US promotes nucleation at relative low supersaturations levels, as was determined by a reduction of the induction time, which means that the required number of nuclei in a batch process can be generated at much lower supersaturation levels [10, 13–18]. Qiu et.al., have reported a reduction in induction time from 340 s to 48 s for magnesium ammonium phosphate, with the application of US in the range of 350

W [18]. Application of US during crystallization was found to overcome problems with agglomeration [8]. Studies in the field of particle size reduction have used US to enhance the attrition and therefore induce a faster deracemization [19], improved solubility and faster dissolution kinetics of the APIs by increasing the specific surface area [10, 20–22]. Good control over particle size distribution has been reported by inducing nucleation at low supersaturations, which helped in avoiding an uncontrolled outburst of nuclei leading to fines generation [10, 16, 23]. Enhanced US induced nucleation rates have been utilized to promote nucleation in systems which are notoriously difficult to nucleate. Through use of US, the nucleation rate improvements have been reported for aminoacids [24], adipic acid [25, 26], roxithromycin [27] [9], ice [28], $BaSO_4$ [15], dodecandioic acid in different solvents [29][12], L-Aspargine monohydrate [30], paracetamol, Dextrose Monohydrate [31], and K_2SO_4 [8]. However, there are studies which also report that the effect of US on nucleation is not strong, for example the use of US to study nucleation of calcium carbonate crystals [32] or with ammonium sulphate system.

The commonly used PAT tools, such as FBRM or imaging probes, all suffer from the inability to detect nucleation events instantaneously, meaning with a delay time required for the nuclei to grow to the detectable size of the instrument. This makes the identification of the optimum conditions for application of US difficult. The inability to precisely characterise nucleation also leads to poor understanding of the US assisted nucleation mechanism, which makes it difficult to predict the nucleation rates. Often the effect of US on the crystallization process is evaluated based on the end product quality which can be misleading as the shape, size or the number of crystals change due to the growth, secondary nucleation or agglomeration. Furthermore, poor understanding of the mechanism behind US assisted nucleation has limited the development of the technology [33]. Often, these used configurations are sub optimal as the spatial distribution of the US field or the power introduced into the system is poorly controlled, leading to poor results.

Cavitation has been the predominant phenomenon believed to behind the US induced nucleation [34]. On applying the US, cavitation bubbles are created which induce very high local temperatures and pressures upon collapse [35, 36]. However, high temperature reduces the supersaturation and high pressures mostly increases the work for nucleation making the exact mechanism unclear. Therefore, alternate mechanisms have been proposed. A rapid increase in supersaturation during bubble expansion or after collapse of the cavitation bubbles has been proposed to be responsible for the enhanced nucleation rates due to creation of thermal gradients with rates approximated to be in the range of 107 to 1010 K/s [9, 12]. A distinction can be made between transient and stable cavitation bubbles. Transient bubbles are short lived and create the extreme local conditions upon collapse, whereas the stable cavities have a longer life time and implode less violently when compared to transient bubbles [37]. Stable cavities have been attributed to promote nucleation through heterogeneous nucleation mechanism, similar to the observations when gas bubble is introduced in supersaturated solution [26]. Another explanation of the enhanced nucleation rates during sono-crystallization is the segregation of the solute species in the vicinity of the bubbles due to large pressure gradients, especially the

bubble oscillations before collapsing promotes high density regions favouring nucleation [38]. The enhanced mass transfer resulting from the improved micromixing upon application of the US has been also been attributed to the nucleation rate enhancement and the resulting crystal shape and surface properties [21]. Devarakonda et. al., reported an US assisted crystallization process where an increase in growth rate was observed owing to breakage of crystals which resulted in increased surface area, whereas Nalajala et. al., described higher nucleation but lower growth rates due to the increased turbulence and breakage of crystals when sonication was applied. The major contribution to the crystal breakage is reported to be particle-shock wave interaction while minor contributions are from interparticle collisions, particle-horn collisions and particle-wall collisions [20]. Most importantly a consistent agreement has been observed with respect to production of smaller particles on application of US [20, 21]. In order to facilitate the design of US application various studies are now focused on, for example, evaluating the effect of US frequency (30-1140 kHz) and US power (4-200 W) on crystal nucleation and breakage, effect of batch or continuous configurations and process conditions on cavitation [37], milli-flow devices to gain spatial control over cavitation [39] and energy efficient application of US [40].

A large number of investigations has demonstrated the potential of US to manipulate the nucleation rate in crystallization processes. On the other hand, the strongly system dependent effects of US highlight the requirement to identify first the dominant phenomenon at which US induces the formation of the nuclei, either by primary or secondary nucleation processes. Also, as the nucleation rate has a strong nonlinear dependence on process conditions, controlled nucleation through use of US can only be ensured at conditions where spontaneous nucleation can be prevented from forming excessive numbers of nuclei.

In line with the motivation of this study, to develop US assisted continuous seeding, the following objectives can be formulated

- Identify the most efficient and robust mechanism for US induced nucleation.

- Generate a US based internal seed generating system for continuous process operation avoiding external seed sources.

- Apply this system to continuous processes to obtain product crystals with narrow size distribution.

We first identify a supersaturation regime at which primary nucleation can be induced by application of US. Nucleation at low supersaturations well within the MSZW is targeted to avoid excessive nucleation . Secondly, two commonly used designs of US application system have been tested in their capability for in-situ seed generation, i.e. to provide a continuously supply of seeds with optimal quality. The two US configurations tested were; one for batch application in which the US horn was inserted directly in a batch crystallizer, and the other for continuous seed generation in which the US was applied in a flow through cell carrying a supersaturated solution. Finally,

the application of the US assisted seed generation in continuous flow processes has been studied in a continuous oscillatory flow baffled crystallizer. A FBRM probe has been used where possible to characterize the crystal phase in the process.

6.2. Materials & Methods

6.2.1. Metastable zone width (MSZW) determination without US

Since studies show that supersaturation ratio at which the US is applied is one of the most important parameter to control crystal properties, metastable zone width has been initially determined in separate experiments. Three systems have been studied, namely, aqueous solution of L-ascorbic acid (AA), paracetamol and melamine. The MSZW was determined under batch conditions by cooling an initially clear, saturated solution until nucleation was observed. The clear saturated solution was made by keeping the solution at 5 $°C$ above the saturation temperature to ensure complete dissolution of the solids. A linear cooling profile (-0.1 $°C/min$) was applied to the solution and the nucleation was observed visually. The batch setup used to characterize the MSZW is same as configuration 'a' detailed in the next section.

6.2.2. US device & setup

A 20 kHz US horn with a diameter of 34 mm and output power rated to be 500 W (model UIP 500HD, Heilscher) has been used throughout the work to apply US. Two equipment configurations have been used in the study. The configurations are: a) Direct contact of the US probe with supersaturated solution in a 1L jacketed glass crystallizer and b) The US probe coupled to a flow through a cell in which the supersaturated solution is pumped for continuous or batch operation with recirculation. The configurations are schematically showing in figure 6.1.

It should be noted here that the working volumes of the configurations are different. Configuration 'a' allows 1 L batch of supersaturated solution to be sonicated, whereas configurations 'b' has a hold up volume of 150 ml which is exposed to US. Moreover configuration 'a' operates in batch mode only whereas the other configuration allow both batch and continuous operation.

In our setup, the input energy to the US horn could be regulated from the signal generator (attached to the US horn) by selecting the mode of operation to be between 50 to 100 % (in step of 10%). In our study the input power selection was fixed at 50% which implied that only half of the maximum rated power (500 W @100%) was supplied to the US horn. We also had a reducer attached to the horn which resulted in the output energy from the horn to be reduced by 50%. The direct characterization of the US energy transferred into the medium is not straightforward. A commonly used measure is the calorimetric energy input due to the heating of the medium by the US energy. The rise in temperature of the medium upon application of the US is measured and the total heat energy is quantified. The calorimetric powers used in our study were in the range of 20-50 W.

In our study, the effect of US on nucleation has been quantified in the batch system (configuration 'a'). To study the application of US for seed generation for continuous systems, configuration 'b' was coupled to the COBC, where growth dom-

inated operation was targeted. FBRM has been used to detected nucleation when possible, otherwise nucleation has been detected visually. In all the experiments, clear supersaturated solution is present before the application of US.
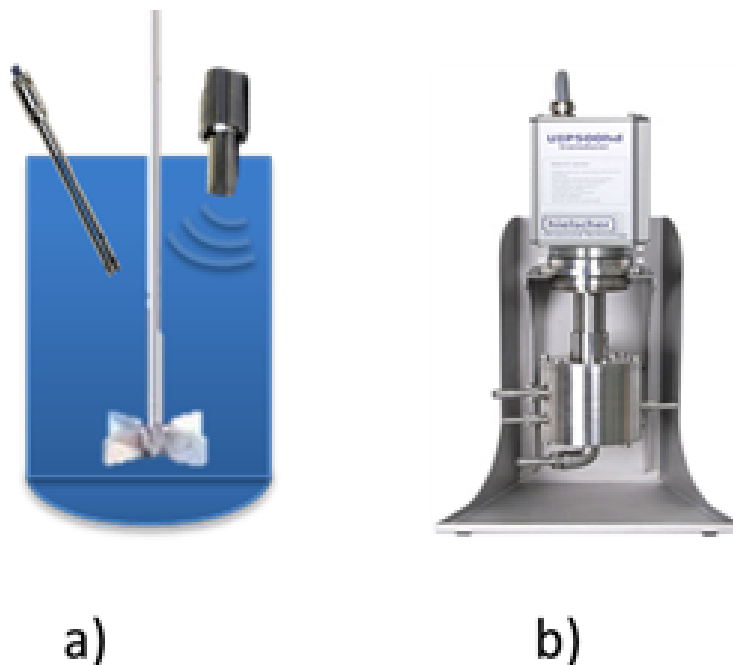

Figure 6.1: Two configuration for US application: a) Direct application of US into the solution in a batch crystallizer and b) US horn attached to flow through cell.

6.3. Results & Discussions

6.3.1. MSZW without US

The metastable zone width depends on the operating conditions which include among others, the cooling profile, volume of the saturated solution, initial saturation concentration, mixing etc. Through experiments the MSZW was determined. Table 1, summarizes the MSZW measured for the different compounds studied along with the working volume, initial concentration and corresponding saturation temperature. To ensure that US is applied in a supersaturation regime where no spontaneous nucleation takes place, the MSZW was quantified. Operating within the MSZW is required as induction of nucleation through US is sought at low supersaturations. As seen from Table 6.1, the MSZW for AA is relatively large compared to Melamine. Due to the narrow MSZW with melamine-water system, the application window for US is small for avoiding spontaneous nucleation.

In light of the two different configurations with different working volume, a high

Table 6.1: Overview of the studied compounds with their corresponding process conditions. The nucleation has been detected visually. MSZW is derived as the difference between saturation and nucleation temperature at the given conditions.

Compound	Concentration (gm/L solvent)	Working Volume for MSZW (mL)	Saturation Temp. (°C)	Avg. Nucleation Temp (°C)	MSZW
L-ascorbic acid (AA)	500	1000	40	24	16
Paracetamol	21	1000	38	25	13
Melamine	10.7	500	50	43	7

variability in MSZW is expected as the working volume is decreased. In literature, the stochastic nature of nucleation has been shown to be very evident at small batch volumes [41]. Using paracetemol-water system (also used in study), it was shown that a variation upto 20 $°C$ in the MSZW was observed between a large number of independent measurements. Whereas, with experiments at a volume of 500 ml or 1 L the variation only around 2 $°C$. The more deterministic MSZW measurements at large volumes was attributed to the higher probability of a single nucleus to form, which is followed by secondary nucleation leading to the observed nucleation. Thus, the supersaturation required to induce nucleation at small volumes can show a high variability and be much higher than the measurements reported in Table 6.1. Use of US introduces new mechanism which may influence nucleation, such as cavitation events may result in higher nucleation probability at a constant supersaturation reducing the variability in nucleation, especially at low working volumes. However, we have not studied in depth the effect of US on the MSZW as a function of volume.

6.3.2. Effect of US on nucleation in batch operation.
Nucleation under the influence of US was characterized in batch process. The paracetamol-water system was studied in configuration 'a', with 1 L capacity. Clear saturated solution (20 gm/l) was cooled down to 35 °C to generate supersaturation (S =1.22) while remaining within the MSZW (refer Table 6.1). Experiments with and without the application of US were carried out. The nucleation was observed visually.

A significantly short induction time was observed with the application of US. Under silent conditions (blank experiment with no US), no nucleation is observed for at least 5 hours. Upon use of US as soon as the supersaturation is generated, a short exposure of 5 minutes is enough to induce nucleation. In several repeat trial of US assisted experiments, within 5 minutes, the solution is observed to become turbid indicating that a large number of nuclei have been produced. On the contrary, spontaneous nucleation under silent conditions goes much slower and hence no nuclei are observed within the limited observation time.

The effect of US on nucleation in melamine-water system has also been studied similarly under batch condition using configuration 'a'. Figure 6.2, shows the reduction in induction time when the US is used in comparison to silent conditions. The induction time is recorded using visual observation. The observed reduction in the induction time clearly shows that the use of US has benefit at low supersaturation where the reduction in induction is drastic. The observed reduction in the induction

time, especially at low supersaturations, clearly shows that the US eenables nucle-ation at low supersaturation levels. The US induced nucleation mechanism can be either primary via a reduction in the nucleation energy barrier or for example, due to the high local supersaturation created by cavitation events. Secondary nucleation, due to attrition of primary nuclei present in the system (which are not easily ob-servable), is also a possibility. The latter mechanism would however implicate that the first nuclei are already present long before they are detected and could originate from heterogeneous nucleation in the solution at the liquid air interface or at the walls [41].

Concluding, application of US has a strong influence on the nucleation in batch operation, enabling nucleation to occur at low supersaturations, well within the metastable zone.
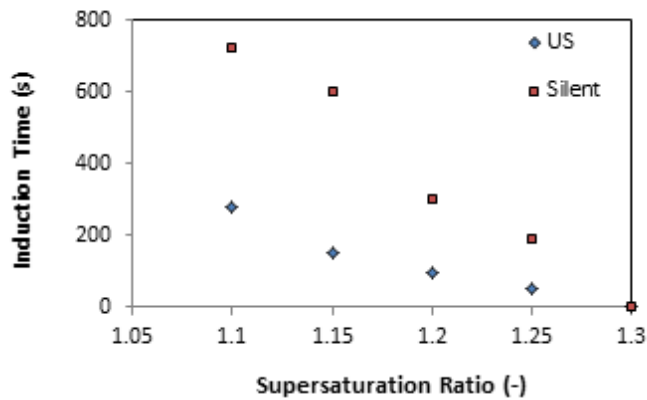

Figure 6.2: Reduction in induction time observed upon application of US at various fixed initial supersat-uration under batch operation (500 ml) using configuration 'a'.

Batch experiments using configuration 'b' were designed to study the effect of US on nucleation of ascorbic acid. The flow through cell was operated in batch mode by recirculating the exit stream from the cell to the feed vessel. To facilitate the monitoring of nucleation the FBRM was placed in the 1 L feed vessel in which the saturated solution was prepared initially. The start-up process lasted for 20 minutes after preparation of the saturated solution (Table 6.1) as the solution was pumped (100 ml/min) through the flow cell and allowed to drain away for two residence time of the flow cell (90 s) before exit of the flow cell was closed for recirculation of the solution. The draining procedure allowed removal of any left-over contaminants from being recirculated. Once the loop was closed, cooling was started to cool down the solution to a temperature within the MSZW. The US was turned on once the desired temperature was reached. The rise in the number of particles in the vessel was continuously recorded to monitor nucleation.

Figure 6.3, shows the rise in particle counts as recorded by FBRM without US under silent conditions (S =1.33) and when the US was continuously applied (S =

1.33 & 1.18). The striking reduction in induction time is observed when the US was applied. In the absence of US it is seen that around 120 minutes are required before nucleation is observed. With the application of US, the nucleation is observed under 30 minutes. Secondly, the rate of change of particle counts is enhanced when US is applied. An approximation of the rate of change of particle counts was estimated based on the time it took for the particle count to rise to the highest values shown in the Figure 6.3. Without US, the counts rose approximately with the rate of 3-4 counts/min on the other hand with US the rise is in the order of 50 counts/min (at same initial supersaturation, S =1.33).

Again the stimulation of the nucleation rate by the US, leading to an increased rate of nuclei generation, can be due to the US induced primary or secondary nucleation as explained earlier. It should be noticed that in the blank experiments no clear signs of crystals is observed with the FBRM for the first 30 minutes of the experiments. Therefore, it is most likely that the application of the US promotes primary nucleation first which is required for secondary nucleation.

The effect of US application on the CSD is shown in Figure 6.4. Samples of the suspension were taken around 120 minutes for the blank process and 60 minutes when US was used. Figure 6.4, shows the laser diffraction based CSD of the samples collected at the exit of flow cell. In the US experiment, almost a mono-modal distribution with a peak at 40 microns is observed, while the experiment without US showed several peaks. Due to the longer batch time required in the blank experiments to reach the counts of 2000, larger crystal sizes are found.

The multiple peaks in the blank experiment can be due to multiple reasons, such as progressive nucleation due to the low nucleation rate and thus slow supersaturation consumption, secondary nucleation and agglomeration. Attrition due to the pump in the recirculation loop does not seem to be responsible for the fine particles as crystals experience a longer residence times in the blank experiment.

Visually some settling of particles was observed in the flow through cell, especially when US was switched of. Some accumulation of particles was observed in the flow cell which might introduce variability in the particle size distribution.

Concluding, the results of the batch experiments in both configuration 'a' and 'b' showed a clear effect of US on inducing nucleation at low supersaturation conditions, which is explored further in the following section, in continuous processes. The experiments with the flow though cell showed that the mixing in flow cell must be improved. Coupling the flow cell with the oscillatory flow in the COBC might result in possible improvement of the mixing in the flow cell, which could result in a robust seeding process for the COBC.

6.4. Application of US for nucleation control in COBC

6.4.1. Applicability of the flow cell for internal seed generation in the COBC

The effectiveness of the flow cell for continuous seed generation was characterized in independent experiments without coupling the flow cell to the COBC. Continuous operation was ensured by pumping (80 ml/min) of the supersaturated paracetamol-
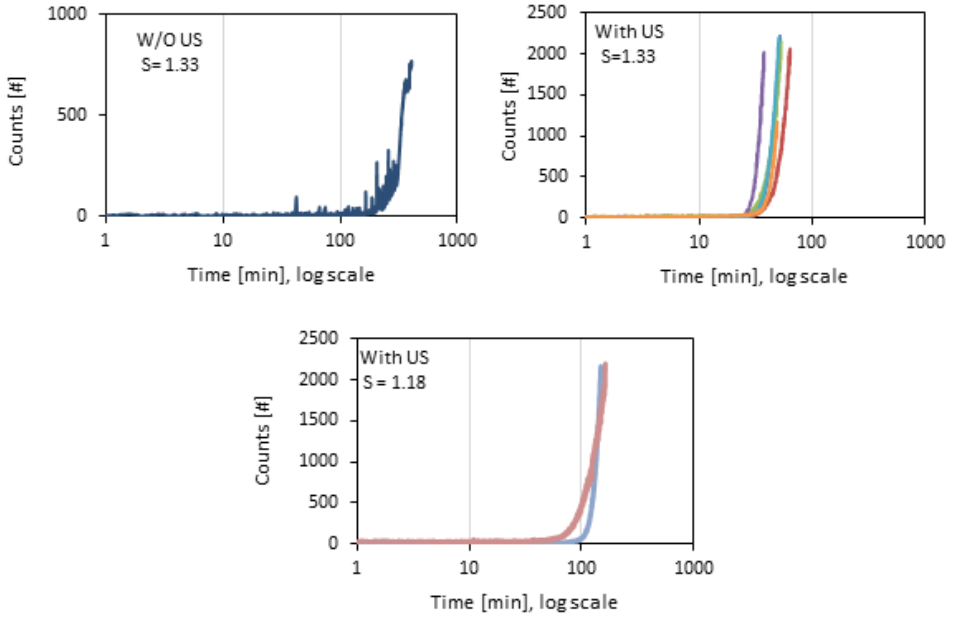
6

Figure 6.3: Effect of US on nucleation kinetics of ascorbic acid in batch operation (at two initial supersaturations).
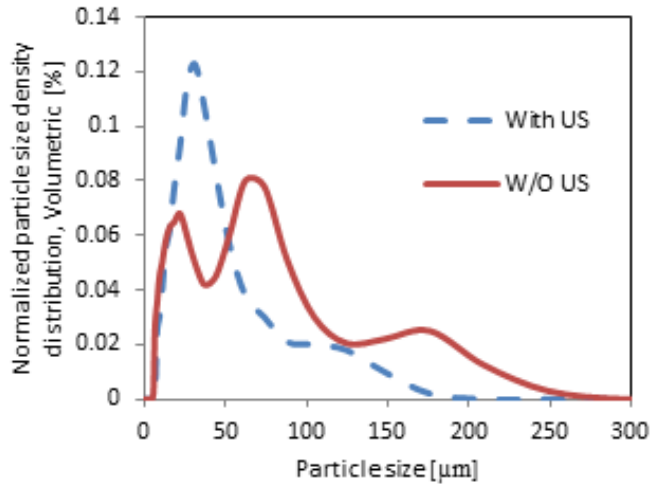

Figure 6.4: Normalized particle size density distribution (volume based) of sample taken from US assisted and blank process (S =1.33) at batch times of 60 min and 120 minutes corresponding to FBRM count of 2000.

water solution (prepared in a 5 L batch crystallizer) through the flow cell. The residence time in the flow cell is estimated to be 2 minutes. The exit temperature of the flow cell was maintained at 32 $°C$, corresponding to S =1.37, which was generated by cooling the supersaturated solution in the batch crystallizer before pumping through the flow cell. The US was switched on after allowing the solution to flow out for 2 residence time. The flow at the exit of the flow cell was allowed to pass through a filtration set-up, so as to capture the crystals coming out of the flow cell. The whole experiment lasted about 1 hour before the whole batch was pumped through the flow cell.

Compared to the US assisted experiments directly in the batch crystallizer (config. 'a'), lower temperature was required (i.e higher supersaturation) in order to observe nucleation with the application of US (5 experiments). The higher supersaturation to observe nucleation is probably due to the reduced working volume in the flow cell. However, with all the experiments nucleation was observed on application of US. Under silent conditions, no nucleation was observed in repeated trials (9 in total) with continuous operation of the flow cell for 1 hour of operation.

The crystals leaving the flow cell which were deposited on the filter paper were characterized. Figure 6.5, shows the volumetric size distribution of the particle sampled at the exit of the flow cell. Also shown in the figure is an typical image of the particles, as observed under microscope. Both show that very small and large particles are present, indicating large differences in crystal residence time in the flow cell. Since the crystals are immediately filtered at the exit, the large crystals must be coming from the flow cell. The hold-up of crystals in the flow cell also introduces uncertainness in the role of US induced nucleation, as secondary nucleation may become dominant after the initial creation of the primary particles. Hence, the current configuration of US application in the flow cell is not ideal for a narrow sized internal seed production.
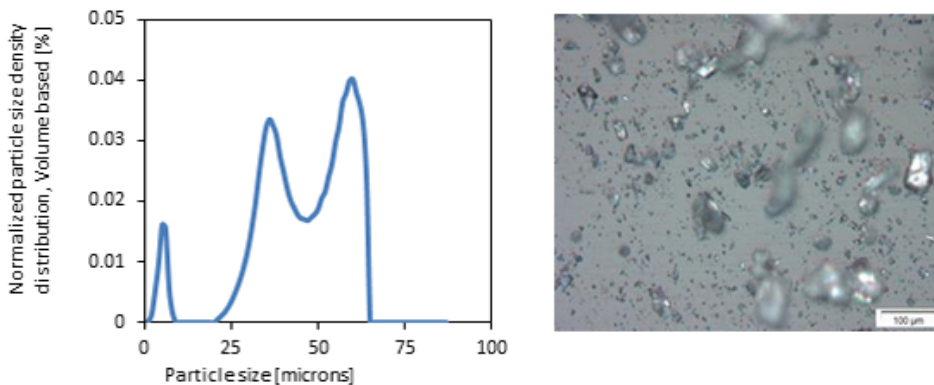

Figure 6.5: Volume based particle size distribution of the paracetamol crystals at the exit of flow cell (left) and the sampled particles as imaged under microscope (right) at S =1.37 of paracetamol-water system.

6.4.2. Coupling of the US flow through cell with the COBC

Coupling of the US flow cell with the oscillatory flow of the COBC will influence the process. The oscillatory flow improves mixing in the flow cell which can avoid the settling of the particles, as previously observed during the operation of the flow cell. On the other hand, the flow cell will introduce some back mixing which will affect the plug flow in the COBC and can thus, lead to difference in the residence time of the crystals in the COBC and the crystal size distribution. Additionally, melamine-water system was chosen to study the role of US assisted seeding in the COBC instead of the paracetamol-water system, as the mixing of the melamine-water system in the COBC is well studied, through extensive characterization of the residence time distribution at various operating conditions (Chapter 4).

To identify the supersaturation regime where spontaneous nucleation can be avoided in the COBC, a series of blank and US assisted experiments were performed with the flow cell coupled to the COBC. The configuration is shown schematically in the figure 6.6. The fluid oscillations in the COBC were chosen such that the operation of COBC was under plug flow conditions (2 Hz and 4 mm) [42]. The start-up process involved circulating clear saturated solution (prepared separately in a temperature controlled stirred vessel) through the COBC. After allowing the flow to displace twice the volume of the COBC, to ensure complete removal of water used in the start-up process, cooling was started. 20 minutes are required to reach the desired temperature of the COBC tubes. Once the tubes are cooled, the hot saturated solution entering the COBC becomes supersaturated in the first three tubes of the COBC. The supersaturation close to S =1.36 is targeted for the blank and US experiments, as this superstation is required for US assisted nucleation. The temperature of the rest of the tube was fixed, so as to not generate additional supersaturation. The supersaturated solution from the third COBC tube was directly allowed to flow into the flow cell and the exit stream from the cell was connected back into the COBC at the entrance of tube 4. The fluid residence time in the COBC was close to 10 minutes and in the flow cell around 1.5 minutes. For US assisted operation, the US was kept on continuously after the desired supersaturation was generated, during the entire duration of the experiments. At the exit of COBC, SOPAT high speed imaging probe was placed to characterize the crystals that flow out of the system. For details on operation of COBC and use of SOPAT image probe, previous chapter should be consulted (Chapter 5).

Figure 6.7, compares the normalized particle counts measured using FBRM within the COBC for one set of blank and US assisted experiment. The triangular markers on the figure show the time point where the desired supersaturation was generated in case of the blank experiment and the same time point where the US was switched on for continuous operation in the US assisted experiment. In context of the residence time in the COBC, the seed crystals entering the COBC from the flow cell should exit the system in 10 minutes. Under the current COBC operating conditions, near plug flow is expected and it is unlikely that the crystals will deviate from the expected residence time in the COBC. Therefore, the nucleation which will happen in the solution at entrance of the COBC will be detected by FBRM one residence time later, at the exit.
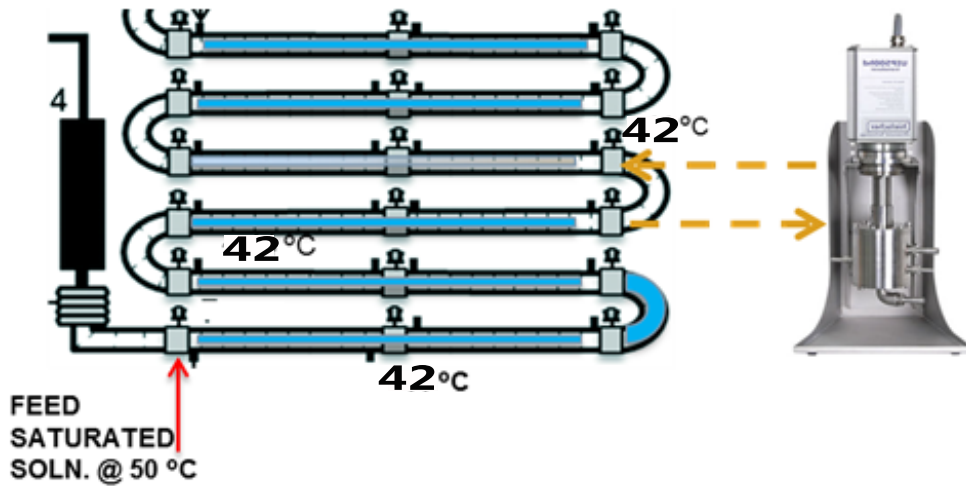
Figure 6.6: Schematic showing the use of US assisted flow through cell as the seed production unit in combination with COBC. Clear supersaturetd solution generated in the COBC was passed through the flow cell for nuclei generation which were transferred back into COBC to grow

Very different trends in the particle counts are observed between the two experiments shown in figure 6.7. In the blank experiments, no crystals are detected in the first 10-12 minutes, indicating that longer induction time is required at the current fixed supersaturation in the set-up. Subsequently, the particle count is seen to rise, which continues over several residence times. Under plug flow, the gradual rise in particle count suggests a high variability in nucleation at the inlet. Knowing the operation of the COBC ensures plug flow, backmixing of the crystals is not expected to cause the crystals to experience a longer residence time in the COBC.

On the other hand, nucleation on the COBC walls could be the most dominant mechanism, which likely causes the crystals to deviate from the expected plug flow. The large surface area offered by the COBC tubes and the baffles, along with the unconsumed supersaturation promotes the nucleation on the surfaces within the COBC. As a result, the nucleation is no longer restricted to the inlet of the COBC and therefore may occur at any position along the tube. Similarly, with the US assisted experiments, nucleation is detected much later than the start of the US application. The particle counts rise initially, which is followed by a drop and again a rising trend in the count is observed. The result, makes the role of US uncertain as nucleation is expected to occur in the flow cell and under plug flow condition, the delay in detection of nucleation is not expected. The variability in nucleation rate which causes the particle counts to vary drastically during the course of the experiment cannot be explained. The decrease is counts can only be attributed to the absence of continued nucleation.

The results from the experiments show the strong presence of nucleation on the walls of the COBC, which overshadows the effect of US (if any), making the control of crystal properties difficult. Presence of secondary nucleation, due to crystal-wall,

crystal-baffle and crystal-crystal collision could be aiding the variation in the number of nuclei in the system arising from the uncontrolled nucleation events. Since, no scaling was observed visually during the experiments, the abrupt rise in the particle count cannot be attributed to crystals originating from the scales on the COBC tubes. Overall, the use of US to localize nucleation in the flow cell was not achieved, as in several additional experiments nucleation on the walls of COBC was observed. The efficiency of US to manipulate nucleation as observed under batch conditions could not be achieved under the conditions investigated with the configuration combining the flow cell and the COBC.
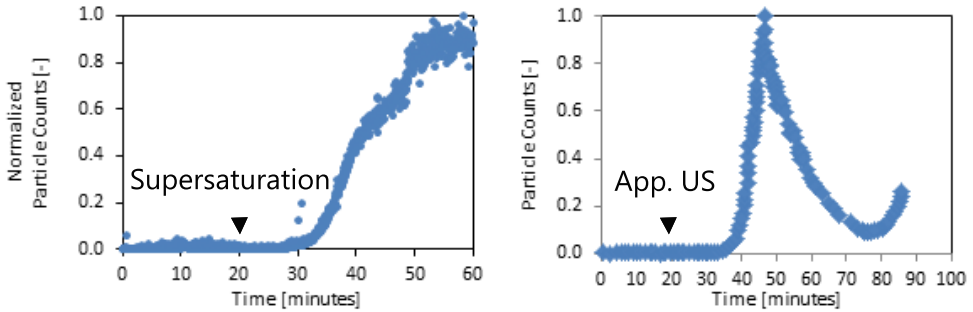

Figure 6.7: Particle counts profile in COBC under silent conditions (left) and under sonicated operation of the flow cell (right). Operating flowrate of 100 ml/min and oscillation frequency of 2 Hz and amplitude of 4 mm with the initial supersaturtion set to (S = 1.36).

6.5. Conclusions & Recommendations

- Under batch configurations a clear effect of US on nucleation has been observed.

- Low supersaturation is critical to the success of nucleation control through the application of US, as at high supersaturation the risk of primary nucleation is high.

- Flow through cell as used in our study offered poor mixing control, which made it an unreliable tool for application of US.

- Unwanted nucleation on the walls of the COBC overshadowed the application of the US assisted flow cell for seeding the COBC. Nucleation on the walls resulted in the deviations in the crystals residence time distribution from the established plug flow mixing.

- Research is still needed to design US application systems, wherein the residence time distribution is minimal and good spatial control of the power of the US is achieved.

- Ideally, it is recommended to have US applicators directly attached to the COBC tubes: This allows avoiding contact of the US applicator with the solution and the complexities arising from the additional unit for applying US, such as pumps and control infrastructure.

6

References

[1] Q. Su, Z. K. Nagy, and C. D. Rielly, *Pharmaceutical crystallisation processes from batch to continuous operation using msmpr stages: Modelling, design, and control,* Chemical Engineering and Processing: Process Intensification **89**, 41 (2015).

[2] R. Lakerveld, J. J.H. van Krochten, and H. J.M. Kramer, *An Air-Lift Crystallizer Can Suppress Secondary Nucleation at a Higher Supersaturation Compared to a Stirred Crystallizer,* Crystal Growth & Design **14**, 3264-3275 (2014).

[3] S. H. Chung, D. L. Ma, and R. D. Braatz, *Optimal seeding in batch crystallization,* The Canadian Journal of Chemical Engineering **77**, 590 (1999).

[4] J. D. Ward, D. A. Mellichamp, and M. F. Doherty, *Choosing an operating policy for seeded batch crystallization,* AIChE Journal **52**, 2046 (2006).

[5] A. N. Kalbasenka, L. C. P. Spierings, A. E. M. Huesman, and H. J. M. Kramer, *Application of seeding as a process actuator in a model predictive control framework for fed-batch crystallization of ammonium sulphate,* Particle & Particle Systems Characterization **24**, 40 (2007).

[6] R. J. P. Eder, E. K. Schmitt, J. Grill, S. Radl, H. Gruber-Woelfler, and J. G. Khinast, *Seed loading effects on the mean crystal size of acetylsalicylic acid in a continuous-flow crystallization device,* Crystal Research and Technology **46**, 227 (2011).

[7] A. Mesbah, A. N. Kalbasenka, A. E. M. Huesman, H. J. M. Kramer, and P. M. J. Van den Hof, *Real-time dynamic optimization of batch crystallization processes,* IFAC Proceedings Volumes **41**, 3246 (2008).

[8] N. Lyczko, F. Espitalier, O. Louisnard, and J. Schwartzentruber, *Effect of ultrasound on the induction time and the metastable zone widths of potassium sulphatelyczko2002,* Chemical Engineering Journal **86**, 233 (2002), 544UQ Times Cited:84 Cited References Count:18.

[9] M. L. de Castro and F. Priego-Capote, *Ultrasound-assisted crystallization (sonocrystallization),* Ultrasonics Sonochemistry **14**, 717 (2007).

[10] J. Chen, B. Sarma, J. M. B. Evans, and A. S. Myerson, *Pharmaceutical crystallization,* Crystal Growth & Design **11**, 887 (2011).

[11] A. Kordylla, T. Krawczyk, F. Tumakaka, and G. Schembecker, *Modeling ultrasound-induced nucleation during cooling crystallization,* Chemical Engineering Science **64**, 1635 (2009).

[12] S. L. Hem, *The effect of ultrasonic vibrations on crystallization processes,* Ultrasonics **5**, 202 (1967).

[13] N. Amara, B. Ratsimba, A.-M. Wilhelm, and H. Delmas, *Crystallization of potash alum: effect of power ultrasound,* Ultrasonics Sonochemistry **8**, 265 (2001).

[14] H. Li, J. Wang, Y. Bao, Z. Guo, and M. Zhang, *Rapid sonocrystallization in the salting-out process,* Journal of Crystal Growth **247**, 192 (2003).

[15] Z. Guo, M. Zhang, H. Li, J. Wang, and E. Kougoulos, *Effect of ultrasound on anti-solvent crystallization process,* Journal of Crystal Growth **273**, 555 (2005).

[16] S. Kaur Bhangu, M. Ashokkumar, and J. Lee, *Ultrasound assisted crystallization of paracetamol: Crystal size distribution and polymorph control,* Crystal Growth & Design **16**, 1934 (2016).

[17] L. d. l. S. Castillo-Peinado and M. D. Luque de Castro, *The role of ultrasound in pharmaceutical production: sonocrystallization,* Journal of Pharmacy and Pharmacology **68**, 1249 (2016).

[18] L. Qiu, L. Shi, Z. Liu, K. Xie, J. Wang, S. Zhang, Q. Song, and L. Lu, *Effect of power ultrasound on crystallization characteristics of magnesium ammonium phosphate,* Ultrasonics Sonochemistry **36**, 123 (2017).

[19] C. Xiouras, J. Van Aeken, J. Panis, J. H. Ter Horst, T. Van Gerven, and G. D. Stefanidis, *Attrition-enhanced deracemization of naclo3: Comparison between ultrasonic and abrasive grinding,* Crystal Growth & Design **15**, 5476 (2015).

[20] J. R. G. Sander, B. W. Zeiger, and K. S. Suslick, *Sonocrystallization and sonofragmentation,* Ultrasonics Sonochemistry **21**, 1908 (2014).

[21] J. Jordens, T. Appermont, B. Gielen, T. Van Gerven, and L. Braeken, *Sonofragmentation: Effect of ultrasound frequency and power on particle breakage,* Crystal Growth & Design **16**, 6167 (2016).

[22] G. Ruecroft, D. Hipkiss, T. Ly, N. Maxted, and P. W. Cains, *Sonocrystallization: the use of ultrasound for improved industrial crystallization,* Organic Process Research & Development **9**, 923 (2005).

[23] L. J. McCausland, P. W. Cains, and M. Maxwell, *Sonocrystallization — the use of power ultrasound to control and manipulate the nucleation of crystals,* Chemie Ingenieur Technik **73**, 717 (2001).

[24] H. Anderson, J. Carberry, H. Staunton, and B. Sutradhar, *Crystallization of adipic acid,* (1995).

[25] O. Narducci, A. G. Jones, and E. Kougoulos, *Continuous crystallization of adipic acid with ultrasound,* Chemical Engineering Science **66**, 1069 (2011).

[26] K. Wohlgemuth, F. Ruether, and G. Schembecker, *Sonocrystallization and crystallization with gassing of adipic acid,* Chemical Engineering Science **65**, 1016 (2010).

[27] M.-W. Park* and S.-D. Yeo, *Antisolvent crystallization of roxithromycin and the effect of ultrasound,* Separation Science and Technology **45**, 1402 (2010), https://doi.org/10.1080/01496391003689538 .

6

[28] R. Chow, R. Blindt, R. Chivers, and M. Povey, *A study on the primary and secondary nucleation of ice by power ultrasound,* Ultrasonics **43**, 227 (2005).

[29] A. Kordylla, S. Koch, F. Tumakaka, and G. Schembecker, *Towards an optimized crystallization with ultrasound: Effect of solvent properties and ultrasonic process parameters,* Journal of Crystal Growth **310**, 4177 (2008).

[30] S. Bhoi and D. Sarkar, *Modelling and experimental validation of ultrasound assisted unseeded batch cooling crystallization of l-asparagine monohydrate,* CrystEngComm **18**, 4863 (2016).

[31] S. Devarakonda, J. M. B. Evans, and A. S. Myerson, *Impact of ultrasonic energy on the crystallization of dextrose monohydrate,* Crystal Growth & Design **3**, 741 (2003).

[32] I. Nishida, *Precipitation of calcium carbonate by ultrasonic irradiation,* Ultrasonics Sonochemistry **11**, 423 (2004).

[33] P. W. Cains, P. D. Martin, and C. J. Price, *The use of ultrasound in industrial chemical synthesis and crystallization. 1. applications to synthetic chemistry,* Organic Process Research & Development **2**, 34 (1998).

[34] V. S. Nalajala and V. S. Moholkar, *Investigations in the physical mechanism of sonocrystallization,* Ultrasonics Sonochemistry **18**, 345 (2011).

[35] E. V. Skorb, H. Möhwald, and D. V. Andreeva, *Effect of cavitation bubble collapse on the modification of solids: Crystallization aspects,* Langmuir **32**, 11072 (2016).

[36] C. Virone, H. J. M. Kramer, G. M. van Rosmalen, A. H. Stoop, and T. W. Bakker, *Primary nucleation induced by ultrasonic cavitation,* Journal of Crystal Growth **294**, 9 (2006).

[37] B. Gielen, J. Jordens, J. Janssen, H. Pfeiffer, M. Wevers, L. C. J. Thomassen, L. Braeken, and T. Van Gerven, *Characterization of stable and transient cavitation bubbles in a milliflow reactor using a multibubble sonoluminescence quenching technique,* Ultrasonics Sonochemistry **25**, 31 (2015).

[38] R. Grossier, O. Louisnard, and Y. Vargas, *Mixture segregation by an inertial cavitation bubble,* Ultrasonics Sonochemistry **14**, 431 (2007).

[39] R. Jamshidi, D. Rossi, N. Saffari, A. Gavriilidis, and L. Mazzei, *Investigation of the effect of ultrasound parameters on continuous sonocrystallization in a millifluidic device,* Crystal Growth & Design **16**, 4607 (2016).

[40] B. Gielen, P. Kusters, J. Jordens, L. C. J. Thomassen, T. Van Gerven, and L. Braeken, *Energy efficient crystallization of paracetamol using pulsed ultrasound,* Chemical Engineering and Processing: Process Intensification **114**, 55 (2017).

6

[41] S. S. Kadam, S. A. Kulkarni, R. Coloma Ribera, A. I. Stankiewicz, J. H. ter Horst, and H. J. M. Kramer, *A new view on the metastable zone width during cooling crystallization,* Chemical Engineering Science **72**, 10 (2012).

[42] R. Kacker, S. I. Regensburg, and H. J. Kramer, *Residence time distribution of dispersed liquid and solid phase in a continuous oscillatory flow baffled crystallizer,* Chemical Engineering Journal **317**, 413 (2017).

6

7

Multi-Parameter Investigation of Laser Induced Nucleation of Supersaturated Aqueous KCl Solutions

7

Various mechanisms have been proposed to explain the non-photochemical laser induced nucleation (NPLIN). Identifying the dominant mechanism requires addressing a large set of experimental parameters with a statistically significant number of samples, forced by the stochastic nature of nucleation [1]. In this study, with aqueous KCl system we focus on the nucleation probability as a function of laser wavelength, laser intensity and sample supersaturation, while the influence of filtration and the laser induced radiation pressure on NPLIN activity is also studied. To account for the nucleation stochasticity 80-100 samples were used. The NPLIN probability showed an increase with increasing laser intensity. The results are different from the previous report, as a supersaturation independent intensity threshold is not observed. No dependence of the NPLIN probability on the laser wavelength (355, 532 and 1064 nm) was observed. Filtration of samples reduced the nucleation probability suggesting a pronounced role of impurities on NPLIN. The magnitude and the propagation velocity of the laser induced radiation pressure were quantified using a pressure sensor under laser intensities ranging from 0.5 to 80 MW/cm^2. No correlation was found between the radiation pressure and NPLIN at our unfocussed laser beam intensities ruling out the radiation pressure as a possible cause for nucleation.

7.1. Introduction

Alternative methods to extend the toolbox for controlling nucleation are sought after. As nucleation is the starting step for the creation of the new crystalline phase, firm control over the nucleation is required to get "first-time-right" crystals. Control of the nucleation rate is required to ensure the formation of a sufficient number of nuclei under optimal conditions for their outgrowth. Moderate supersaturations are used, which maximize the growth while avoiding impurity uptake, the emergence of metastable forms and undesired crystal shapes. Non-Photochemical Laser Induced Nucleation (NPLIN) has been suggested as a promising method to alter the nucleation kinetics. Transparency of supersaturated solutions to the incident light distinguishes NPLIN from the photo-chemically initiated reactions that lead to reactive crystallization. Several reports point out that non-photochemical laser irradiation dramatically reduces the nucleation induction time and controls polymorphism in various fine chemicals relevant for industrial practice [2–7]. Despite the large set of experimental literature on NPLIN, there is no consensus on the working mechanism. Several working mechanisms have been hypothesized so far. The Optical Kerr effect has been first suggested to influence the nucleation due to the density fluctuations resulting from the anisotropic polarization of the pre-nucleation clusters due to electric field of the laser beam [8]. The use of DC fields to control the nucleation of polymorphic forms has supported this hypothesis [9]. On the other hand, simulation of nucleation under the influence of the laser induced electrical field has shown that the field strengths at the laser intensities commonly used in NPLIN studies are too low to influence nucleation [10]. In addition, recent experiments using digital imaging to quantify the orientation of the grown urea crystals with respect to the polarization of the incident laser light during NPLIN did not support the previously claimed influence of laser polarization on the crystal orientation [11]. Laser trapping [12, 13], cavitation [14–17], formation of bubbles [18**?**] and presence of impurities [19] have also been proposed as mechanisms for aiding NPLIN. Other studies using KCl solutions have explained the observed NPLIN to be due to isotropic electronic polarizability of the KCl clusters [20]. Molecular dynamic simulations carried out on KCl system have also corroborated the existence of electronically polarizable clusters with a relaxation time in the order of $100\ ps$ which is comparable to the laser pulse duration [21]. NPLIN studies using potassium halides (KCl & KBr) showed in general a strong dependence of the nucleation probability on the laser beam intensity, with a probability of 1 being achieved at laser intensities higher than 25 MW/cm^2 and no NPLIN effect was observed below 5 MW/cm^2 [22]. Furthermore KCl system, required no prior ageing of the supersaturated samples to achieve NPLIN with a single laser pulse and no effect of laser polarization on nucleation was observed [23]. Extensive studies have been carried out to extend the understanding of NPLIN by varying the width of the laser pulse [24], by limiting the penetration depth of the laser into the sample by use of an evanescent wave [25] and by using micro droplets and gel solutions to gain spatial and temporal control over nucleation [26, 27]. Interestingly, recent work has shown the tendency of the supersaturated solutions of various sodium salts and tartaric acid to nucleate under the influence of the laser induced pressure wave (sound/shock wave) passing through the solution [28]. The

study claimed that the crystals form as a result of the pressure waves appearing in the sample when the laser is focused into the solution or on the opaque wall of the container containing the solution. The variation of the local pressure and temperature caused by the shock wave was reasoned to alter the chemical potential and hence the nucleation rates. The laser induced shock wave thus adds yet another potential working mechanism for NPLIN. In this work, we contribute to the current understanding of the NPLIN phenomenon by investigating multiple parameters such as, the laser wavelength & intensity, the supersaturation of the solution and the influence of filtration of the aqueous KCl solution using a statistical significant number of samples. In addition, we have investigated whether the laser induced pressure wave can be correlated to NPLIN. The stochastic nature of nucleation has been taken into account by studying 80-100 samples for quantifying the nucleation probability. The study has been carried out by shining a single pulse of the unfocussed laser beam of different wavelengths (355, 532 and 1064 nm) through aqueous supersaturated solution of KCl. The laser induced pressure has been quantified and its effect on nucleation probability is studied. The radiation pressure caused by the interaction of the unfocussed laser beam with the experimental system (the solution and the glass vial) is quantified by measuring the pressure signal with a piezo-electric transducer placed just below the air-liquid interface. NPLIN was studied with samples at supersaturations (S =1.055 & 1.035) which were found to be stable to mechanical disturbances and nucleate only when exposed to laser pulse. We showed that a single laser pulse at relatively low beam intensity (around 0.5 MW/cm^2) compared to previous reports [22] can induce nucleation. We discuss our results in depth along with an assessment of potential NPLIN mechanisms.

7.2. Materials & Methods

7.2.1. Materials and sample preparation

KCl (≥99%, Sigma Aldrich) and purified water (Elga PURELAB Ultra, Type I+ >18 $M\Omega.cm$) have been used in this study. Solution of KCl in water, with concentration of 369 mg of KCl / g of water and 377 mg of KCl / g of water, was prepared corresponding to a respective supersaturation of 1.035 and 1.055 at 24 $°C$. The solution was prepared by dissolving KCl in water at 50 $°C$. 6 ml of heated solution was then transferred into borosilicate glass vials 1.3 cm in diameter and sealed. The vials were again heated overnight in an oven at 50 °C to ensure complete dissolution before being taken out and allowed to cool to the room temperature maintained at 24 ±1$°C$. Therefore, the required supersaturation was maintained with an error of ±2%. In addition, a set of samples were also filtered through a syringe filter (0.45 μm, Whatman Puradisc) when hot as a part of the sample preparation procedure. The syringe filters with cellulose acetate as the filtration media were used which can be autoclaved at 121 $°C$ for sterilization. The control samples (both filtered and un-filtered) which were brought to the same supersaturation and handled in the same way but not exposed to laser did not nucleate over a period of 1-2 weeks.
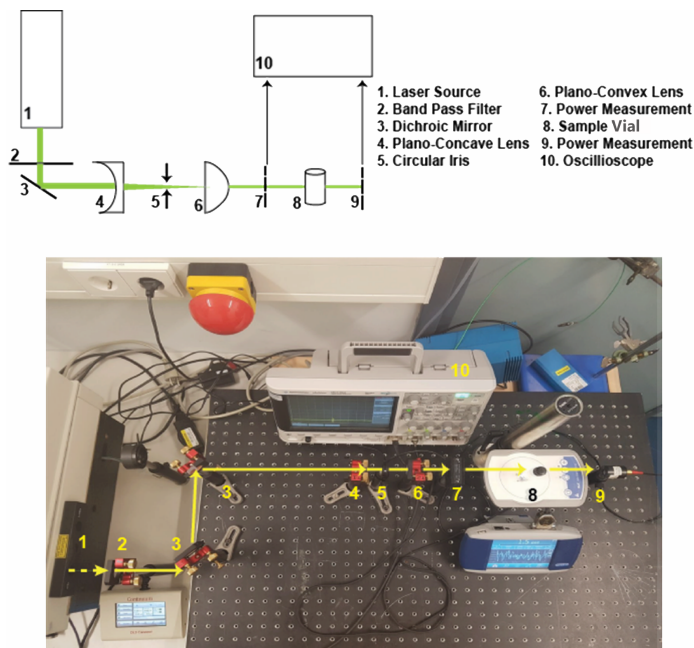
Figure 7.1: Schematic of the experimental set-up showing different components and path of the laser beam (a) and Photograph of the experimental set-up with the beam path illustrated (b).

7.2.2. Experimental setup and method

A Q-switched Nd:YAG laser, Continuum Powerlite DLS 8000 model, was used to generate a train of 7 ns linearly polarized light pulses at (the repetition rate of 10 Hz) the fundamental wavelength of 1064 nm. The fundamental beam was further doubled and tripled in frequency via second harmonic generation (SHG) and third harmonic generation (THG) processes in potassium dihydrogenphosphate (KDP) nonlinear crystals to produce wavelengths of 532 nm and 355 nm respectively. The output powers at the new wavelengths could be varied by gently changing the alignment of the KDP crystals and thus altering their SHG/THG conversion efficiencies. The laser beam was then passed through a home-made 2-lens system telescope to shrink beam diameter from 9 mm to 4.5 mm. The energy of the light pulses was measured behind the telescope using a power/energy meter, Gentec Electro Optique- Maestro Monitor, while their duration was precisely monitored with a high-speed photodetector, Thorlabs DET10A 1-ns rise time. The schematic of the set-up is shown in figure 7.1

To study the NPLIN phenomenon and the resulting nucleation kinetics, vials were exposed to a single pulse of laser at a particular constant intensity and wavelength. The effect of laser wavelengths on NPLIN was studied at 355, 532, and 1064 nm. For each parameter 80-100 samples were used to ensure a robust set of data. In order to visually detect crystals, a wait period of 60 minutes was observed for each experiment, which was sufficient in all the cases studied in this work. Precautions were taken to handle the supersaturated sample carefully during experiments to

avoid any unwanted mechanical shocks. The number of vials that showed nucleation was recorded and the results were reported as fraction of the total number of vials exposed to the laser pulse, from now on termed as the nucleation probability. The blank samples which were not exposed to the laser pulse were not labile to nucleation for many days at same constant supersaturation. The interaction of the laser with the sample generates a pressure wave; the pressure fluctuation was quantified in separate set of experiments by dipping a pressure transducer (KISTLER Type 601H with sensitivity of 0.001 bar) just below the air-liquid interface of saturated KCl solution in ultrapure water.

7.3. Results and Discussions

Figure 7.2, shows the nucleation probability as a function of the incident laser intensity at different wavelengths (355, 532 and 1064 nm) for a fixed supersaturation level, S = 1.055. The vials exposed crystalized even at low intensities (below 1.5 MW/cm^2). At all the three laser wavelengths used in the study, we report 100% nucleation probability at intensities above of 5 MW/cm^2 (indicating that NPLIN was observed in all the samples exposed to the single pulse of laser within the observation time of 60 min). These results are in conflict with a recent paper, which reported a supersaturation independent threshold intensity (about 6 MW/cm^2) for NPLIN, in aqueous KCl system using single laser pulses at 1064 nm [20]. The paper reported a very low nucleation probability (about 10%) with the intensity of approximately 6 MW/cm^2. In addition, the nucleation probability of KCl system has been reported to increase linearly with laser intensity in the range of 6-35 MW/cm^2. We see 5 MW/cm^2 to be the saturation intensity above which nucleation probability was 100% while below this intensity value, a decreasing trend in the nucleation probability is seen. It should be noted that the procedure for cleaning the vials and filtering of the solution was different in the reported literature and the present paper. This difference in impurity level has been addressed further in this paper. Our observation is comparable to reports with an aqueous solution of glycine where NPLIN activity has been reported to be a non-linear function of the laser intensity, approaching a saturation value [3]. Based on our observations, the threshold intensity to trigger NPLIN is low, irrespective of the wavelength of the incident laser. The strong dependence of NPLIN on the laser beam intensity can also be speculated to be due to NPLIN mechanisms such as electronic polarizability which theoretically depend on the laser electric field strength.3 Additionally, the nucleation probabilities are higher with the 355nm wavelength. To ensure that the role of photochemistry is ruled out at the shorter wavelength of 355 nm, the intensity of the pulse was checked before and after it passed the vial. The variation in the intensity measurements were similar to measurements at wavelength of 532 and 1064 nm, confirming the transparency of the solution. Although, with the present results, it is difficult to reason the higher nucleation probability at 355 nm.

The nucleation probability was measured as a function of the laser intensity also at a lower supersaturation (S =1.035). Figure 7.3, shows the nucleation probability (at 60 mins after laser irradiation) as a function of laser intensity at 532 nm and at two supersaturations, S =1.055 & 1.035. As expected, the nucleation probabilities
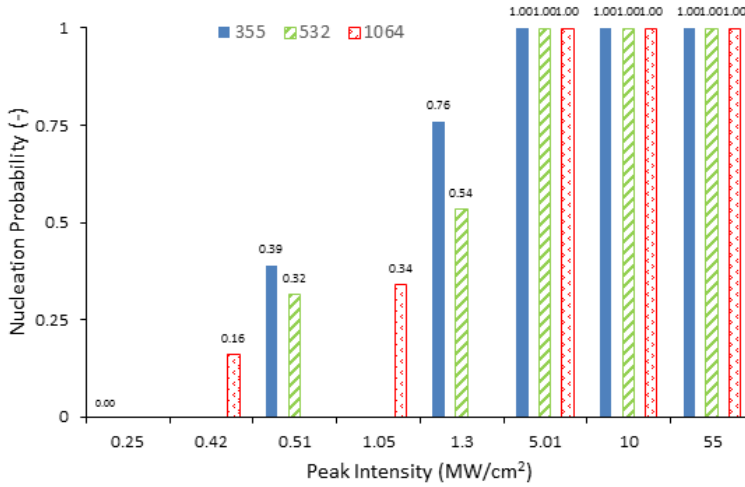
Figure 7.2: Nucleation probability (the ratio of number of samples nucleated to the number of samples exposed- the commonly used terminology in literature) at 60 mins after laser irradiation as a function of the laser intensity at different wavelengths (355, 532 & 1064 nm) and at a fixed supersaturation (S =1.055). Experiments were done with 80-100 unfiltered samples for each parameter.

are lower at the lower supersaturation. Unlike the relatively high nucleation probability of the samples at S =1.055 at the two lowest intensities, no NPLIN took place at S =1.035. NPLIN at the higher supersaturation (S =1.055) and low intensities (below 10 MW/cm^2) resulted in only a few crystals (2-4 in number). As per classical nucleation theory, due to the strong non-linear dependence of nucleation rate on supersaturation, the nucleation probability is significantly reduced at the lower supersaturation (S =1.035). However, the growth rates will not drastically differ due to the mostly linear dependence with the supersaturation. Therefore, even if only a few nuclei would have been formed in the experiments with the lower supersaturation, the detection probability would be about equal.

Our results do not show a supersaturation independent laser intensity threshold as reported in literature. The existence of a supersaturation independent intensity threshold (6 MW/cm^2) was explained to be due to the inability of the weak electric field to bring about isotropic electronic polarization.21 Thus, our observation showing supersaturation dependent NPLIN threshold (Figure 7.3) at very low intensities cannot be explained solely based on the proposed isotropic electronic polarizability mechanism. Interplay of several mechanisms such as optical Kerr effect, susceptibility of samples to mechanical shocks or presence of impurities has been suggested during NPLIN. An explanation to our observation of high nucleation probability at low laser intensities could be the presence of impurities, which have been reported to enhance the NPLIN effect [19, 30]. Our results showing a high nucleation probability are based on unfiltered samples. Experiments with samples filtered using a 0.45 μm syringe filter resulted in significantly reduced nucleation probabilities (based on 20
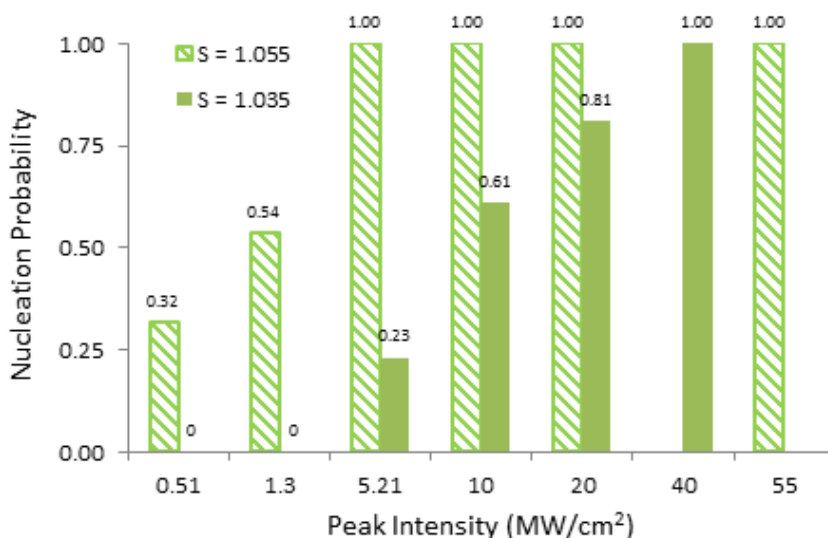
Figure 7.3: Nucleation probability (at 60 mins after laser irradiation) as a function of the laser intensity at two supersaturations (S = 1.055 & 1.035) and fixed wavelength of 532 nm (based on 100 unfiltered samples).

7

samples at each intensity). Figure 7.4, shows the difference in the nucleation probabilities between the filtered and unfiltered samples at two wavelengths, 532 and 1064 nm respectively and at a fixed supersaturation of 1.055. Irrespective of the wavelength, the nucleation probability is lowered upon filtration and no NPLIN is observed at intensities below 0.5-1.5 MW/cm^2. Our observation shows that presence of impurities may aid NPLIN which is in agreement with the earlier reported results. In blank experiments, employing unfiltered samples and no laser light, the impurities alone are not able to cause nucleation as none of the supersaturated samples nucleated for days. A possible mechanism could be that the impurities facilitate the laser induced nucleation process by lowering the free energy required to make the solute clusters critical (heterogeneous nucleation). Alternatively, NPLIN could be the direct result of laser-impurity interaction that can cause local heating and the formation of bubbles/cavity which act as nucleation sites [18]. Since filtration reduces the amount of impurities the laser-impurity interaction will also be reduced explaining the reduced nucleation probability.

In literature, the presence of impurities larger than 200 nm are not suspected to affect the NPLIN phenomenon as use of clean environment, ultrapure ingredients and rigorous cleaning of the vials did not result in significantly different nucleation probabilities [20]. However, unfiltered samples have been reported to be more labile to laser induced nucleation. It is also believed that filtering the solution may reduce the pre-existing subcritical clusters, thereby reducing the nucleation probability. On the other hand addition of nano-particles has been shown to enhance NPLIN [19].
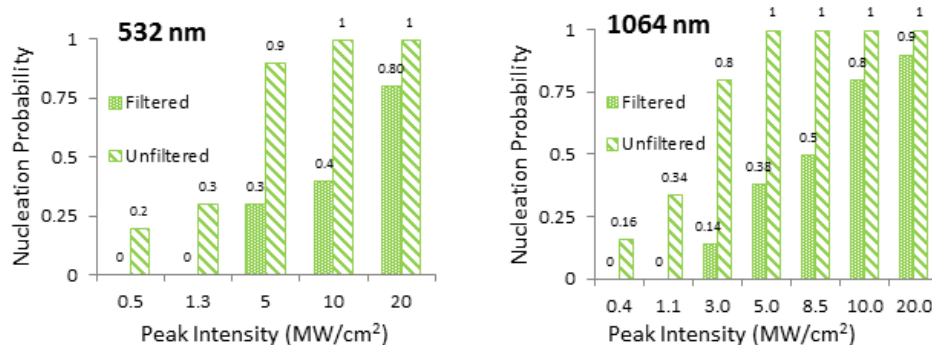
Figure 7.4: Comparison of nucleation probabilities (at 60 mins after laser irradiation) using 20 each of the filtered and unfiltered samples as a function of the laser intensity at two wavelengths of 532 and 1064 nm and at a fixed supersaturation (S = 1.055).

In our case we remove large impurities only (above 0.45 μm) and make sure there is no crystallization during filtration which can reduce supersaturation.

In a recent study, a laser induced pressure wave is identified as an potential mechanism triggering nucleation [28]. The pressure wave generated by the inter-action of the laser beam with an opaque surface in contact with the supersaturated solution was able to induce nucleation. The study estimated that a pressure variation in the order of 1 MPa was required to influence the nucleation kinetics. Similarly laser focused directly into the supersaturated solution has also been reported to promote nucleation via a shockwave resulting from collapsing vapor bubble [14]. However these studies were carried out with a focused laser which transfers very high intensity into the solution, about 2 orders of magnitude higher than the unfocused laser beam used in this study and also in conventional NPLIN experiments. In our study with the unfocused laser beam, a pressure signal was measured after a single pulse of laser passed the sample. Vials containing KCl solution or water were used to measure the pressure signal at a fixed distance from the path of the laser beam through sample vial. Figure 7.5 shows the peak pressure values as a function of the laser intensity in vials containing aqueous KCl solution. Pressure signal in the 2-20 $mbar$ range is measured at characteristic laser intensities used in our study (0.5 - 80 MW/cm^2). At higher laser intensities, the pressure signal is higher. The use of a low energy unfocused laser beam at 532 nm, rules out cavitation induced shockwave as the so-lution is transparent to the beam. Even though the laser pulse lasts only for 7 ns, the pressure signal has a decay time of a few milliseconds possibly due to reflections of the acoustic wave within the sample vials (see Appendix A). The pressure signal may originate from the momentum transfer of laser photons to the solution as the refractive index changes along the beam path through air-glass and glass-solution interfaces [29]. Reflections at the glass surface of sample vial also contributes to the generation of the pressure wave. In order to test the effect of the laser induced

pressure on nucleation, we prepared two sets of samples filled with identical solutions: one "masked sample" where we blocked the incident laser beam (intensity 80 MW/cm^2) by placing a small piece of black tape on the surface of the vials the other "unmasked" control sample where the laser can pass through and interact with the solution in vials. Figure 6, shows the masked and "control" vials and the resulting nucleation probability (S =1.055) as well as the measured pressure signals. A much higher pressure signal (around 200 $mbar$) was measured for the masked samples probably due to the transfer of all the energy onto the tape. As shown in figure 7.6, no nucleation was observed in the masked vials. 100 samples were tested (also at a lower supersaturation S = 1.035) and none of the samples nucleated. Nucleation only occurred in control samples where the laser was allowed to pass through the solution. Our experiments confirm the presence of laser induced pressure wave however it does not contribute to nucleation at laser intensities and supersaturations used in our experiments. When the laser is absorbed into the sample, for example, in the case of a laser absorbing dye, a high amount of energy is transferred which can result in cavitation generating localized shockwaves [13]. Then the resulting nucleation is probably due to the cavitation. In our study the laser pulse passes through the transparent solution and hence the transferred energy is small hence unable to cause cavitation. Since we observed NPLIN at very low laser intensity (0.5 MW/cm^2) we believe that the interaction between laser energy field and the solute molecules is more likely to be the plausible mechanism for NPLIN. Moreover, the pressure signals we measure are in the same order of magnitude as the predicted theoretical values of the radiation pressure (see Appendix A) and the magnitude is too low to influence nucleation kinetics. Our observations are in agreement with the various mechanisms proposed to influence NPLIN. We do not ascertain a single mechanism to be in play during NPLIN, but it is shown that the nucleation is not due to the radiation pressure at laser intensities commonly achieved with an unfocussed laser beam.
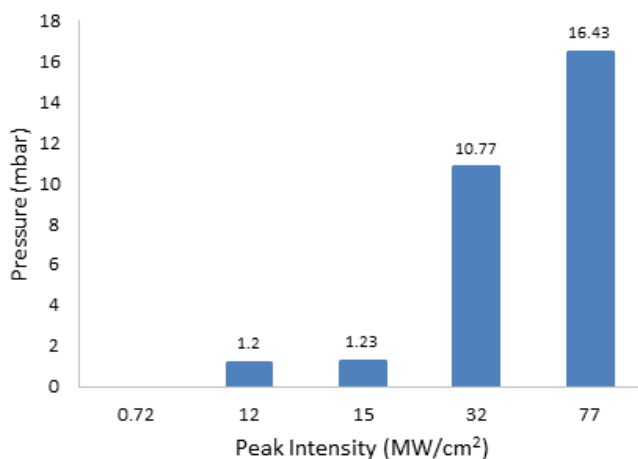
Figure 7.5: The pressure signal upon irradiation of the vials with unfiltered saturated aqueous KCl solution with a single shot of laser at 532 nm at different laser intensities.
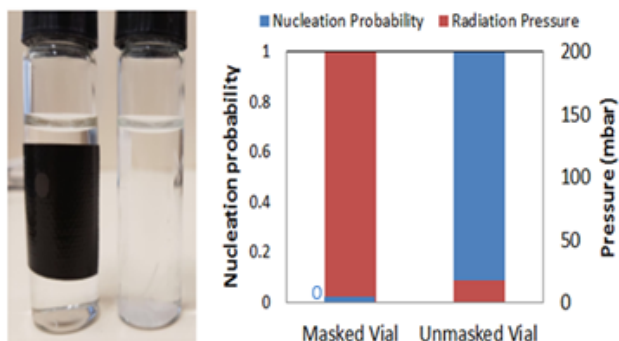

Figure 7.6: The resulting peak pressure signal and nucleation probability (S =1.055) in the masked and the unmasked vial upon irradiation of a single laser pulse at intensity of 80 MW/cm^2. Despite the higher induced pressure in the masked vial (shown in red in the bar graph), no nucleation was observed (shown in blue in the bar graph) compared to the "unmasked" control case where laser pulse could pass through.

7.4. Conclusions

We focused on the laser induced nucleation phenomenon in aqueous KCl solutions in a multi parameter study spanning laser wavelength, intensity and supersaturation. We also studied the influence of filtration and the correlation between NPLIN activity and laser induced radiation pressure. The NPLIN kinetics is found to depend on the laser intensity and the supersaturation but independent of the laser wavelength at 355, 532, 1064 nm. In contrast to previous reports, we did not observe a supersaturation independent intensity threshold below which no nucleation is observed. High nucleation probabilities were observed with unfiltered samples; a 100% nucleation probability emerged at laser intensities where in literature low nucleation probability has been reported. Filtering the samples prior to studying NPLIN resulted in lowering of the nucleation probabilities, which highlights the role of submicron impurities in enhancing NPLIN. But our results do not rule out the presence of NPLIN mechanisms such as electronic polarization.

We characterized the magnitude of the laser induced pressure wave. Based on our measurements (estimation of the pressure wave velocity shown in Appendix A), the resulting wave is not a shock wave but a sound wave at the laser intensities used in the study. Blocking the laser beam at the surface of the sample vials resulted in larger induced pressure compared to the "unmasked" control case where laser pulse did pass through the sample vials. However, nucleation was completely absent in masked samples. The quantification of the pressure wave intensity and velocity along with the nucleation probability experiments with masked samples enabled us to rule out shock wave induced crystallization as a potential working mechanism for NPLIN. We believe our multi-parameter study will contribute to mechanistic understanding of NPLIN as it examines a single model system evoking all the key experimental parameters with statistically significant repetitions-a commonly critiqued point in NPLIN literature.

7

References

[1] Y. Xiao, S. K. Tang, H. Hao, R. J. Davey, and T. Vetter, *Quantifying the inherent uncertainty associated with nucleation rates estimated from induction time data measured in small volumes,* Crystal Growth & Design **17**, 2852 (2017), http://dx.doi.org/10.1021/acs.cgd.7b00372 .

[2] J. Zaccaro, J. Matic, A. S. Myerson, and B. A. Garetz, *Nonphotochemical, laser-induced nucleation of supersaturated aqueous glycine produces unexpected gamma-polymorph,* Crystal Growth & Design **1**, 5 (2001),.

[3] J. Matic, X. Y. Sun, B. A. Garetz, and A. S. Myerson, *Intensity, wavelength, and polarization dependence of nonphotochemical laser-induced nucleation in supersaturated aqueous urea solutions,* Crystal Growth & Design **5**, 1565 (2005),.

[4] X. Y. Sun, B. A. Garetz, and A. S. Myerson, *Polarization switching of crystal structure in the nonphotochemical laser-induced nucleation of supersaturated aqueous l-histidine,* Crystal Growth & Design **8**, 1720 (2008),.

[5] A. Ikni, B. Clair, P. Scouflaire, S. Veesler, J. M. Gillet, N. El Hassan, F. Dumas, and A. Spasojevic-de Bire, *Experimental demonstration of the carbamazepine crystallization from non-photochemical laser-induced nucleation in acetonitrile and methanol,* Crystal Growth & Design **14**, 3286 (2014),.

[6] B. Clair, A. Ikni, W. J. Li, P. Scouflaire, V. Quemener, and A. Spasojevic-de Bire, *A new experimental setup for high-throughput controlled non-photochemical laser-induced nucleation: application to glycine crystallization,* Journal of Applied Crystallography **47**, 1252 (2014),.

[7] W. J. Li, A. Ikni, P. Scouflaire, X. X. Shi, N. El Hassan, P. Gemeiner, J. M. Gillet, and A. Spasojevic-de Bire, *Non-photochemical laser-induced nucleation of sulfathiazole in a water/ethanol mixture,* Crystal Growth & Design **16**, 2514 (2016),.

[8] B. A. Garetz, J. E. Aber, N. L. Goddard, R. G. Young, and A. S. Myerson, *Nonphotochemical, polarization-dependent, laser-induced nucleation in supersaturated aqueous urea solutions,* Physical Review Letters **77**, 3475 (1996),.

[9] J. E. Aber, S. Arnold, B. A. Garetz, and A. S. Myerson, *Strong dc electric field applied to supersaturated aqueous glycine solution induces nucleation of the gamma polymorph,* Phys Rev Lett **94**, 145503 (2005),

[10] B. C. Knott, M. F. Doherty, and B. Peters, *A simulation test of the optical kerr mechanism for laser-induced nucleation,* The Journal of Chemical Physics **134**, 154501 (2011).

[11] Y. Liu, M. R. Ward, and A. J. Alexander, *Polarization independence of laser-induced nucleation in supersaturated aqueous urea solutions,* Physical Chemistry Chemical Physics **19**, 3464 (2017).

7

[12] K.-i. Yuyama, T. Sugiyama, and H. Masuhara, *Laser trapping and crystallization dynamics of l-phenylalanine at solution surface,* The Journal of Physical Chemistry Letters **4**, 2436 (2013).

[13] T. Sugiyama, K.-i. Yuyama, and H. Masuhara, *Laser trapping chemistry: From polymer assembly to amino acid crystallization,* Accounts of Chemical Research **45**, 1946 (2012).

[14] A. Soare, R. Dijkink, M. R. Pascual, C. Sun, P. W. Cains, D. Lohse, A. I. Stankiewicz, and H. J. M. Kramer, *Crystal nucleation by laser-induced cavitation,* Crystal Growth & Design **11**, 2311 (2011).

[15] I. Kenji, M. Mihoko, T. Yoshinori, M. Yoichiro, Y. Y. Hiroshi, O. Shino, A. Hiroaki, S. Shigeru, T. Kazufumi, M. Satoshi, M. Hiroyoshi, I. Tsuyoshi, Y. Masashi, and M. Yusuke, *Selective crystallization of the metastable phase of indomethacin at the interface of liquid/air bubble induced by femtosecond laser irradiation,* Applied Physics Express **8**, 045501 (2015).

[16] R. Murai, H. Y. Yoshikawa, Y. Takahashi, M. Maruyama, S. Sugiyama, G. Sazaki, H. Adachi, K. Takano, H. Matsumura, S. Murakami, T. Inoue, and Y. Mori, *Enhancement of femtosecond laser-induced nucleation of protein in a gel solution,* Applied Physics Letters **96**, 043702 (2010).

[17] H. Y. Yoshikawa, R. Murai, S. Sugiyama, G. Sazaki, T. Kitatani, Y. Takahashi, H. Adachi, H. Matsumura, S. Murakami, T. Inoue, K. Takano, and Y. Mori, *Femtosecond laser-induced nucleation of protein in agarose gel,* Journal of Crystal Growth **311**, 956 (2009).

[18] M. R. Ward, W. J. Jamieson, C. A. Leckey, and A. J. Alexander, *Laser-induced nucleation of carbon dioxide bubbles,* The Journal of Chemical Physics **142**, 144501 (2015).

[19] M. R. Ward, A. M. Mackenzie, and A. J. Alexander, *Role of impurity nanoparticles in laser-induced nucleation of ammonium chloride,* Crystal Growth & Design **16**, 6790 (2016).

[20] A. J. Alexander and P. J. Camp, *Single pulse, single crystal laser-induced nucleation of potassium chloride,* Crystal Growth & Design **9**, 958 (2009).

[21] J. O. Sindt, A. J. Alexander, and P. J. Camp, *Structure and dynamics of potassium chloride in aqueous solution,* The Journal of Physical Chemistry B **118**, 9404 (2014).

[22] M. R. Ward, and A. J. Alexander, *Nonphotochemical Laser-Induced Nucleation of Potassium Halides: Effects of Wavelength and Temperature,* Crystal Growth & Design **9**, 4554-4561 (2012) .

[23] I. S. Lee, J. M. B. Evans, D. Erdemir, A. Y. Lee, B. A. Garetz, and A. S. Myerson, *Nonphotochemical laser induced nucleation of hen egg white lysozyme crystals,* Crystal Growth & Design **8**, 4255 (2008).

[24] M. R. Ward, I. Ballingall, M. L. Costen, K. G. McKendrick, and A. J. Alexander, *Nanosecond pulse width dependence of nonphotochemical laser-induced nucleation of potassium chloride,* Chemical Physics Letters **481**, 25 (2009).

[25] M. R. Ward, A. Rae, and A. J. Alexander, *Nonphotochemical laser-induced crystal nucleation by an evanescent wave,* Crystal Growth & Design **15**, 4600 (2015),.

[26] K. Fang, S. Arnold, and B. A. Garetz, *Nonphotochemical laser-induced nucleation in levitated supersaturated aqueous potassium chloride microdroplets,* Crystal Growth & Design **14**, 2685 (2014),.

[27] C. Duffus, P. J. Camp, and A. J. Alexander, *Spatial control of crystal nucleation in agarose gel,* Journal of the American Chemical Society **131**, 11676 (2009).

[28] N. Mirsaleh-Kohan, A. Fischer, B. Graves, M. Bolorizadeh, D. Kondepudi, and R. N. Compton, *Laser shock wave induced crystallization,* Crystal Growth & Design **17**, 576 (2017).

[29] O. Capeloto, V. Zanuto, M. Baesso, G. Luckasievicz, S. Bialkowski, and N. Astrath, *Quantitative assessment of radiation force effect at the dielectric air-liquid interface,* Scientific Reports **6**, 20515 (2016).

[30] N. Javid, T. Kendall, I. S. Burns, and J. Sefcik, *Filtration suppresses laser-induced nucleation of glycine in aqueous solutions,* Crystal Growth & Design **16**, 4196 (2016).

7

8

Conclusion

The work presented in the thesis focussed on control of nucleation. Development of novel approaches, which allow the manipulation of the number of crystals in batch or continuous processes and thereby control the crystal properties, i.e. size and shape distribution, is addressed. Chapters 2 and 3 addressed the efficiency enhancement of the model free direct nucleation control (DNC), which manipulates the number of crystals via temperature cycling in batch cooling crystallization processes. Chapter 4, addressed identification of the optimal operating conditions required to obtain plug flow conditions in a continuous oscillatory flow baffled crystallizer (COBC). Operation under plug flow conditions ensures narrow residence time distribution and in combination with supersaturation control allows controlled growth of the crystals. Chapter 5, presented the implementation and development of imaging based in-situ nucleation monitoring and crystal phase characterization, which is an essential part of designing and implementation of control strategies. Pattern based and segregation based image analysis algorithms have been compared for robust characterization of the number, shape and the size distribution of the crystals exiting the COBC. Ideally under plug flow conditions in tubular crystallizers, secondary nucleation cannot be relied upon to avoid primary nucleation, especially at the inlet where the supersaturation is expected to be high. Hence, seeding is preferred to avoid nucleation and to maintain a steady number of crystals in continuous COBC, which ensures a consistent product quality. Thus chapters 6 and 7 addressed the use of alternate energy as additional levers to manipulate the nucleation rate and the use external fields as a tool for continuous in-situ seed crystals production through controlled nucleation. The key outcomes and the challenges pertaining to the different nucleation control approaches studied in the thesis are summarized with respect to the key questions raised in the beginning:

Can direct nucleation control efficiency be enhanced through restriction of nucleation and optimization of dissolution cycles using rapid microwave heating?

Can a novel crystallizer design be realized where microwave application is integrated in the crystallizer for direct nucleation control? Due to the slow response of conventional heating, usually limited by the heat transfer, DNC requires many control cycles (temperature cycles) to manipulate the supersaturation and steer the batch process to maintain the desired number of crystals required for reaching the targeted mean size and crystal size distribution. Thus, by manipulating the number of the crystals control over the mean size and the size distribution of the product crystals is gained. As a result of the slow response, to curb the rapid nucleation process and to prevent excessive dissolution of the crystals which requires nucleation again to generate new crystals, large number of control cycles is experienced making the batch time undesirably long. In the chapters 2 and 3, the efficiency of the direct nucleation control (DNC) has been enhanced by ensuring a reduction in the number of control cycles because of the rapid response against nucleation achieved by the implementation of microwave heating. First, the efficiency enhancement has been demonstrated in the proof of concept crystallizer where rapid heating and quick temperature cycles were achieved via the introduction of microwaves in a circulation loop. Chapter 3 specifically, covered the development of a novel crystallizer with integrated microwave heating for rapid temperature cycling required for realizing an efficient DNC process. A number of challenges were addressed to realize the novel crystallizer with integrated microwave heating. The Labotron 4000 unit (4 L in capacity) from Sairem with its internal transmission line technology was redesigned to enable integration of microwave heating directly into a crystallizer. Safe implementation of PAT in presence of microwave fields was guaranteed for process monitoring and control. In the new crystallizer, the unseeded crystallization using paracetamol-IPA system under microwave assisted DNC, resulted in strong efficiency enhancement when compared to the performance using conventional heating. The application of rapid heating countered the bulk nucleation and prevented excessive nuclei to be created. Consequently, the impact of nucleation could be strongly mitigated and resulted in a remarkable reduction in the number of heating cycles needed to keep the particle counts at their set-point value at the end of the batch. The use of microwave heating resulted in decoupling of heating and cooling mechanisms, which resulted in faster switching between heating and cooling. Overall, the effectiveness of DNC was improved as the batch time was reduced by 50% in comparison to the case with conventional heating. A narrow particle size distribution was achieved similar to experiments with conventionally heated DNC but with significantly reduced batch time. The novel crystallizer design promises to be a convenient tool for optimizing processes based on temperature cycling. At lab/pilot scale, the microwave assisted crystallizer equipped with DNC can be used for mapping the process space to facilitate the process design with good control over nucleation and the growth of crystals.

Can optimal mixing conditions in the COBC be obtained for controlled growth of crystals?

Chapter 4, presented the optimum operating conditions in the (COBC) for the first time by taking into account the dispersion of both the bulk and the crystal phase. The identified operation conditions allowed COBC to be operated under plug flow

conditions where crystals and the bulk solvent experienced narrow residence time distribution. As a result of the operation under plug flow, the controlled mixing conditions can ensure homogenous temperature and supersaturation distribution which is critical to supress unwanted primary and secondary nucleation. Thus, the fluid oscillation amplitude and frequencies resulting in near plug flow conditions in the COBC were ascertained by analysing the residence time distribution (RTD) using both homogeneous (methylene blue-water) and heterogeneous tracer system (melamine-water). Contrary to the findings in the literature, it was shown that the velocity ratio Ψ (the ratio between the oscillatory velocity and the superficial velocity of the imposed flow) alone is not sufficient to identify the optimal plug flow operating conditions in the COBC. Since, a combination of the operating frequency and amplitude result in dimensional numbers usually used to characterize mixing in the COBC, both high and low frequencies were identified to be optimal for minimizing dispersion. But in general, our knowledge showed operating at high amplitudes of fluid oscillations increased dispersion and should be avoided. Comparable responses were obtained with both the tracer systems showing both the bulk and the dispersed phase (crystals) achieve plug flow. However, the bulk and the dispersed phase residence times do not necessarily resemble, hence characterization of both the phases is required to ensure a good process design. Our study addressed the existing gap in understanding handling of solids in a COBC by showing that operation at 2 Hz and 2 mm was optimal to homogenously suspend the melamine crystals and obtain a plug flow like residence time distribution at four different slurry concentrations (upto 10 % , w/w).

Can in-situ imaging be applied as a robust tool for monitoring and control of nucleation through characterization of shape and size distribution of the newly formed crystals?

Process monitoring and characterization is an essential part of realizing and implementing process control. In-situ visualization of the crystals and the characterization of the crystal properties, for example size and shape distribution, helps in monitoring and ensuring steady operation of processes without disturbances due to product sampling. When coupled with other PAT tools and development of faster image processing, in-situ monitoring presents an opportunity to realize real time control. In chapter 5, in-situ imaging technology has been developed to achieve accurate characterization of the crystal size, the shape and the number of particles of melamine crystals in the COBC. Two image analysis approaches were examined for particle characterization which appeared non-spherical and irregular in shape. The pattern matching algorithm and a segmentation based object recognition algorithm were compared. Due to simultaneous presence of both nucleation and growth, smaller and larger crystals were observed to be present in the COBC which had different appearances. The edges of the smaller particles could not be clearly distinguished due to limitation of the resolution, whereas the large particles had clearly identifiable edges and a more consistent shape making the image analysis challenging. Therefore, a single pattern with sets of features which covered both the small and the larger crystals could not be generated; highlighting the need of several patterns for the pattern matching based image analysis. Also with the pattern matching approach,

8

the crystal edge estimation using circles lead to a mismatch of the estimated crystal boundary with the actual crystals. As a result, overestimation of the particle sizes was observed. Alternatively, the segmentation based algorithm resulted in reliable crystal size and shape characteristics. The segmentation based algorithm having the flexibility in edge detection was better in identifying crystals differing in appearance. The aspect ratios estimated from the projections of the particles suggested close to circular particles. The skewness of the aspect ratio toward the circular shape was attributed to the large number of fine particles, which limited by resolution, presented no clear shape. The in-situ imaging system offered to be a reliable tool for inline characterization of the crystals during the cooling crystallization process in the COBC. A comparison of the number of particles estimated using imaging could also be made with the data from FBRM. Particle counts trend obtained from the imaging analysis were comparable to the trend obtained using the FBRM. The gradually increasing number of particles measured at the exit of COBC over several residence times implied that the nucleation was not localized but occurred over the length of the tubes. Further investigation into the size dependent backmixing of the particles (where the very small nuclei may mix different from large crystals) and the kinetics of secondary nucleation under the oscillatory flow conditions is required to design the COBC process better.

Can application of laser pulses and ultrasound fields lead to a process actuator that realizes a reproducible seed generation system?

To generate right number and quality of seed crystals directly within the flow crystallization process, a better grip over the nucleation rate is required. Use of US and laser have been explored as alternative levers to control the nucleation rate. Chapters 5 and 6 investigated the process conditions i.e. supersaturation, which is required to induce nucleation only when US or lasers is applied. Nucleation rate has been characterized by monitoring the number of the crystals which form upon application of the energy fields and the resulting crystal size distribution has been characterized.

Under batch conditions a strong effect of US on nucleation rate was observed. High nucleation rates resulted at low supersaturations where under blank conditions (when no US is applied) no nucleation was observed. At supersaturation where primary nucleation was observed, a significant reduction in induction time has been obtained by application of US. For application of US to the inlet stream flowing into the COBC, a flow through cell was used to produce the seed nuclei. However, much higher supersaturation than the supersaturation determined under batch conditions was required. The flow conditions and the smaller working volume of the flow through cell could be the reasons for the high supersaturation requirement. As a consequence of the higher supersaturation, unwanted primary nucleation was observed in the COBC, even under blank conditions where no US was applied. As a result, poor control over number of crystals and crystal size distribution was obtained. In contrast to plug flow condition in the COBC, the flow cell behaved as a well-mixed vessel which lead to broad crystal size distribution. Also, accumulation of the crystals due to settling was observed in the flow cell.

Laser induced nucleation rate has been characterized by determining the nucleation probability in batch conditions (80-100 vials) at various supersaturations and at various levels of input laser energy and wavelengths. No dependence of the NPLIN probability on the laser wavelength (355, 532 and 1064 nm) was observed. The results showed that the nucleation rate is a function of the laser energy, which can be utilized for manipulating the number of crystals in the process. Since various mechanisms have been proposed to explain the non-photochemical laser induced nucleation (NPLIN), the dominant mechanism needs to be identified for gaining control over nucleation. Filtration of samples reduced the nucleation probability suggesting a pronounced role of impurities on NPLIN. The magnitude and the propagation velocity of the laser induced radiation pressure were quantified using a pressure sensor under laser intensities ranging from 0.5 to 80 MW/cm2. No correlation was found between the radiation pressure and NPLIN at our unfocussed laser beam intensities ruling out the radiation pressure as a possible cause for nucleation.

8

Acknowledgements

First and foremost, I am forever grateful to my parents. Through their never-ending love and support, I continue to flourish and bring my dreams into realization. I am also grateful to my grandparents, uncle, aunt and the extended family who have, advertently or inadvertently, played a role in shaping me as a person. Special thanks to my sister who is always ready to extend her support.

I would also like to thank my loving wife, Hanaa. She holds a special place in my life. The special bond which we share is full of warmth, openness and encouragement to dream. She has played an important role during my journey as a student at Delft University of Technology, by extending her by unrelenting support for me. Especially, during my PhD she has contributed by reviewing my planning, evaluating my progress and by providing constructive critique, which immensely improved my work.

Not enough can be said about the valuable knowledge and learning that has been passed to me by my teachers and mentors at Delft University of Technology. Dr. Herman Kramer has immensely contributed to my learning and education through his valuable feedback on my work. Dr. Andrzej Stankiewicz has always extended his support and encouragement towards the research that I carried out. Dr. Burak Eral has been very encouraging in letting me independently guide the research and work together with him on new ideas. A special thank goes out to Dr. Joop ter Horst who encouraged me in the very first place to take the step towards the doctoral programme.

Last but not the least, I would like to thank my colleagues at the Process & Energy department. I acknowledge the support lent to me by the colleagues at DEMO and especially by Michel van den Brink, without which the experiments would not have been possible. During my stay at the department, I found some very good friends. I cherish the moments that we had as a group together at department meetings, conferences and during fun events, such as the drinks and the dinner. Many of these events I have enjoyed together with Javier, which has been a pleasure.

This journey, with all the wonderful memories created along the way, will be forever cherished.

Appendix A

Solubility data aqueous KCl system

In order to determine the operating supersaturation for the NPLIN experiments, it was necessary to ascertain the solubility of KCl in water. The solubility has been measured by using the Crystal 16 (Avantium) parallel crystallizer system. The integrated turbidity sensor in the system allowed the recoding of the event when excess KCl in water completely dissolved upon reaching the saturation temperature in a linearly increasing temperature trajectory (0.1 K/min) by means of change in the laser transmissivity through the sample slurry to 100%. Slurry of aqueous KCl (1 ml in volume) with different concentrations was subjected to the user-defined heating-cooling cycles and the laser transmissivity was recorded throughout the experiment. Figure 8.1 shows the measured solubility data and compares it with the literature[1] values. The solutions in our study are made based on the measured solubility.
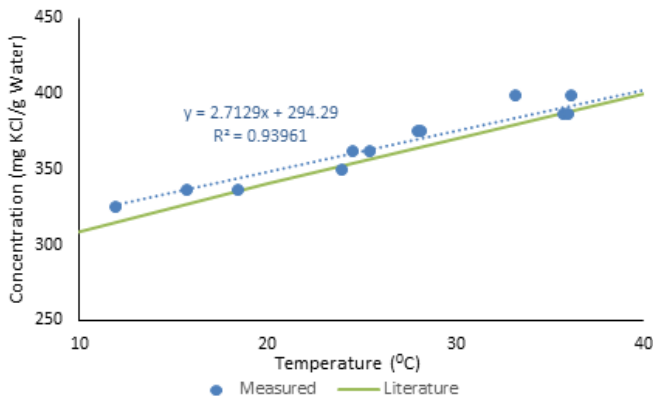

Figure 8.1: Measured solubility data and the solubility data from the literature[1].

1 A. Myerson, Handbook of industrial crystallization. Elsevier, 2001.

Cumulative nucleation probability as a function of time

The figure 8.2 shows that even at low power the nucleation probability does not change beyond 30 $mins$. In our experiments wait period of 60 $mins$ is therefore sufficient for observing nucleation.
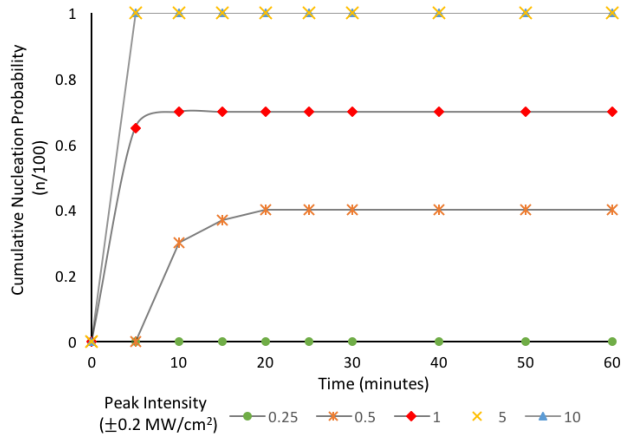

Figure 8.2: Evolution of cumulative nucleation probability vs time based on set of 100 samples at different laser beam intensities. The measurements are carried out at S =1.055 and laser pulse at with wavelength 532 nm is used.

8

Radiation pressure measurement and characterization

A piezoelectric pressure sensor (KISTLER type 601H, range: 0 to 1000 bar, sensitivity: $-16\ pCbar^{-1}$) submerged in the sample solution was used for dynamic pressure measurements. The electrostatic charge signal generated by the pressure transducer was further converted to a proportional voltage signal by using a charge amplifier (KISTLER type 5011B, range: 10 to $10^5\ pC$, sensitivity: 0.01 to $10^3\ pCbar^{-1}$). All the signals were analysed on an oscilloscope procured from Agilent Technologies (DSO-X 3054A).

The solutions were exposed to a single pulse of laser at different peak intensities and wavelengths. Figure 8.3 shows the measured pressure due to the exposure to a single pulse of laser at different laser intensities and at different wavelengths, using Ultrapure water in sample vials used in the study. Factors such as transparency of the borosilicate glass vial containing water with respect to the laser wavelength and the absorption (if any) of the laser will play a role in the resulting pressure signal. Therefore the dependence of the pressure signal on the laser wavelength is not trivial. However a clear trend showing the increase in pressure signal with the increased laser intensity is observable.
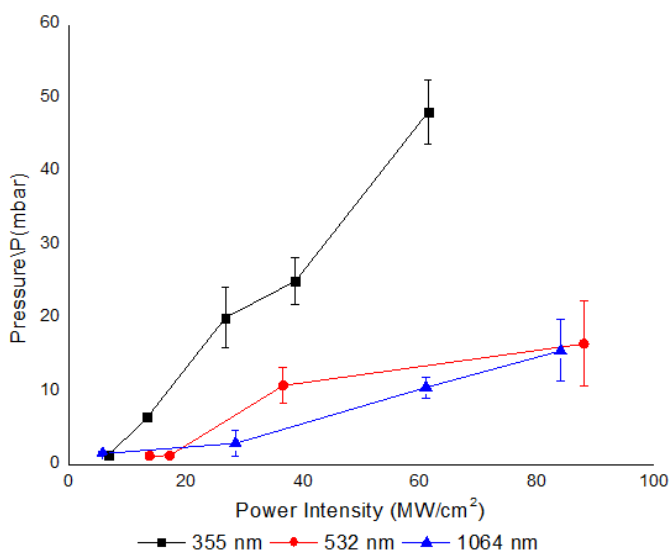

Figure 8.3: Measured pressure upon exposure of Ultrapure water in sample vials to a single pulse of laser at different laser intensities and at wavelengths of 355, 532 and 1064 nm

2 A. Kumar, "Speed of sound in concentrated aqueous kcl solutions from 278.15 to 338.15 k", Journal of Chemical & Engineering Data, vol. 48, no. 2, pp. 388–391, 2003. DOI: 10.1021/je025605k.

The nature of the pressure wave being generated when the single pulse of the laser passed through the sample was characterized by measuring the time lag between the laser pulse and the pressure signal. Simultaneously recordings of the laser and the pressure signals were made using a photo-detector and the transducer respectively. As the photo-detector has a quick rise time of 1 ns, it enabled the detection of the travelling laser beam as soon as it is shot. Figure 8.4 shows the time lag between the laser pulse and the detection of the pressure wave. Assuming that the acoustic wave emerges near the path of the laser within the sample vial, the measured time lag between the two signals can be attributed to time required for the pressure wave to travel the distance between the beam path and the pressure transducer. 2.6 cm was estimated to be the distance. This assumption allowed us to compute the speed of the pressure wave to be around 1383 m/s. This is in close approximated speed of sound in KCl solution (1468 ms^{-1}) as mentioned in the literature[2]. Thus, the induced pressure wave can be called as an acoustic wave which lasts in the vials for a period of 3 to 4 ms before attenuating completely.
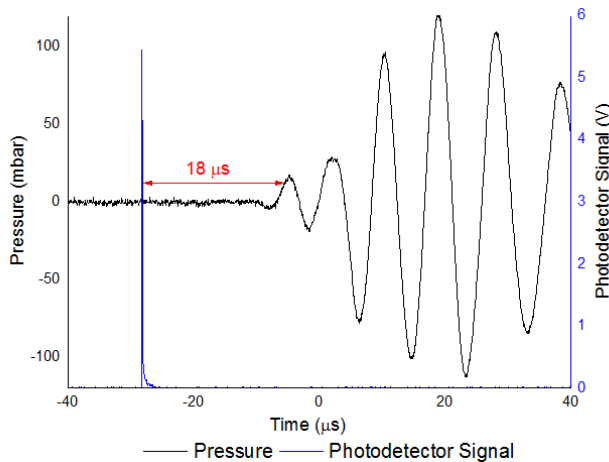

Figure 8.4: Time lag between the shot of a single laser pulse passing through the sample vials and the resulting pressure signal measured by the pressure transducer.

Due to the dual nature of the EM wave the momentum (p) arising from the translational motion of the elementary particles of the EM waves (the photons) can be expressed as:

$$p = Energy\_carried\_by\_the\_wave(E)/Speed\_of\_light\_in\_vacuum(c) \quad (8.1)$$

3 L. Zhang, W. She, N. Peng, and U. Leonhardt, "Experimental evidence for abraham pressure of light", New Journal of Physics, vol. 17, no. 5, p. 053 035, 2015. DOI: 10.1088/1367-2630/17/5/053035.

Further, radiation pressure (P_rad) is defined as the rate of change of momentum in time (t) of the EM wave per unit area and is expressed using the peak intensity of light (I) and speed of light in vacuum (C) as:

$$P\_rad = I/c \qquad (8.2)$$

Three different cases arises where the laser can be absorbed, reflected or pass through a transparent medium with a refractive index (n). In these cases the radiation pressure is expressed as follows[3]:

$$P\_rad = \begin{cases} I/C & \text{Absorption} \\ 2I/C & \text{Reflection} \\ I(1-n)/cn & \text{Transparent} \end{cases}$$

This estimation doesn't take into account the dampening of the wave due to the fluid's inertia but an order of magnitude estimation of the radiation pressure can be made. Figure 8.5 shows the radiation pressure at various intensities used in our studies for the three cases of absorption, reflection and when the laser passes through a transparent medium. The pressure calculated is in the range of the experimental observations. Thus, this mechanism contributing to the measured acoustic wave could be the radiation pressure induced by the laser passing through the transparent medium.
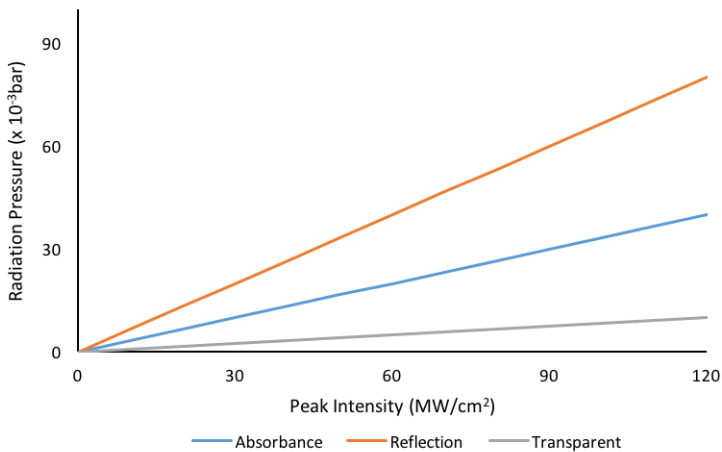

Figure 8.5: Shown in the figure, the calculated radiation pressure at various intensities used in our studies for the three cases of absorption, reflection and when the laser passes through a transparent medium..

Curriculum Vitæ

Rohit Kacker was born in Lucknow, India on 6th of February 1986. Since childhood he was inquisitive and curious, which developed his natural affinity towards science. After finishing school, he pursed Bachelor's in Chemical Engineering from R.V. College of Engineering in Bangalore, India. He put to test his passion for research and engineering by joining the Unilever R&D Centre in Bangalore as a Process Technology Researcher, where he worked for 3 years. At Unilever, he significantly contributed to the innovative combination of drying and distillation technology, which lead to a patented process. He further led the technology transfer activities to develop a new pilot processing capacity to facilitate extensive technology and consumer trials.

In the middle of 2011, he decided to strengthen his research skills by continuing his education through the master's programme followed by a doctoral programme at Delft University of Technology, in The Netherlands. In 2013, he obtained the degree of Masters of Science and continued his research work in the subsequent years, which contributed to the degree of Doctor of Philosophy in 2018. The PhD dissertation dealt with the use of microwave, ultrasound and laser energy as alternative driving forces to design novel nucleation control approaches, during crystallization. Currently, he is working as a consultant and is engaged by Unilever R&D Vlaardingen for developing virtual product development capabilities by combining the formulation specification & processing knowledge on a common scientific data platform.

It would be great to connect on LinkedIn: `linkedin.com/in/rohit-kacker`

List of Publications

Recent Journal Articles:

1. **R. Kacker**, S. Maaß, J. Emmerich, H.J.M. Kramer. *Application of Inline Imaging for Monitoring Crystallization Process in a Continuous Oscillatory Baffled Crystallizer (COBC)*, DOI: 10.1002/aic.16145 AIChE Journal (2018).

2. **R. Kacker**, S. Dhingra, D. Irima, A.I. Stankiewicz, M.K. Ghatkesar, H.J.M. Kramer and H.B. Eral. *Multiparameter Investigation of Laser-Induced Nucleation of Supersaturated Aqueous KCl Solutions*, DOI: 10.1021/acs.cgd.7b01277 Crystal Growth & Design **18(1)**, 312-317 (2018).

3. **R. Kacker**, M. Radoiu and H.J.M. Kramer. *Novel design integrating a microwave applicator into a crystallizer for rapid temperature cycling. A Direct Nucleation Control study*, DOI: 10.1021/acs.cgd.7b00368, Crystal Growth & Design **17**, 3766−3774 (2017).

4. **R. Kacker**, S. Regensburg and H.J.M. Kramer. *Residence time distribution of dispersed liquid and solid phase in a continuous oscillatory flow baffled crystallizer*, DOI: 10.1016/j.cej.2017.02.007 Chemical Engineering Journal **317**, 413-423 (2017).

5. **R. Kacker**, P.M. Salvador, G.S.J. Sturm, G.D. Stefanidis, R. Lakerveld, Z.K. Nagy and H.J.M. Kramer. *Microwave assisted Direct Nucleation Control for batch crystallization: crystal size control with reduced batch time*, DOI: 10.1021/acs.cgd.5b01444, Crystal Growth & Design **16**, 440-446 (2016).

Conference Proceedings & Oral Presentations

1. **R. Kacker** and H.J.M. Kramer. *Investigations into the Use of Ultrasounds for Seed Generation for Continuous Cooling Crystallization Process in an Oscillatory Flow Baffled Crystallizer*, Proceedings of the 16th annual meeting of the American Institute for Chemical Engineers, AIChE (2016).

2. **R. Kacker**, S. Regensburg and H.J.M. Kramer. *Ultrasound assisted tubular crystallization in a COBC*, Proceedings of the 22nd International Workshop on Industrial Crystallization BIWIC(2015).

3. **R. Kacker**, M. Radoiu and H.J.M. Kramer. *Microwave assisted fines control during crystallization*, Proceedings of the 21st International Workshop on Industrial Crystallization, BIWIC (2014), p. 97-104.

Recent Poster Presentation

1. **R. Kacker**, S. Dhingra, D. Irima, A.I. Stankiewicz, M.K. Ghatkesar, H.J.M.
   Kramer and H.B. Eral. *Multiparameter Investigation of Laser-Induced Nucle-
   ation of Supersaturated Aqueous KCl Solutions*. In International Symposium
   on Industrial Crystallization, ISIC20 (2017).